Binghamton University
The Open Repository @ Binghamton (The ORB)

Graduate Dissertations and Theses | Dissertations, Theses and Capstones

2017

# Harnessing solar energy: vapor phase polymerized poly(3,4-Ethylenedioxythiophene) for solid state dye-sensitized solar cells and the photodegradation of organic toxicants

Steven M. Boyer
*Binghamton University--SUNY*, sboyer2@binghamton.edu

Follow this and additional works at: https://orb.binghamton.edu/dissertation_and_theses

 Part of the Chemistry Commons

## Recommended Citation

Boyer, Steven M., "Harnessing solar energy: vapor phase polymerized poly(3,4-Ethylenedioxythiophene) for solid state dye-sensitized solar cells and the photodegradation of organic toxicants" (2017). *Graduate Dissertations and Theses*. 14.
https://orb.binghamton.edu/dissertation_and_theses/14

This Dissertation is brought to you for free and open access by the Dissertations, Theses and Capstones at The Open Repository @ Binghamton (The ORB). It has been accepted for inclusion in Graduate Dissertations and Theses by an authorized administrator of The Open Repository @ Binghamton (The ORB). For more information, please contact ORB@binghamton.edu.

# HARNESSING SOLAR ENERGY: VAPOR PHASE POLYMERIZED POLY(3,4-ETHYLENEDIOXYTHIOPHENE) FOR SOLID STATE DYE-SENSITIZED SOLAR CELLS AND THE PHOTODEGRADATION OF ORGANIC TOXICANTS

BY

STEVEN M. BOYER

BS, Elizabethtown College, 2012

DISSERTATION

Submitted in partial fulfillment of the requirements for
the degree of Doctor of Philosophy in Chemistry
in the Graduate School of
Binghamton University
State University of New York
2017

© Copyright by Steven M. Boyer 2017
All Rights Reserved

Accepted in partial fulfillment of the requirements for
the degree of Doctor of Philosophy in Chemistry
in the Graduate School of
Binghamton University
State University of New York
2017

April 28, 2017

Professor Alistair J. Lees, Chair
Department of Chemistry, Binghamton University

Professor Wayne E. Jones, Jr., Faculty Advisor
Department of Chemistry, Binghamton University

Professor Chuan-Jian Zhong, Member
Department of Chemistry, Binghamton University

Professor Gerard S. McGrady, Member
Department of Chemistry, Binghamton University

Professor Louis F. J. Piper, Outside Examiner
Department of Physics, Binghamton University

**Abstract**

Solar energy is the most abundant energy resource available and can be utilized for a variety of applications such as photovoltaics and promote chemical reactions. Dye-sensitized solar cells (DSSCs) are a class of photovoltaic cells that have been well studied for their low cost and environmentally friendly materials. Previous research focused on developing more efficient liquid phase solar cells, but little work has gone into solid state DSSCs. Moving towards the solid state would improve the lifetime of the cells, preventing leaking of electrolyte and corrosion of the electrode while potentially being a more scalable process for mass production, improving feasibility. Our focus is exploring the use of vapor phase polymerized (VPP) poly(3,4-ethylenedioxythiophene) (PEDOT) as a solid electrolyte to replace the liquid electrolyte commonly used. The challenge in fabricating solid state DSSCs is the interaction between the photosensitizer dye and the solid state electrolyte acting as the hole transport layer. Since VPP occurs in the vapor phase, it has the potential to penetrate the mesoporous titanium dioxide ($TiO_2$) which can improve the interaction between the dye and hole transport layer PEDOT.

There has also been an increased interest in $TiO_2$ fibers as a photocatalyst for the degradation of persistent organic and biopharmaceutical toxins in the environment. The photocatalytic efficiency of $TiO_2$ fibers is typically limited to UV irradiation due to its wide semiconductor bandgap. In DSSCs a photosensitizer dye is used to absorb visible light and

inject an electron into the $TiO_2$ electron transfer material. Our focus is utilizing this concept in the fabrication of ruthenium dye-sensitized $TiO_2$ fibers to enhance the degradation of the biopharmaceutical pollutant phenazopyridine under visible irradiation.

*To My Parents*

**Acknowledgments**

I would like to express my appreciation for my research advisor, Professor Wayne E. Jones, Jr. for providing me with more opportunities than I knew was possible. Dr. Jones changed my life before I ever stepped foot on campus, meeting him at Elizabethtown College my senior year. I know I would not be here today if he did not take the time that day to talk to me. I would also like to thank Dr. Jones for his endless support, encouragement, and enthusiasm while guiding me throughout my graduate career. I am thankful for the broad range of research opportunities in various areas of chemistry, I learned so much from those experiences. I would also like to extend my gratitude for his support of my career goal of becoming a chemistry faculty member. I have become a better teacher, and mentor because of my work with him during Go Green, the NSF Smart Energy REU, the Intermediate Inorganic class and as Instructor of Record for CHEM101. He also provided me the opportunity to work with industries and government on projects for Asbury Carbon, Advanced Pierre Foods, Battelle and the DoD. I am fortunate to have had Dr. Jones as a mentor because he made me better chemist, teacher, mentor and person. As I move on in professional career, I am happy to say I have gained an important mentor and friend in Dr. Jones.

I would also like to extend my gratitude to my committee members, Professor Alistair Lees, Professor Chuan-Jian Zhong, Professor Gerard S. McGrady, and Professor Louis Piper for their time and input on my dissertation, the useful discussions, their guidance and their support during my graduate studies. I would also like to the Dr. James

Dix for serving as a committee member for my preliminary oral exam. In addition, I would like to thank Dr. William Bernier for his advice and guidance on research projects, papers and presentations throughout my time in the Jones group. His support and knowledge has greatly helped in my development as a chemistry researcher. I consider all of these faculty wonderful professional role models and thank them for their help and support.

I consider myself lucky to have worked with Dr. Alexsa Silva, who I consider my teaching mentor. She was always willing to share her knowledge and experiences while taking an interest in my goals. Dr. Silva took the time and personal interest to teach me how to be a better teacher, mentor and professional. I will always appreciate her enthusiasm, support and confidence in me as an educator, giving me the opportunities to be Head TA and Instructor of Record. I feel Dr. Silva has prepared me to be successful, and am grateful for all that she's done for me.

Joining the Jones research group was like becoming a part of a second family. I am grateful to have spent time both professionally and socially with the current and past group members. I would like to especially thank Dr. Kenneth Skorenko for helping me become acclimated to graduate school and the research group. He taught me how to use different instrumentation and experimental procedures that I frequently used with my work on solar cells. I am thankful to have worked closely with Linyue Tong throughout our time together in the group. She has been a valuable person to work with and have discussions about chemistry. I would also like to thank Dr. Jian Liu and Dr. Danielle McCarthy for their help with the photodegradation project. I would also like to thank the undergraduate students I had the pleasure of mentoring and working with: Kevin Fischer, Sandy Zhang, Frank Schreffler, Matthew Ehrilch, and John Kinsley. I appreciate their hard work,

dedication, and allowing me to grow as a research mentor. I extend gratitude to the rest of the graduate students in the group I had the pleasure of working with including Anting Chen, Wei Wu, Ziqi Qing and Boxio Li. Thank you to the entire Jones group for your support, suggestions, and kindness.

I am grateful for the support from the entire Chemistry Department throughout my graduate studies. I would like to thank all the faculty and staff members on all the committees that convened and decided to grant me with the fellowships, assistantships and awards I received during my graduate career. Thank you to Renee Sersen, Connie Dowling, and Lynn Hickey for their support and help making my experience pleasant and memorable. I would like to thank Mary Bridge and Dr. Benjamin Turnpenny for their support with teaching and outreach and Bob Gonzales for instrumentation support. Thank you to all of my former students, in lab and lecture, for providing me with a positive experience and allowing me to grow as an educator. I would also like to thank Dr. Abhishek Nandur from the Physics Department and Dallas Fisher and Professor Tara Dhakal from the Electrical Engineering Department for their collaborations in the CASP Lab. I have gained many friends during my time in the department and would like to especially thank Dr. Tim Owen, Bryan Trimm, Zakiya Skeete, Stephen Ambrozik, Heather Crapo, Yinguang Zhao, Jing Zhang, Derek Dwyer, Xiaohui, and Kaitlin McCardle. You were always there to help me either in the lab or out and provided me a lifetime of memories.

I would also like to express my gratitude for my family who gave me the greatest gift, their unwavering belief in me. My parents taught me a lot of life lessons that helped me achieve success but also handle the failures. I can never thank my parents enough for

their sacrifices and guidance to become the person I am today. I would also like to thank my brother for his endless support of me. Thank you to the rest of my family and friends for their love and support throughout my life, especially throughout my education.

Lastly, I would like to thank my fiancé Hannah Cronk for her endless support through everything. Hannah has seen me at my best and my worst through my studies, and I appreciate that she was by my side through it all. Hannah always knew what I needed to hear, usually before I knew it. I am amazed at the support you were able to offer me while also performing your graduate studies. I am lucky to have you, and I look forward to our next journey together.

## Table of Contents

## List of Tables

**Chapter 1**



**Chapter 2**



**Chapter 3**



**Chapter 4**



**Chapter 5**

## List of Figures

### Chapter 1



### Chapter 2

## List of Schemes

### Chapter 1



### Chapter 4



### Chapter 5

## List of Abbreviations

| | |
|---|---|
| $CuCl_2$ | Copper (II) chloride |
| cm | Centimeter |
| $cm^{-1}$ | Wavenumber |
| CVD | Chemical vapor deposition |
| DSSC | Dye-sensitized solar cell |
| EDOT | 3,4-ethylenedioxythiophene |
| EPA | Environmental Protection Agency |
| FeCl | iron (III) chloride |
| FePTs | iron(III) p-toluenesulfonate |
| FF | Fill factor |
| FTIR | Fourier transform infrared spectra |
| FTO | Fluorine doped tin oxide |
| GNP | Graphene nano platelets |
| ICP | Intrinsically conducting polymer |
| Imp | Current at maximum power |
| Isc | Short-circuit current |

| | |
|---|---|
| ITO | Indium tin oxide |
| IV | Current-voltage |
| $J_{SC}$ | Short-circuit current density |
| mL | Milliliter |
| nm | Nanometer |
| NMR | Nuclear magnetic resonance |
| PAP | Pyridinediamine,3-(phenylazo) monohydrochloride |
| PEDOT | Poly(3,4'ethylenedioxythiophene) |
| PEDOT:PSS | Poly(3,4'ethylenedioxythiophene) polystyrene sulfonate |
| PEP | Photoelectrochemical polymerization |
| Pin | Power input |
| $P_{max}$ | Maximum power |
| PMMA | Poly(methyl methacrylate) |
| PVDF | Polyvinylidene fluoride |
| PVDF-HFP | Poly(vinylidene fluoride-hexafluoro propylene) |
| $R_s$ | Series resistance |
| $R_{sh}$ | Shunt resistance |
| $Ru(dcbpyH_2)_2Cl_2$ | cis-dichlorobis(2,2'-bipyridyl-4,4'-dicarboxylic acid)ruthenium (II) |

| | |
|---|---|
| SEM | Scanning electron microscopy |
| spiro-OMeTAD | 2,2', 7, 7'-tetrakis(N,N'-di-p-methoxyphenylamine)-9, 9' – spirobifluorene |
| t | Time |
| TCE | Transparent conducting electrode |
| $TiO_2$ | Titanium dioxide |
| TTIP | Titanium isopropoxide |
| ttp-Br | 4′-{4-[2-(2,5-Dibromothiophen-3-yl)-vinyl]phenyl}-2,2′:6′,2″- terpyridine |
| ttp-H | 4′-[4-(thiophen-3-yl-methoxymethyl)phenyl]-2,2′: 6′,2″-terpyridine |
| Twy | Terawatt year |
| UV | Ultraviolet |
| Vis | Visible |
| Vmp | Voltage at maximum power |
| Voc | Open-circuit voltage |
| VPP | Vapor phase polymerization |
| XPS | X-ray photoelectron spectroscopy |
| XRD | X-ray diffraction |
| λ | Wavelength |
| η | Solar cell efficiency |

# Chapter 1 Introduction to Dye-Sensitized Solar Cells

## 1.1 Overview of Solar Energy

According to the Environmental Protection Agency (EPA), 90% of energy consumed in the United States in 2015 was produced by nonrenewable energy resources including coal, oil, natural gas and nuclear. While these resources are the most common, they are also limited and have been linked to greenhouse gas emissions. For these reasons, there has been an effort to increase the use or renewable energy resources such as wind, solar and bio fuels. Looking at the energy available for each renewable source per year, solar is the most abundant as shown in Table 1-1. In addition to being the most abundant energy resource, solar does not require a combustion reaction which produces carbon dioxide, a known green house gas. This makes solar an available and clean alternative to fossil fuels that are currently the standard.

Table 1-1: Available energy for renewable energy resources per year.

| Energy Resource | Available Energy (TWy/year) |
|---|---|
| Solar | 23, 000 |
| Wind | 25-70 |
| Bio Mass | 2-6 |
| Hydro | 3-4 |
| Geothermal | 0.3-2 |

There are several methods solar energy can be converted to useable energy including direct solar, photovoltaics, and water splitting. Photovoltaics and water splitting offer the most promise as they require less area compared to direct solar. Water splitting or artificial photosynthesis can be used to generate hydrogen. Hydrogen has gained interest as an alternative fuel source to be used in fuel cells. Finding a cheap, clean source of hydrogen will be important if fuel cells are to become feasible for consumers. Photovoltaics directly convert solar energy to electricity, making it a strong candidate to power homes and businesses. While solar energy is the most abundant and reaches most places on the planet every day, there are fluctuations in the amount of energy reaching the earth's surface.[1] With advances is energy storage devices such as batteries and capacitors, unused energy generated during the day can be stored for when solar is not available.[1]

Photovoltaics convert light energy into current by creating electron-hole pairs at a junction between two materials, creating an electric potential difference across the interface as shown in Figure 1-1.[2] On one side of the junction is an n-type material which electrons

travel through, the other is a p-type material for holes. To date, most commercially available solar cells use doped forms of crystalline or amorphous silicon. While these solar cells are efficient, they can also be expensive from the high temperature processing leading to the development of new classes such as the dye-sensitized solar cell (DSSC).[2]

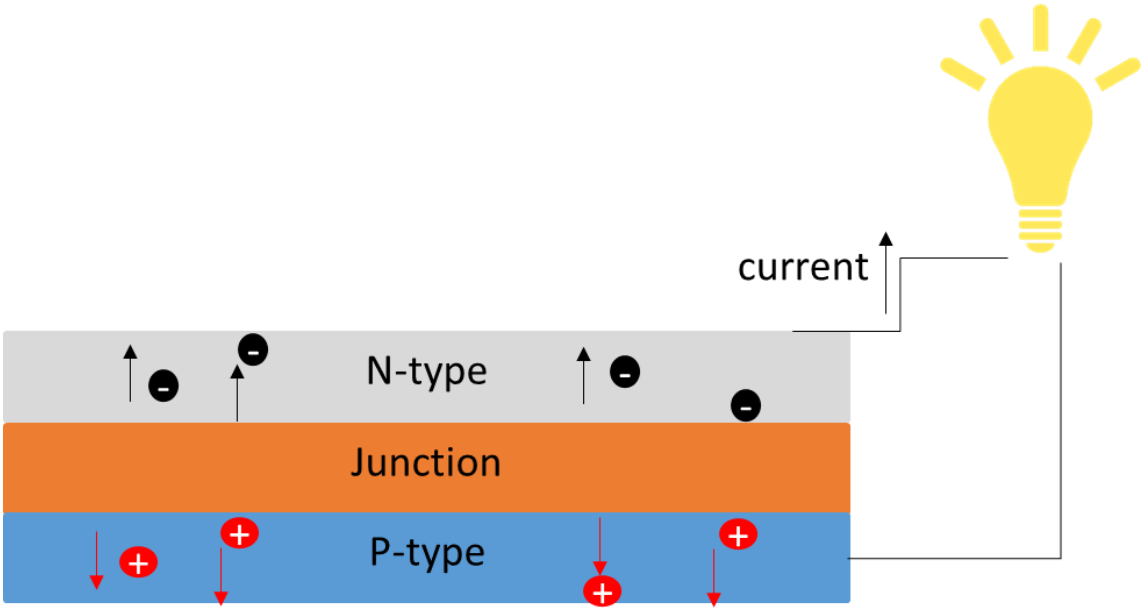


Figure 1-1: General overview of how photovoltaic cells produce energy.

The solar cell efficiency (η) is calculated from the short-circuit current ($I_{SC}$), open-circuit voltage ($V_{OC}$) the fill factor (FF) and the power input ($P_{in}$) which accounts for the area of the cell and the intensity of light.[3]

$$\eta = \frac{I_{SC}V_{OC}FF}{P_{in}} \quad (1)$$

The FF is a term that is calculated from the maximum power ($P_{max}$), $V_{OC}$ and $I_{SC}$ and illustrates how close to the theoretical maximum the solar cell is based on loss from series and shunt shunt resistance.[3] The $P_{max}$ term is the product of the photocurrent and photovoltage where the power output is maximal.[3]

$$FF = \frac{P_{max}}{I_{SC}V_{OC}} \quad (2)$$

A current-voltage curve (IV) curve is used to measure the variables needed to calculate the efficiency of a solar cell. A representative IV curve is shown in Figure 1-2. The $I_{SC}$ and $V_{OC}$ are where the curve crosses the x and y-axis. The current at maximum power ($I_{mp}$) and voltage at maximum power ($V_{mp}$) are used to determine the $P_{max}$. Based on this the FF can be calculated, allowing of the solar cell efficiency to be calculated. Factors that can decrease the solar cell efficiency include series and shunt resistance ($R_s$ and $R_{sh}$ respectively). Series resistance is the loss of energy from electrons moving through the layers of the solar cell. Shunt resistance is the resistance that prevents early recombination of the electron-hole pair which would result in a short in the system. For highly efficient solar cells, a low $R_s$ and high $R_{sh}$ is required.

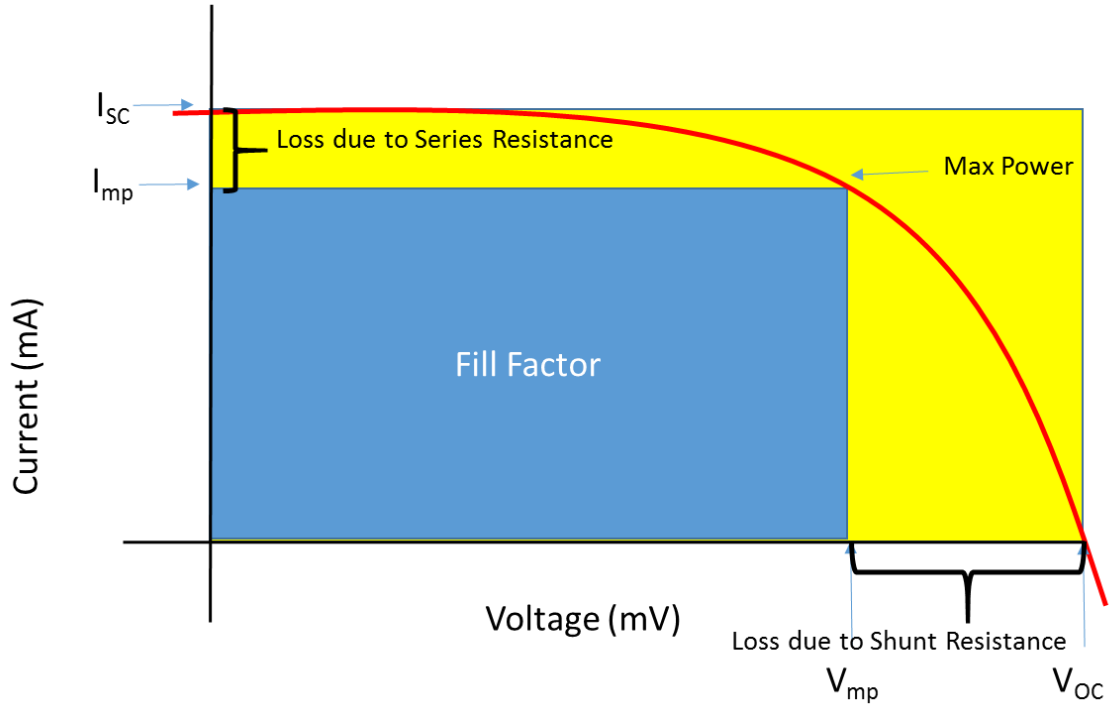


Figure 1-2: A representative IV curve used to determine the $I_{SC}$, $V_{OC,}$ and $P_{max}$ which are used to calculate the solar cell efficiency.

### 1.2 Dye-sensitized Solar Cell Overview

The first reported efficient DSSC demonstrated the potential for a solar cell with <7% efficiency using inexpensive materials and processes.[4] Although this was not the first DSSC, the breakthrough for the technology was the use of a titania nanoparticle layer instead of a thin film of titania.[4-6] The nanoparticles formed a mesoporous n-type anode that increased the surface area and the available surface for the anchored photosensitizer by over a thousand fold.[4] The increase in dye loading drastically improved power-conversion efficiencies to become competitive with other generations of solar cells.[7] The schematic of a general DSSC is shown in Figure 1-3.[8] The dye photosensitizer is bound to the semiconductor mesoporous material such as $TiO_2$ or ZnO is used as the n-type material

on a transparent electrode such as indium tin oxide (ITO) or fluorine doped tin oxide (FTO). The p-type material is most commonly a liquid electrolyte, especially an iodide/triiodide system. While a liquid electrolyte, specifically an iodide triiodide solutions is the most common, solid-state electrolytes have been explored as well. Liquid electrolytes undergo an oxidation/reduction reaction and diffusion to shuttle an electron from the electrode to the dye molecule. Solid electrolytes use a tunneling or hoping mechanism, depending on the material that is being used in the system.

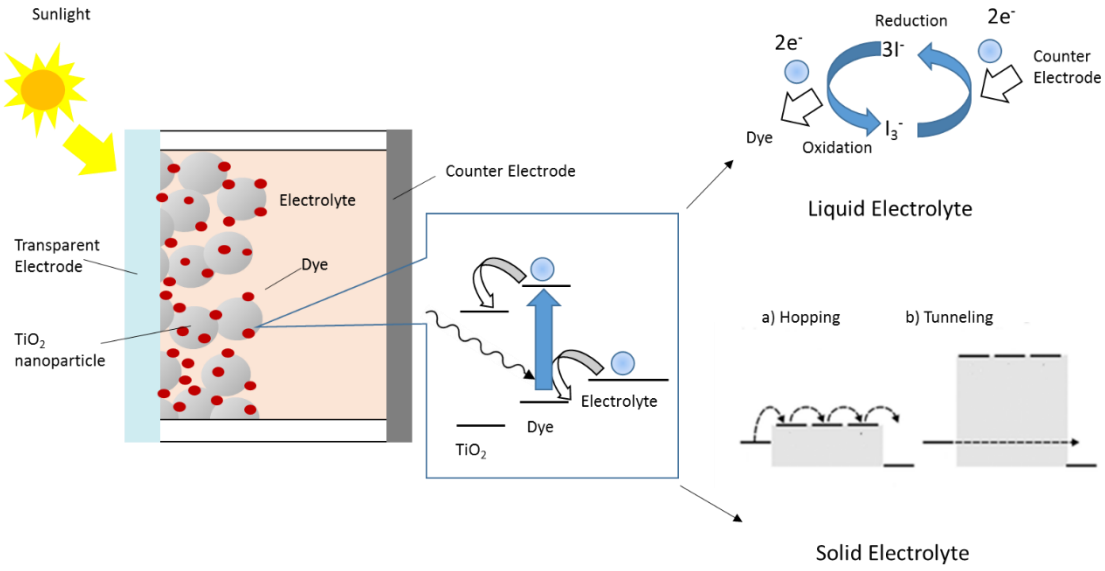


Figure 1-3: Liquid and solid state DSSC device schematic (adapted from Ref. 3).

While there have been a range of photosentizers used in DSSCs including porphyrins, metal complexes and organic molecules, ruthenium polypyridyl complexes. Of the photosensitizers, ruthenium polypyridyl complexes have been extensively studied for their broad absorption spectra, suitable ground and excited state energy levels, relatively long excited-state lifetimes and good (electro)chemical stability.[3] The properties of the complexes can be tuned based on the substituents on the bipyridine ligands as shown

in Figure 1-4 which has led to the numerous dye structured studied.[3, 9] While there has been a range of dyes synthesized and studied, there are common components such as an anchoring group and an electron donating ligand such as isothiocyante.[7] The anchoring group is needed for the dye to bind to the semiconductor layer which is especially important when a liquid electrolyte is used to prevent removal of the dye. The electron donating ligand helps with the regeneration of the dye from the electrolyte and broadens the absorbance spectrum, allowing for more light to be utilized.[3]

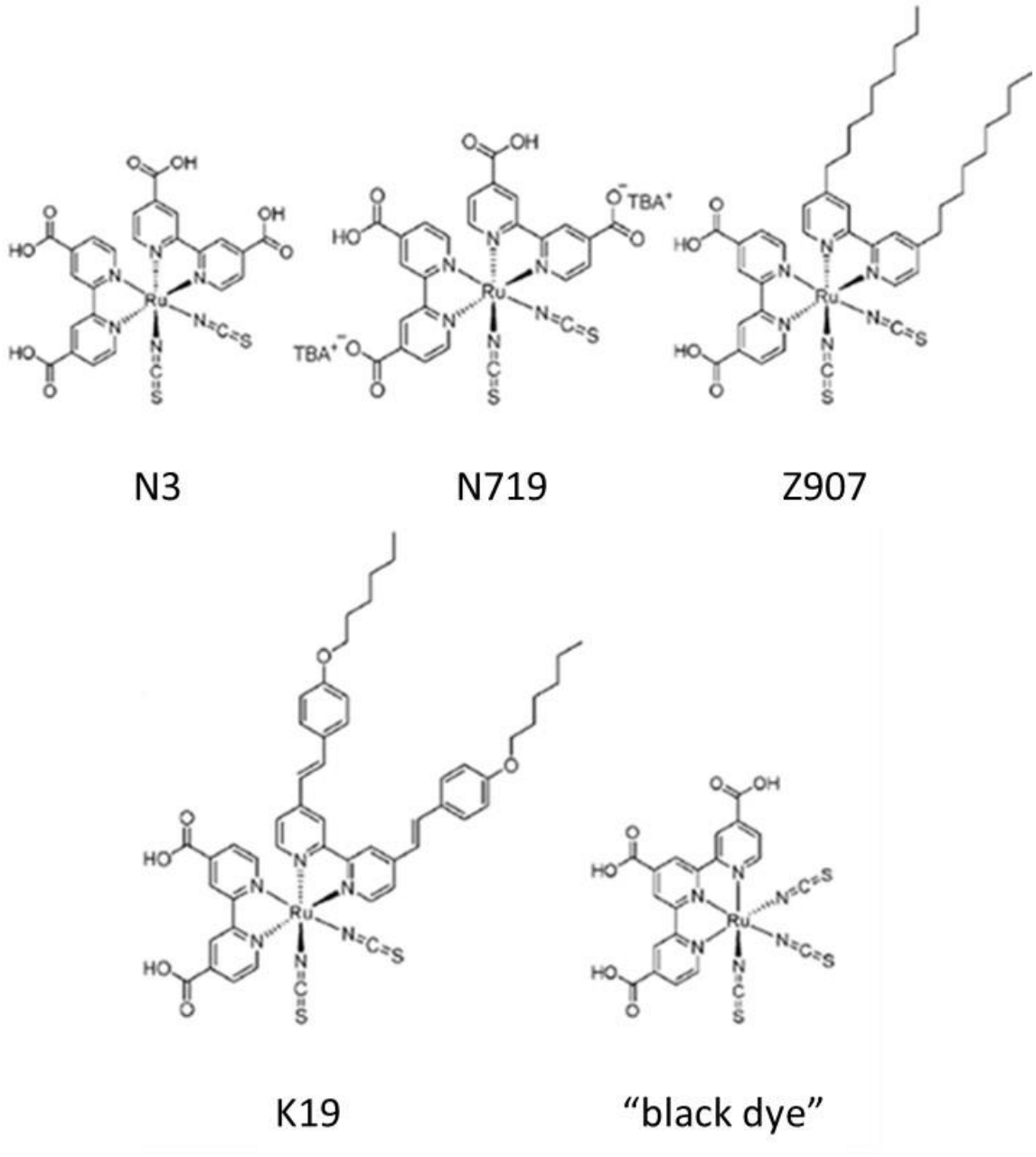


Figure 1-4: Structure of some common ruthenium polypyridyl complexes used as photosensitizers in DSSCs.

A common component of the dyes is the presences of an anchoring group such as a carboxylate, ester, acid chloride, sulfonate, silane or phosphate group.[3, 10, 11] Although phosphates have been shown to bind stronger than carboxylates, the stability and easy of synthesis has made carboxylates the most common anchoring group.[3] In addition to

adhering to the n-type semiconductor, the anchoring group plays an important role in the rate of electron injection as the functional group plays a role in the wave function overlap with the semiconductor.[12] Carboxylates have been shown to favor electron injection by allowing delocalization of the dye LUMO over the anchoring group towards the semiconductor surface.[13-15] Studies adjusting the distance between the anchoring group and the sensitizer with nonconjugated spacers showed an exponential decrease in injection rate.[16] This suggests the mechanism of the electron injection is through the anchoring group not through space as shown in Figure 1-5.

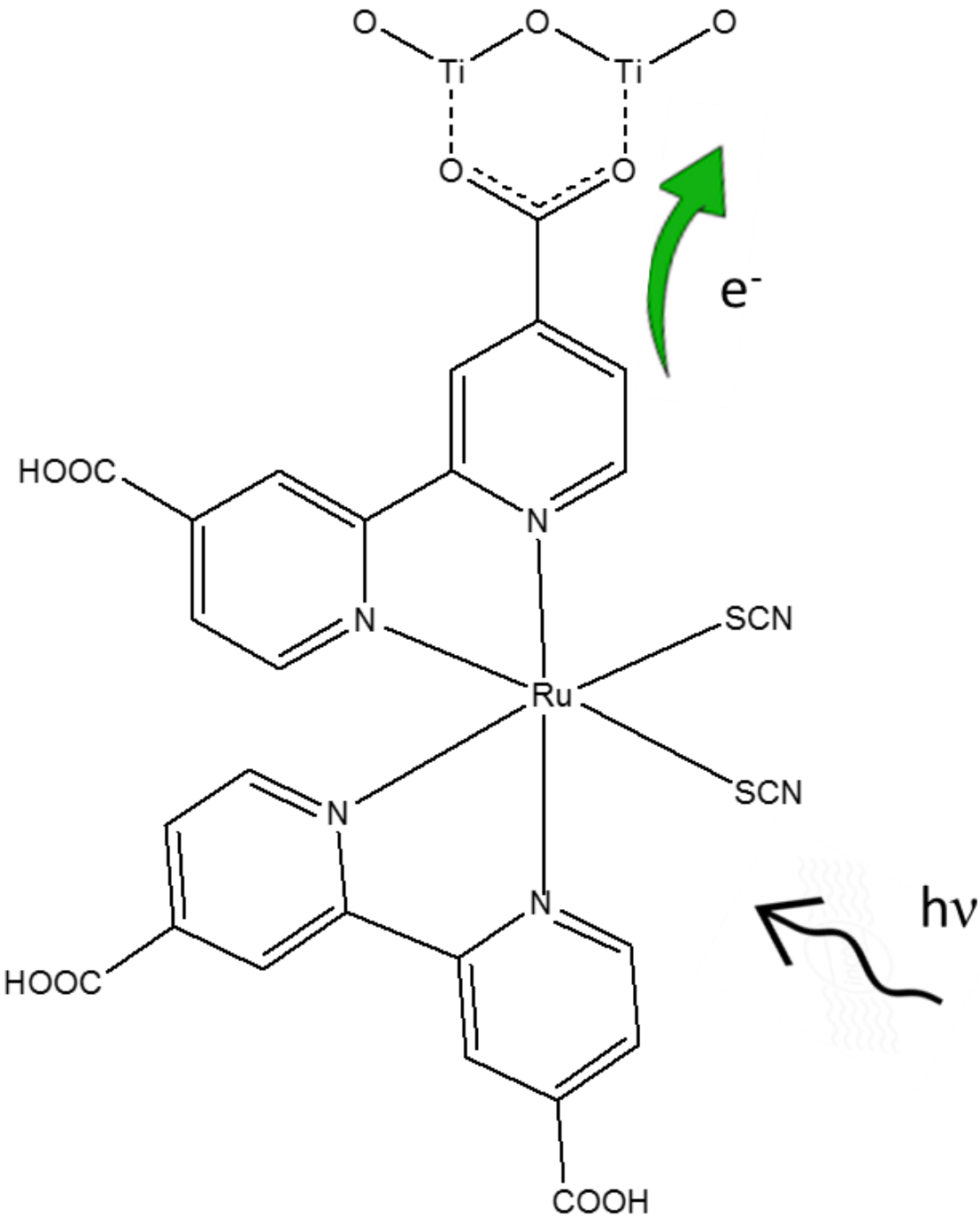


Figure 1-5: Proposed mechanism of dye absorbing a photon of light and undergoing a MLCT followed by injection of an electron into the conduction band of $TiO_2$ through the carboxylate anchoring group.

### 1.3 Regeneration of Photosensitizer with Liquid Electrolytes

After the sensitizer injects an electron into the semiconductor, for the reaction to occur again the oxidized molecule must be reduced. A liquid electrolyte is commonly used because of a liquid's ability to fill the mesoporous $TiO_2$ layer. The iodide/triiodide system in an organic solvents has been commonly used because of the slow recombination kinetics between the electrons in the titania with the oxidized dye and the triiodide electrolyte.[17-19] There are several drawbacks of the liquid electrolyte though including corroding of the electrode, leaking and requiring special sealants.[7] In addition to the lack of long term stability, the regeneration of the dye is slow based on the mechanism for the reduction of the oxidized sensitizer ($S^+$) as shown in Scheme 1-1.[3] The first step is likely the binding of iodide to the thiocyanate ligand of the dye, followed by a transfer of one electron between $S^+$ and $I^-$.[20] The second step is the addition of a second iodide forming a complex. The $I_2^-$ will leave and form triiodide and iodide.[21]

Scheme 1-1: Mechanism for the reduction of an oxidized sensitizer with an iodide/triiodide electrolyte.

$$S^+ + I^- \longrightarrow (S\text{---}I)$$

$$(S\text{---}I) + I^- \longrightarrow (S\text{---}I_2^{-\bullet})$$

$$(S\text{---}I_2^{-\bullet}) \longrightarrow (S + I_2^{-\bullet})$$

$$2I_2^{-\bullet} \longrightarrow I_3^- + I^-$$

As mentioned previously, there have been a lot of research into the development of new dyes with larger extinction coefficients and broader absorbance yet DSSC efficiencies have not improved greatly. To understand why, it is important to look at the electron transfer kinetics as shown in Figure 1-6.[12] The through bond electron transfer from the

excited sensitized dye to the $TiO_2$ following excitation has been reported on the picosecond time scale.[12] The regeneration of the dye is much slower on a microsecond time scale.[12] The slower regeneration rates could be a result of the regeneration of the dye being less favorable, resulting in a low regeneration efficiency and requiring an overpotential to drive the redox reaction.[22 23] It has been proposed if the overpotential is reduced, the efficiency of DSSCs can reach over 20%, competing with the efficiency of thin-film and silicon based solar cells, making DSSCs feasible for consumers.[23] For this to happen, an alternative to the currently used liquid is required.

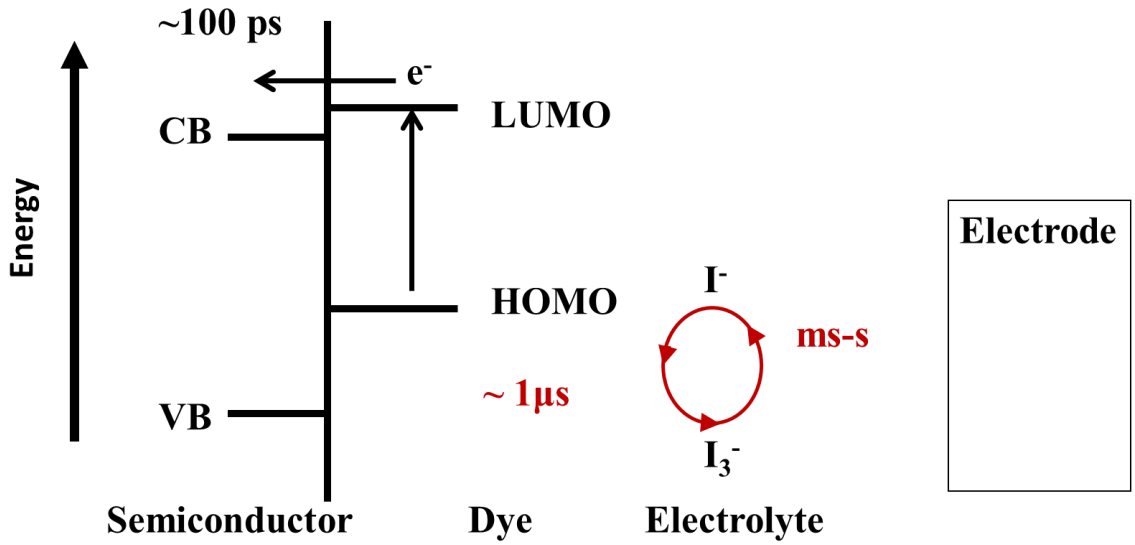


Figure 1-6: Electron transfer kinetics in a DSSC determined using transient absorption spectroscopy (adapted from Ref. 12).

### 1.4 Inorganic p-type Semiconductors

When considering alternatives to the liquid electrolyte in a DSSC, there are certain properties that are required of the material. The material needs to transfer holes from the photosensitizer dye efficiently, fill the porous n-type material layer, fabrication of the layer cannot damage previous layers, and be transparent in the visible region or be as efficient

as the dye at electron injection.[24] Common p-type semiconductors such as SiC and GaN cannot be used in the fabrication of DSSCs because their high temperature depositions would degrade the dye layer. For this reason other p-type materials have been explored including CuI, CuBr and CuSCN.[25-27]

Of the copper semiconductors, the most studied is CuI which was first used by Tennakone et al.[27] By replacing cyanidin with N3 dye, the group was able to fabricate a solar cell with an efficiency of 2.4%.[28] The drawback of CuI is the material is unstable, degrading faster than liquid-state DSSCs.[29] The films were found to oxidize under constant illumination from interaction with the $TiO_2$ layer while excess iodine from the synthesis decreased the photocurrent of the solar cell.[30, 31] To overcome the stability issues of CuI, CuSCN was used as an alternative. While the stability of the cells were found to improve, the efficiency of the cells were lower, likely due to the lower hole conductance.[24] While other p-type semiconductor materials have been explored, there has not been a material found that can replace the liquid electrolyte efficiently.

### 1.5 Molecular Hole Transporting Materials

An alternative to p-type semiconductors is organic small molecules with the most popular currently 2,2', 7, 7'-tetrakis(N,N'-di-p-methoxyphenylamine)-9, 9' – spirobifluorene (spiro-OMeTAD) shown in Figure 1-7. While DSSCs with spiro-OMeTAD has reached efficiencies of 7.2%, they have not yet been able to match efficiencies with liquid electrolytes.[32] Spiro-OMeTAD has produced the highest efficiencies of solid state DSSCs, likely because its HOMO level is optimally located to balance the hole transfer yield and the open circuit voltage, allows oxygen induced doping in the presence of chemical oxidants and shows good pore filling.[33] Spiro-OMeTAD has

shown promise, there are limitations including a strong absorption band in the visible when oxidized and a relatively low hole mobility.[34, 35] The major challenge with using a solid state electrolyte like spiro-OMeTAD the most efficient solar cells have been thinner than liquid state DSSCs. The reason thinner $TiO_2$ layers are needed could be more efficient is a lack of penetration into the mesoporous layer, lack of conductivity or the filtering of light from reaching the photosensitizer.[33] Decreasing the thickness can minimize these however it also decreases the dye loading possible which will decrease the maximum efficiency achievable. For a solid state DSSC to match the efficiency of liquid DSSCs, the mesoporous layer must be thicker to increase dye loading but still effectively fill the semiconductor layer, have high hole mobility and be transparent. While other molecules have been explored, nothing has been found better than Spiro-OMeTAD.[33]

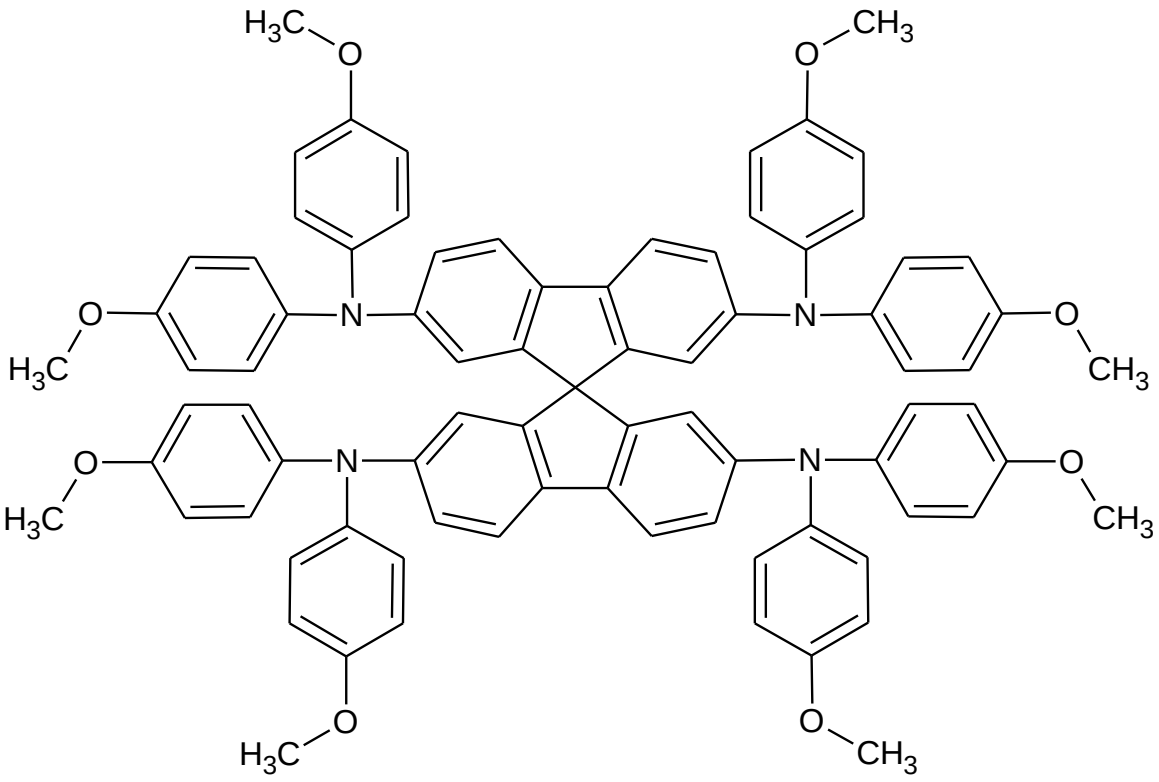


Figure 1-7: Chemical structure of the hole transport material spiro-OMeTad.

## 1.6 Intrinsically Conducting Polymers as Hole Transport Materials

One possible alternative to small molecules such as spiro-OMeTad as a hole transport material is an intrinsically conducting polymer (ICP). While there are numerous ICPs, poly(3,4'ethylenedioxythiophene) (PEDOT) has shown the most promise as a hole transport material. PEDOT is a p-type conducting polymer that transfers electrons through a redox process as shown in Figure 1-8. PEDOT is an insoluble polymer but copolymerizing it with polystyrene sulfonate (PSS) produces PEDOT:PSS which is soluble, allowing for solution processing. The PSS however is an insulator and reducing the conductivity of the material. An alternative to PEDOT:PSS solution processing is utilizing an *in-situ* method such as electrochemical, chemical vapor deposition (CVD), chemical oxidation polymerization and vapor phase polymerization (VPP).[36]

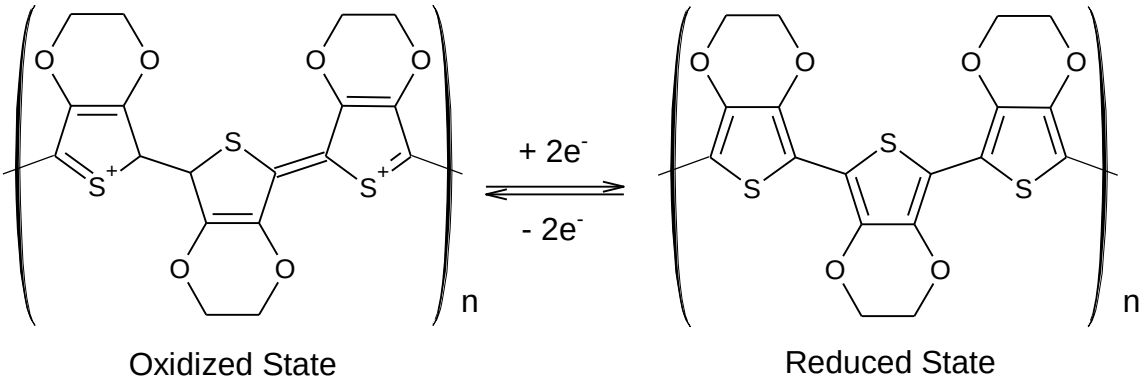


Figure 1-8: Mechanism of electron transfer from the oxidized and reduced states of PEDOT.

Currently the most commonly used method of forming PEDOT as a hole transport material in a DSSC is using an *in-situ* photoelectrochemical polymerization (PEP) method.[37-41] First reported by Saito et al in 2003, the original PEP-PEDOT solar cell had an efficiency of 0.53% which at the time was one of the most efficient solid state DSSC using an organic polymer as a hole transport material.[41] The efficiency was attributed to

an increase is the transparency and charge transport properties of PEDOT.[41] The efficiency of PEP-PEDOT solar cells improved as the polymerization conditions were optimized including the anion dopant, the photosensitizer, solvent, and irradiation conditions.[38-40] The current record for a PEP-PEDOT solar cell is 7.11%, rivaling the record for spiro-OMeTAD which is 7.2%.[37] The high efficiency was attributed to the higher doping of the PEDOT which resulted in a hole conductivity of 2.0 S/cm.[37]

Another method reported of using PEDOT as a hole transport material is a thermal polymerization of the brominated monomer.[42] Kim et al compared the conducting polymers PEDOT and poly(3,4-ethylenedithiathiophene) (PEDTT) as hole transport materials and found solar cells with PEDOT were more efficient as shown in Table 1-2.[42] The higher efficiency was attributed to the higher conductivity of PEDOT which is supported by the conductivity measured with a 4-point probe and short-circuit current density ($J_{SC}$). Based on the increase of efficiency in the PEP-PEDOT solar cell and when comparing PEDOT to PEDTT, the conductivity of the hole transport material is important in the overall efficiency of a solid state DSSC.[42] This suggests developing a more conductive PEDOT layer in a solid state DSSC could further increase the efficiency of the solar cell.

Table 1-2: Solar cell efficiency and other values based on using PEDOT or PEDTT as a hole transport material.

| **Sample** | **$V_{oc}$ (V)** | **$J_{sc}$ (mA/cm$^2$)** | **FF** | **η (%)** | **σ (S/cm)** |
|---|---|---|---|---|---|
| PEDOT | 0.64 | 18.6 | 0.56 | 6.8 | 10 |
| PEDTT | 0.66 | 11.2 | 0.56 | 4.1 | 0.5 |

Based on the literature, to further improve the efficiency of solid state DSSCs with PEDOT as a hole transport material, more conductive PEDOT is needed. The method and conditions of polymerizing PEDOT can greatly change the chemical and physical properties of the resulting films, including the transparency and conductivity.[36, 43] Of the reported methods, CVD and VPP have resulted in the most conductive films, which have exceeded 1000 S/cm.[36, 43, 44] While the CVD method requires specialized equipment to sublime the oxidant, the VPP method coats the substrate using solution processing such as spin coating.[44] This makes the VPP method of interest for its combination of simplified setup for processing while still achieving high conductivity.

The conductivity of VPP PEDOT can vary based on the oxidant initiator, vapor pressure and environmental conditions such as temperature.[44-47] When iron(III) p-toluenesulfonate (FePTs) is used as an oxidant, there are several reports of PEDOT thin films with conductivity greater than 1000 S/cm.[44, 48, 49] High conductivities are possible and have been reported using iron (III) chloride (FeCl) as an oxidant to produce single-crystal PEDOT nanowires with conductivities of 7619 S/cm.[50] These reported conductivities are several orders of magnitude greater than the conductivities of PEDOT found as hole transport materials in solid state DSSCs.

In addition to being highly conductive, VPP PEDOT has shown to be highly transparent in the visible region, preventing light filtering in solid state DSSCs.[44, 46] While other conducting polymers such as polypyrole, (poly[2,6-(4,4-bis-(2-ethylhexyl)-4H-cyclopenta[2,1-b;3,4-b0]dithiophene)-alt-4,7-(2,1,3-benzothiadia-zole)] (PCPDTBT) and poly(3-hexylthiophene-2,5-diyl) (P3HT) have been explored, they absorb visible light and reduce the number of photons reaching the dye.[33, 51-55] Absorbing light in the conductive

oxidized state is also a limit of small molecules such as spiro-OMeTAD which supports DSSCs with PEDOT could someday become the most efficient solid state DSSC.

Using an *in-situ* polymerization such as PEP has shown to allow for penetration of the mesoprous $TiO_2$ layer, one of the major challenges transitioning to a solid electrolyte.[54] VPP is another *in-situ* method of polymerization where the monomer is in the vapor phase which has been shown to fill the mesoporous layer.[56] Other p-type conducting polymers such as polythiophene and poly-[2-methoxy-5-(2-ethylhexyloxy)-1,4-phenylenevinylene] (PMEHPV) were explored in DSSCs but were limited by pore filling.[38, 57, 58] Based on the ability to fill the mesoporous $TiO_2$ layer, the high transparency in the visible region and the high conductivity, VPP PEDOT could lead to improved solid state DSSCs.

Previous work in the group has demonstrated the ability to fabricate highly conductive, transparent PEDOT thin films using VPP PEDOT, however no working DSSC has been fabricated.[44, 46, 56] It was proposed using the oxidant FePTs reduced the $TiO_2$ layer based on x-ray photoelectron spectroscopy (XPS) results before and after soaking $TiO_2$ in the oxidant solution. To overcome this, it was proposed copper (II) chloride ($CuCl_2$) could be used as an oxidant. While the conductivities of VPP PEDOT fabricated with $CuCl_2$ is lower than FePTs, the conductivities are still greater than PEP-PEDOT or the thermal polymerization of brominated EDOT.[56]

## 1.7 Dye Sensitized $TiO_2$ to Enhance Photocatalytic Properties Under Visible Irradiation

While use of dyes to expand the absorbance of DSSCs into the visible has been well studied, the concept could also be applied to other systems. $TiO_2$ is a well-studied photocatalyst for the degradation organic pollutants but uses UV irradiation based on the wide band gap.[59, 60] To make $TiO_2$ a more feasible photocatalyst, efforts have been made to extend the absorption into the visible region which makes up more of the solar spectrum. Modifying $TiO_2$ through metal, metalloid, and non-doping or through surface modification can increase the photoactivity of $TiO_2$ under visible irradiation.[60, 61] There are several examples of doping $TiO_2$, there is less investigation of utilizing a dye sensitizer like is a DSSC. By attaching a dye to the surface of $TiO_2$ the dye can absorb a photon of light, and inject the excited electron into the conduction band of $TiO_2$ as shown in Figure 1-9. The transfer of an electron from the photosensitizer to the $TiO_2$ layer has been well studied in DSSC systems which should transfer to the photodegradation system.

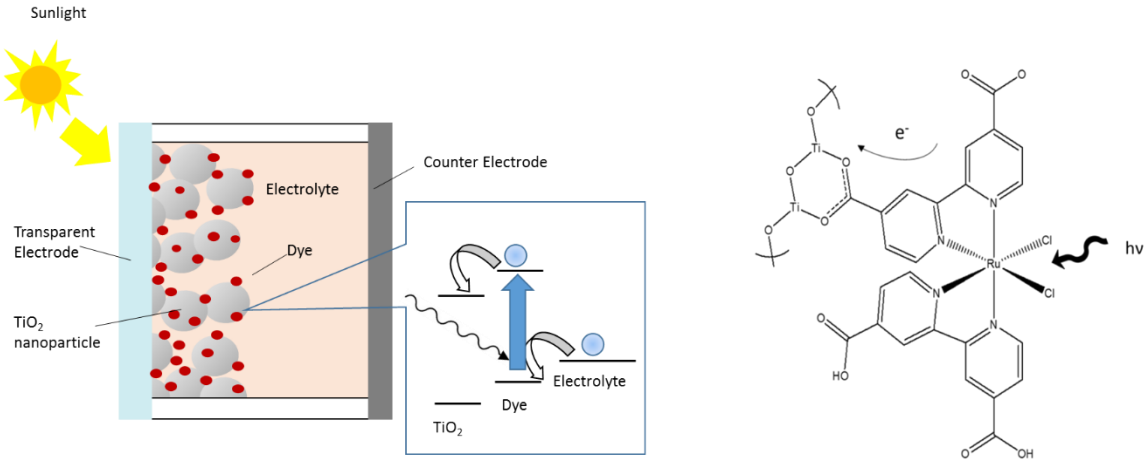


Figure 1-9: Utilization of dye photosensitizers in DSSC to expand region of absorbance into the visible region, promoting electron injection into the conduction band of $TiO_2$.

### 1.8 Problem Statement and Dissertation Overview

This dissertation has been broken into six chapters. The introduction chapter has covered the need to utilize solar energy as a clean, abundant renewable energy resource through photovoltaics. It describes the mechanism for converting solar energy to electricity and the importance of the development of the DSSC which offers a cheaper alternative to semiconductor and thin film solar cells. The first chapter highlights the commonly used p-type materials in current DSSCs and how VPP PEDOT could make solid state DSSCs as efficient as other generations of solar cells. Lastly, the chapter discussed how utilizing dye-sensitized $TiO_2$ could improve photocatalytic activity of $TiO_2$ under visible irradiation, making it more feasible to use with solar irradiation.

The second chapter will discuss the fabrication of solid state DSSCs using VPP PEDOT or PEDOT:PSS as hole transport materials. The chapter will demonstrate the importance of using both a VPP and PEDOT:PSS layer for an efficient solar cell It will look at the effects of $TiO_2$ thickness as well as the duration of the VPP PEDOT polymerization. The chapter will also compare using $CuCl_2$ and FePTs as an oxidant for the VPP PEDOT.

Chapter three will discuss the progress in the synthesis and characterization of thiophene containing ligands for the polymerization into the PEDOT hole conducting material. The ligands were polymerized with EDOT to form a new copolymer using an oxidant initiated solution polymerization to prepare thin films. It will also discuss the synthesis of new ruthenium dyes containing the two new ligands.

Chapter four will focus on the use of dye-sensitized $TiO_2$ fibers for the degradation of phenazopyridine under visible irradiation. It will compare the photocatalytic activity of

bare $TiO_2$ fibers to the dye-sensitized fibers under visible/UV irradiation and visible irradiation. The chapter will discuss the proposed mechanism of electron transfer in the material to produce the radicals used in the degradation of phenazopyridine.

Chapter five will discuss the fabrication and characterization of conducting fibrous materials using electrospinning and VPP PEDOT. It will compare the use of different template polymers and show the effects of electrospinning conditions and oxidant loading on the conductivity of the fibers. The chapter will demonstrate the use of electrospinning to fabricate polyvinylidene fluoride forms β-phase of the polymer which is a known piezoelectric material but typically requires a poling process to form. The fabrication of new dye materials and further experiments are discussed in the sixth chapter.

## 1.9 Current and Pending Publications

### 1.9.1 Publications

1. Boyer, S.M.; Tong, L.; Schreffler, F.H.; Fisher, D.A.; Dhakal, T.; Bernier, W.E.; Jones Jr., W.E. Solid-state dye-sensitized solar cells using vapor phase polymerized poly(3,4-ethylenedioxythiophene) as a hole transport layer *(In preparation)*
2. McCarthy, D.L.; Liu, J.; Dwyer, D.B.; Troiano, J.B.; Boyer, S.M.; DeCoste, J.B.; Bernier, W.E.; Jones Jr.; W.E. Electrospin metal-organic framework polymer composites for the catalytic degradation of methyl paroxon. *(Submitted New Journal of Chemistry)*

3. Tong, L.; Liu, J.; Boyer, S.M.; Sonnenburg, L.; Fox, M.; Ji, D.; Feng, J.; Bernier, W.E.; Jones Jr., W.E. Vapor-phase polymerized poly(3,4-ethylenedioxythiophene) (PEDOT)/$TiO_2$ composite fibers as electrode materials for supercapcitors. Electrochimica Acta **2016,** 224, 133-141.
4. Liu, J., McCarthy, D.L., Tong, L., Cowan, M.J., Kinslet, J.M., Sonnenberg, L., Skorenko, K.H., Boyer, S.M., DeCoste, J.B., Bernier, W.E., Jones Jr., W.E. RSC Advances **2016,** 115, 113884-113892.
5. Boyer, S.M., Liu, J., Zhang, S., Ehrlich, M.I., McCarthy, D.L., Tong, L., DeCoste, J.B., Bernier, B.E., Jones Jr., W.E. The role of ruthenium photosensitizers in the degradation of phenazopyridine with $TiO_2$ electrospun fibers. Journal of Photochemistry and Photobiology A:Chemistry **2016,** 329, 46-53.
6. Ding, J.; Li, Z.; Cui, K.; Boyer, S.; Karpuzov, D.; Mitlin, D., Heteroatom enhanced sodium ion capacity and rate capability in a hydrogel derived carbon give record performance in a hybrid ion capacitor. Nano Energy **2016,** 23, 129 - 137.
7. Liu, J.; McCarthy, D. L.; Cowan, M. J.; Obuya, E. A.; DeCoste, J. B.; Skorenko, K. H.; Tong, L.; Boyer, S. M.; Bernier, W. E.; Jones Jr., W. E., Photocatalytic activity of TiO2 polycrystalline sub-micron fibers with variable rutile fraction. Applied Catalysis B: Environmental **2016,** 187, 154 - 162.
8. Tong, L.; Skorenko, K. H.; Faucett, A. C.; Boyer, S. M.; Liu, J.; Mativetsky, J. M.; Bernier, W. E.; Jones Jr., W. E., Vapor-phase polymerization of poly(3,4-ethylenedioxythiophene) (PEDOT) on commercial carbon coated aluminum foil as enhanced electrodes for supercapacitors. Journal of Power Sources **2015,** 297, 195 - 201.

### 1.9.2 Preprints

1. Linyue Tong, Kenneth H. Skorenko, Austin C. Faucett, Steven M. Boyer, Jian Liu, Jefferey M. Mativetsky, William E. Bernier, Wayne E. Jones Jr Supercapacitor Electrodes Prepared with Vapor Phase Polymerization of Poly(3,4-ethylenedioxythiophene). Prepr. Pap.-Am. Chem. Soc.,Div. Energy Fuels **2015**.

## 1.10 Select Presentation

### 1.10.1 Invited Presentations

1. "Working Towards a Solid-State Dye Sensitized Solar Cell using Vapor Phase Polymerized PEDOT with Polymerizable Ruthenium Dyes" , Chemistry Department Colloquium, Binghamton, NY, Fall 2015
2. "Design and synthesis of ruthenium-EDOT based coordination polymers for use in inorganic organic hybrid dye sensitized solar cells", Disappearing Boundaries, Lebanon Valley College, PA 2015

### 1.10.2 Other Presentations

1. "Solid-state dye sensitized solar cells using vapor phase polymerized poly(3,4-ethylenedioxythiophene) as a hole transport", ACS North East Regional Meeting, Binghamton, NY, Fall 2016 (oral)
2. "Working towards a solid-state dye sensitized solar cell using vapor phase polymerized PEDOT", 252nd ACS National Meeting, Philadelphia, PA, Fall 2016 (oral)
3. "Design and synthesis of ruthenium-EDOT based coordination polymers for use in inorganic-organic hybrid dye sensitized solar cells" , 250th ACS National Meeting, Boston, MA, Fall 2015 (oral)

4. “Design and Synthesis of Ruthenium Coordination Polymers for use in Dye Sensitized Solar Cells.” DAAD, Leipzig, Germany 2014 (Oral)
5. “Design and Synthesis of Ruthenium Coordination Polymers for use in Dye Sensitized Solar Cells.”, 247th ACS National Meeting Dallas, TX, Spring 2014 (Poster)

## 1.11 References


1. Urmee, T.; Harries, D.; Holtorf, H.-G., *Photovoltaics for Rural Electrification in Developing Countries*. Springer International: Switzerland, 2016.

2. Gratzel, M., Photoelectrochemical cells. *Nature* **2001,** *414* (6861), 338-344.

3. Hagfeldt, A.; Boschloo, G.; Sun, L. C.; Kloo, L.; Pettersson, H., Dye-Sensitized Solar Cells. *Chemical Reviews* **2010,** *110* (11), 6595-6663.

4. O'Regan, B.; Gratzel, M., A low cost, high-efficiency solar-cell based on dye-sensitized collodial $TiO_2$ films. *Nature* **1991,** *353* (6346), 737-740.

5. Gerischer, H.; Tributsch, H., Elektrochemische Untersuchungen zur spektralen Sensibilisierung von ZnO-Einkristallen. *Berichte der Bunsengesellschaft für physikalische Chemie* **1968,** *72* (3), 437-445.

6. Gerischer, H.; Michel-Beyerle, M. E.; Rebentrost, F.; Tributsch, H., Sensitization of charge injection into semiconductors with large band gap. *Electrochimica Acta* **1968,** *13* (6), 1509 - 1515.

7. Hardin, B. E.; Snaith, H. J.; McGehee, M. D., The renaissance of dye-sensitized solar cells. *Nat Photon* **2012,** *6* (3), 162-169.

8. Nagata, T.; Murakami, H., Development of Dye-sensitized Solar Cells. *ULVAC Technical Journal* **2009,** *70*, 1-5.

9. Ardo, S.; Meyer, G. J., Photodriven heterogeneous charge transfer with transition-metal compounds anchored to TiO2 semiconductor surfaces. *Chemical Society Reviews* **2009,** *38* (1), 115-164.

10. Murakoshi, K.; Kano, G.; Wada, Y.; Yanagida, S.; Miyazaki, H.; Matsumoto, M.; Murasawa, S., Importance of binding states between photosensitizing molecules and the $TiO_2$ surface for efficiency in a dye-sensitized solar-cell. *Journal of Electroanalytical Chemistry* **1995,** *396* (1-2), 27-34.

11. Li, J. R.; Nilsing, M.; Kondov, I.; Wang, H. B.; Persson, P.; Lunell, S.; Thoss, M., Dynamical simulation of photoinduced electron transfer reactions in dye-semiconductor systems with different anchor groups. *Journal of Physical Chemistry C* **2008,** *112* (32), 12326-12333.

12. Listorti, A.; O'Regan, B.; Durrant, J. R., Electron Transfer Dynamics in Dye-Sensitized Solar Cells. *Chemistry of Materials* **2011,** *23* (15), 3381-3399.

13. Gillaizeau-Gauthier, I.; Odobel, F.; Alebbi, M.; Argazzi, R.; Costa, E.; Bignozzi, C. A.; Qu, P.; Meyer, G. J., Phosphonate-based bipyridine dyes for stable photovoltaic devices. *Inorganic Chemistry* **2001,** *40* (23), 6073-6079.

14. Odobel, F.; Blart, E.; Lagree, M.; Villieras, M.; Boujtita, H.; El Murr, N.; Caramori, S.; Bignozzi, C. A., Porphyrin dyes for TiO2 sensitization. *Journal of Materials Chemistry* **2003,** *13* (3), 502-510.

15. She, C. X.; Guo, J. C.; Irle, S.; Morokuma, K.; Mohler, D. L.; Zabri, H.; Odobel, F.; Youm, K. T.; Liu, F.; Hupp, J. T.; Lian, T., Comparison of interfacial electron transfer through carboxylate and phosphonate anchoring Groups. *Journal of Physical Chemistry A* **2007,** *111* (29), 6832-6842.

16. Anderson, N. A.; Ai, X.; Chen, D. T.; Mohler, D. L.; Lian, T. Q., Bridge-assisted ultrafast interfacial electron transfer to nanocrystalline SnO2 thin films. *Journal of Physical Chemistry B* **2003,** *107* (51), 14231-14239.

17. Huang, S. Y.; Schlichthorl, G.; Nozik, A. J.; Gratzel, M.; Frank, A. J., Charge recombination in dye-sensitized nanocrystalline TiO2 solar cells. *Journal of Physical Chemistry B* **1997,** *101* (14), 2576-2582.

18. Boschloo, G.; Hagfeldt, A., Characteristics of the Iodide/Triiodide Redox Mediator in Dye-Sensitized Solar Cells. *Accounts of Chemical Research* **2009,** *42* (11), 1819-1826.

19. Bisquert, J.; Fabregat-Santiago, F.; Mora-Sero, I.; Garcia-Belmonte, G.; Gimenez, S., Electron Lifetime in Dye-Sensitized Solar Cells: Theory and Interpretation of Measurements. *Journal of Physical Chemistry C* **2009,** *113* (40), 17278-17290.

20. Antila, L. J.; Myllyperkiö, P.; Mustalahti, S.; Lehtivuori, H.; Korppi-Tommola, J., Injection and Ultrafast Regeneration in Dye-Sensitized Solar Cells. *The Journal of Physical Chemistry C* **2014,** *118* (15), 7772-7780.

21. Nogueira, A. F.; De Paoli, M. A.; Montanari, I.; Monkhouse, R.; Nelson, J.; Durrant, J. R., Electron transfer dynamics in dye sensitized nanocrystalline solar cells using a polymer electrolyte. *Journal of Physical Chemistry B* **2001,** *105* (31), 7517-7524.

22. Jennings, J. R.; Liu, Y. R.; Wang, Q., Efficiency Limitations in Dye-Sensitized Solar Cells Caused by Inefficient Sensitizer Regeneration. *Journal of Physical Chemistry C* **2011,** *115* (30), 15109-15120.

23. Snaith, H. J., Estimating the Maximum Attainable Efficiency in Dye-Sensitized Solar Cells. *Advanced Functional Materials* **2010,** *20* (1), 13-19.

24. Li, B.; Wang, L.; Kang, B.; Wang, P.; Qiu, Y., Review of recent progress in solid-state dye-sensitized solar cells. *Solar Energy Materials and Solar Cells* **2006,** *90* (5), 549 - 573.

25. Tennakone, K.; Senadeera, G. K. R.; De Silva, D.; Kottegoda, I. R. M., Highly stable dye-sensitized solid-state solar cell with the semiconductor 4CuBr 3S(C4H9)(2) as the hole collector. *Applied Physics Letters* **2000,** *77* (15), 2367-2369.

26. Kumara, G.; Konno, A.; Senadeera, G. K. R.; Jayaweera, P. V. V.; De Silva, D.; Tennakone, K., Dye-sensitized solar cell with the hole collector p-CuSCN deposited from a solution in n-propyl sulphide. *Solar Energy Materials and Solar Cells* **2001,** *69* (2), 195-199.

27. Tennakone, K.; Kumara, G.; Kumarasinghe, A. R.; Wijayantha, K. G. U.; Sirimanne, P. M., A dye-sensitized nano-porous solid-state photovoltaic cell. *Semiconductor Science and Technology* **1995,** *10* (12), 1689-1693.

28. Tennakone, K.; Perera, V. P. S.; Kottegoda, I. R. M.; Kumara, G., Dye-sensitized solid state photovoltaic cell based on composite zinc oxide tin (IV) oxide films. *Journal of Physics D-Applied Physics* **1999,** *32* (4), 374-379.

29. Sirimanne, P. M.; Jeranko, T.; Bogdanoff, P.; Fiechter, S.; Tributsch, H., On the photo-degradation of dye sensitized solid-state TiO2-dye-CuI cells. *Semiconductor Science and Technology* **2003,** *18* (7), 708-712.

30. Perera, V. P. S.; Tennakone, K., Recombination processes in dye-sensitized solid-state solar cells with CuI as the hole collector. *Solar Energy Materials and Solar Cells* **2003,** *79* (2), 249-255.

31. Kumara, G. R. A.; Kaneko, S.; Okuya, M.; Tennakone, K., Fabrication of dye-sensitized solar cells using triethylamine hydrothiocyanate as a CuI crystal growth inhibitor. *Langmuir* **2002,** *18* (26), 10493-10495.

32. Bach, U.; Lupo, D.; Comte, P.; Moser, J. E.; Weissortel, F.; Salbeck, J.; Spreitzer, H.; Gratzel, M., Solid-state dye-sensitized mesoporous TiO2 solar cells with high photon-to-electron conversion efficiencies. *Nature* **1998,** *395* (6702), 583-585.

33. Docampo, P.; Guldin, S.; Leijtens, T.; Noel, N. K.; Steiner, U.; Snaith, H. J., Lessons Learned: From Dye-Sensitized Solar Cells to All-Solid-State Hybrid Devices. *Advanced Materials* **2014,** *26* (24), 4013-4030.

34. Poplavskyy, D.; Nelson, J., Nondispersive hole transport in amorphous films of methoxy-spirofluorene-arylamine organic compound. *Journal of Applied Physics* **2003,** *93* (1), 341-346.

35. Abate, A.; Leijtens, T.; Pathak, S.; Teuscher, J.; Avolio, R.; Errico, M. E.; Kirkpatrik, J.; Ball, J. M.; Docampo, P.; McPherson, I.; Snaith, H. J., Lithium salts as "redox active" p-type dopants for organic semiconductors and their impact in solid-state dye-sensitized solar cells. *Physical Chemistry Chemical Physics* **2013,** *15* (7), 2572-2579.

36. Martin, D. C.; Wu, J. H.; Shaw, C. M.; King, Z.; Spanninga, S. A.; Richardson-Burns, S.; Hendricks, J.; Yang, J. Y., The Morphology of Poly(3,4-Ethylenedioxythiophene). *Polymer Reviews* **2010,** *50* (3), 340-384.

37. Zhang, J. B.; Vlachopoulos, N.; Jouini, M.; Johansson, M. B.; Zhang, X. L.; Nazeeruddin, M. K.; Boschloo, G.; Johansson, E. M. J.; Hagfeldt, A., Efficient solid-state dye sensitized solar cells: The influence of dye molecular structures for the in-situ photoelectrochemically polymerized PEDOT as hole transporting material. *Nano Energy* **2016,** *19*, 455-470.

38. Fukuri, N.; Masaki, N.; Kitamura, T.; Wada, Y.; Yanagida, S., Electron transport analysis for improvement of solid-state dye-sensitized solar cells using poly(3,4-ethylenedioxythiophene) as hole conductors. *Journal of Physical Chemistry B* **2006,** *110* (50), 25251-25258.

39. Xia, J. B.; Masaki, N.; Lira-Cantu, M.; Kim, Y.; Jiang, K. J.; Yanagida, S., Influence of doped anions on poly(3,4-ethylenedioxythiophene) as hole conductors for iodine-free solid-state dye-sensitized solar cells. *Journal of the American Chemical Society* **2008,** *130* (4), 1258-1263.

40. Zhang, J. B.; Jarboui, A.; Vlachopoulos, N.; Jouini, M.; Boschloo, G.; Hagfeldt, A., Photoelectrochemical Polymerization of EDOT for Solid State Dye Sensitized Solar Cells: Role of Dye and Solvent. *Electrochimica Acta* **2015,** *179*, 220-227.

41. Saito, Y.; Kitamura, T.; Wada, Y.; Yanagida, S., Poly(3,4-ethylenedioxythiophene) as a hole conductor in solid state dye sensitized solar cells. *Synthetic Metals* **2002,** *131* (1-3), 185-187.

42. Kim, J.; Koh, J. K.; Kim, B.; Ahn, S. H.; Ahn, H.; Ryu, D. Y.; Kim, J. H.; Kim, E., Enhanced Performance of I2-Free Solid-State Dye-Sensitized Solar Cells with Conductive Polymer up to 6.8%. *Advanced Functional Materials* **2011,** *21* (24), 4633-4639.

43. Shi, W.; Zhao, T. Q.; Xi, J. Y.; Wang, D.; Shuai, Z. G., Unravelling Doping Effects on PEDOT at the Molecular Level: From Geometry to Thermoelectric Transport Properties. *Journal of the American Chemical Society* **2015,** *137* (40), 12929-12938.

44. Skorenko, K. H.; Faucett, A. C.; Liu, J.; Ravvin, N. A.; Bernier, W. E.; Mativetsky, J. M.; Jones Jr, W. E., Vapor phase polymerization and mechanical testing of highly electrically conductive poly(3,4-ethylenedioxythiophene) for flexible devices. *Synthetic Metals* **2015,** *209*, 297 - 303.

45. Im, S. G.; Gleason, K. K., Systematic control of the electrical conductivity of poly(3,4-ethylenedioxythiophene) via oxidative chemical vapor deposition. *Macromolecules* **2007,** *40* (18), 6552-6556.

46. Madl, C. M.; Kariuki, P. N.; Gendron, J.; Piper, L. F. J.; Jones, W. E., Vapor phase polymerization of poly (3,4-ethylenedioxythiophene) on flexible substrates for enhanced transparent electrodes. *Synthetic Metals* **2011,** *161* (13-14), 1159-1165.

47. Cho, M. S.; Kim, S. Y.; Nam, J. D.; Lee, Y., Preparation of PEDOT/Cu composite film by in situ redox reaction between EDOT and copper(II) chloride. *Synthetic Metals* **2008,** *158* (21-24), 865-869.

48. Metsik, J.; Saal, K.; Maeorg, U.; Lohmus, R.; Leinberg, S.; Mandar, H.; Kodu, M.; Timusk, M., Growth of Poly(3,4-ethylenedioxythiophene)Films Prepared by Base-Inhibited Vapor Phase Polymerization. *Journal of Polymer Science Part B-Polymer Physics* **2014,** *52* (8), 561-571.

49. Winther-Jensen, B.; Forsyth, M.; West, K.; Andreasen, J. W.; Bayley, P.; Pas, S.; MacFarlane, D. R., Order-disorder transitions in poly(3,4-ethylenedioxythiophene). *Polymer* **2008,** *49* (2), 481-487.

50. Cho, B.; Park, K. S.; Baek, J.; Oh, H. S.; Lee, Y. E. K.; Sung, M. M., Single-Crystal Poly(3,4-ethylenedioxythiophene) Nanowires with Ultrahigh Conductivity. *Nano Letters* **2014,** *14* (6), 3321-3327.

51. Murakoshi, K.; Kogure, R.; Wada, Y.; Yanagida, S., Fabrication of solid-state dye-sensitized TiO2 solar cells combined with polypyrrole. *Solar Energy Materials and Solar Cells* **1998,** *55* (1–2), 113 - 125.

52. Wu, J.; Lan, Z.; Lin, J.; Huang, M.; Huang, Y.; Fan, L.; Luo, G., Electrolytes in Dye-Sensitized Solar Cells. *Chemical Reviews* **2015,** *115* (5), 2136-2173.

53. Yang, L.; Cappel, U. B.; Unger, E. L.; Karlsson, M.; Karlsson, K. M.; Gabrielsson, E.; Sun, L. C.; Boschloo, G.; Hagfeldt, A.; Johansson, E. M. J., Comparing spiro-OMeTAD and P3HT hole conductors in efficient solid state dye-sensitized solar cells. *Physical Chemistry Chemical Physics* **2012,** *14* (2), 779-789.

54. Yanagida, S.; Yu, Y. H.; Manseki, K., Iodine/Iodide-Free Dye-Sensitized Solar Cells. *Accounts of Chemical Research* **2009,** *42* (11), 1827-1838.

55. Grancini, G.; Kumar, R. S. S.; Abrusci, A.; Yip, H. L.; Li, C. Z.; Jen, A. K. Y.; Lanzani, G.; Snaith, H. J., Boosting Infrared Light Harvesting by Molecular Functionalization of Metal Oxide/Polymer Interfaces in Efficient Hybrid Solar Cells. *Advanced Functional Materials* **2012,** *22* (10), 2160-2166.

56. Skorenko, K. H. Fabrication of solid state dye sensitized solar cells utilizing vapor phase polymerized poly (3,4-ethylenedioxythiopene) hole conducting layer. Binghamton Univeristy, State University of New York at Binghamton, Department of Chemistry, 2015.

57. Spiekermann, S.; Smestad, G.; Kowalik, J.; Tolbert, L. M.; Gratzel, M., Poly(4-undecyl-2,2 '-bithiophene) as a hole conductor in solid state dye sensitized titanium dioxide solar cells. *Synthetic Metals* **2001,** *121* (1-3), 1603-1604.

58. Li, J.; Osasa, T.; Hirayama, Y.; Sano, T.; Wakisaka, K.; Matsumura, M., Solid-state dye-sensitized solar cells using poly 2-methoxy-5-(2-ethylhexyloxy)-1,4-phenylene-vinylene as a hole-transporting material. *Japanese Journal of Applied Physics Part 1-Regular Papers Brief Communications & Review Papers* **2006,** *45* (11), 8728-8732.

59. Chen, X.; Mao, S. S., Titanium dioxide nanomaterials: Synthesis, properties, modifications, and applications. *Chemical Reviews* **2007,** *107* (7), 2891-2959.

60. Teh, C. M.; Mohamed, A. R., Roles of titanium dioxide and ion-doped titanium dioxide on photocatalytic degradation of organic pollutants (phenolic compounds and dyes) in aqueous solutions: A review. *Journal of Alloys and Compounds* **2011,** *509* (5), 1648-1660.

61. Park, H.; Park, Y.; Kim, W.; Choi, W., Surface modification of TiO2 photocatalyst for environmental applications. *Journal of Photochemistry and Photobiology C-Photochemistry Reviews* **2013,** *15*, 1-20.

# Chapter 2

## Investigation of Vapor Phase Polymerized Poly(3,4-Ethylene Dioxythiophene) as a Hole Transport Layer is a Solid State Dye Sensitized Solar Cell

### 2.1 Introduction

Dye sensitized solar cells (DSSCs) have gained interest for their high efficiency, simple fabrication and low cost of production.[1] [2] [3] Commonly, DSSCs use a liquid electrolyte as the p-type material or hole transport material to regenerate the dye molecule following electron injection. The liquid electrolyte allows for penetration of the mesoporous $TiO_2$ layer, providing a close interaction with the adsorbed dye.[3, 4] Liquid-phase DSSCs have the highest reported efficiencies for DSSCs, but are known to be relatively unstable. The electrolyte is known to leak, evaporate, or corrode the electrode, reducing the longevity of the solar cell.[3] In addition to the stability concerns, the liquid phase may play a role in limiting the efficiency. With a liquid electrolyte, the regeneration of the dye is limited by the rate of diffusion of iodide and triiodide, making it the slow step in the process as shown in Figure 2-1.[5] [6] In addition to the slow rate of diffusion, the electron transfer for the redox reactions involving the electrolyte solution is several orders of magnitude slower than the rate of electron injection into the $TiO_2$.[5, 6]

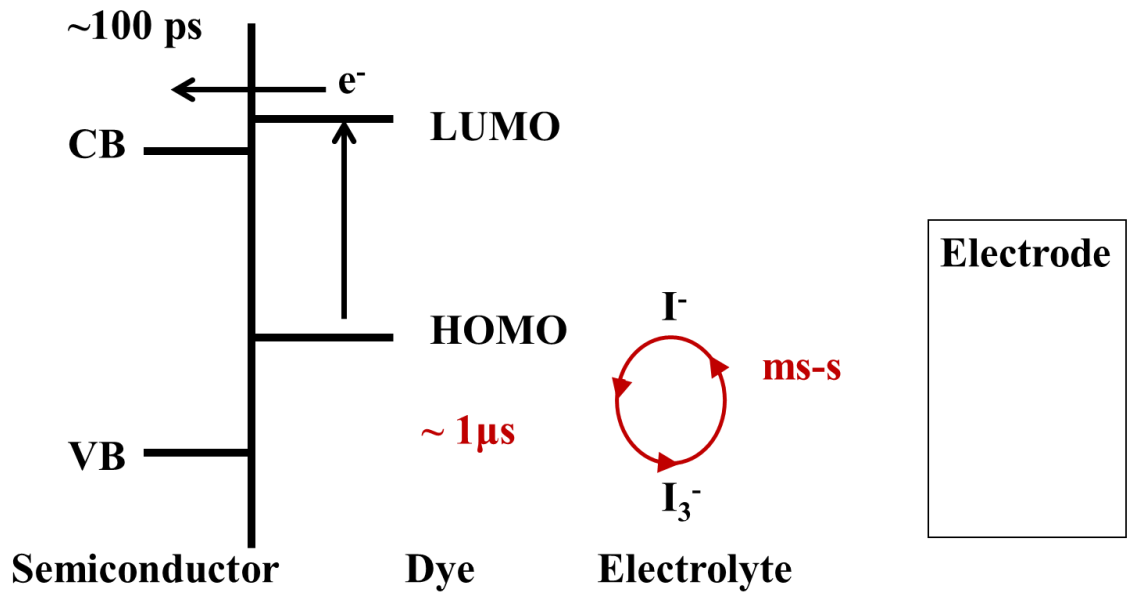


Figure 2-1: Rate of electron injection from dye and regeneration of the dye from a liquid electrolyte (modified from Ref. 5).

An alternative to liquid phase DSSCs is the solid-state dye sensitized solar cell (ssDSSC). Using a solid electrolyte can make the solar cell more stable and provide a faster electron transfer using a hopping or tunneling mechanism instead of diffusion.[7] To date ssDSSCs have shown lower efficiencies than their liquid counterparts, however. The lower efficiencies can be attributed to the challenges of producing a solid state material that is highly conductive, penetrates into the mesoporous layer, mild processing conditions and is transparent in the visible region of the spectrum.[8] There are several materials that have been used as a solid HTL including inorganic, organic, molecular and polymeric materials each having their advantages and disadvantages.[8 3 9 7] One of the challenges is having a solid material that can fill the mesoporous semiconducting layer.[8] One method to overcome this challenge is the use of an in-situ polymerization of a conducting polymer.

Poly(3,4-ethylenedioxythiophene (PEDOT), shown in Figure 2-2, is a material that has been explored as a HTL. PEDOT is a conjugated polymer that is chemically stable and

a known hole-conductor, but is insoluble.[10] To process PEDOT, it can be copolymerized with Poly(3,4-ethylenedioxythiophene polystyrene sulfonate (PEDOT:PSS) that is water solution allowing for solution processing.[10] In addition to PSS making the polymer soluble, it also reduces the conductivity since it is an insulating material. PEDOT:PSS has been explored as a HTL however it lacks the ability to fill the nano pores in the $TiO_2$ layer.[7] This can limit the amount of active dye in the solar cell which decreases the efficiency of the solar cell. An alternative to PEDOT:PSS is using an *in situ* polymerization to grow the PEDOT within the $TiO_2$ layer, increasing the interaction with the dye molecules compared to PEDOT:PSS.

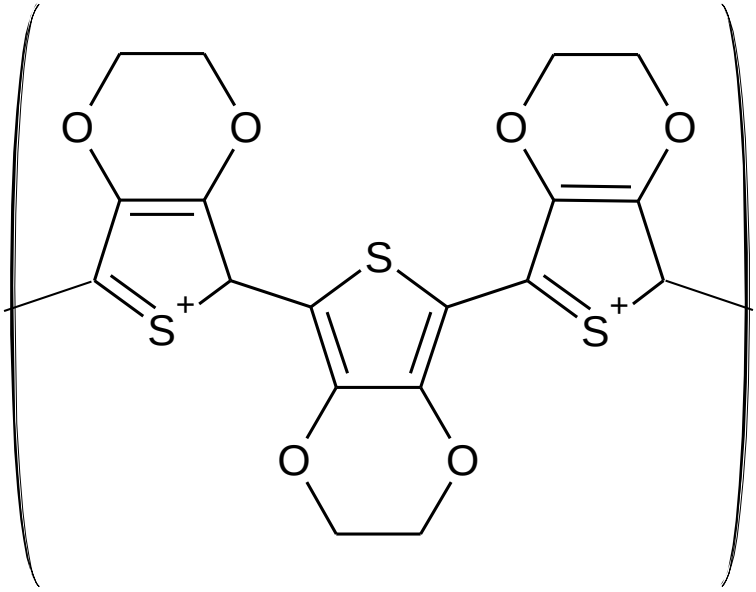


Figure 2-2: Structure of PEDOT in the doped state.

There are several mechanisms of EDOT polymerization that are considered *in situ* methods. These methods include chemical vapor-deposition (CVD), electrochemical deposition, oxidant initiated *in situ* and vapor phase polymerization (VPP).[10] An oxidant initiated *in situ* method was reported, but the best performance was 0.012% after post polymerization treatment.[11] The low efficiency was attributed to a poor contact between

the dye and HTL however it is also possible the PEDOT had low conductivity. The oxidant initiated method has some of the lowest reported conductivities in the literature because of the poor crystallinity and short polymer length. To have a more efficient solar cell it is important to use methods that produce highly conductive PEDOT. A more promising method uses a photoelectrochemical polymerization (PEP).[12 13 14 15 16 17 18 19 20] After using post-polymerization treatment and optimizing the energy overlap of the dye and PEDOT, these ssDSSCs have exceeded 7% efficiency which is approaching the record for the liquid phase DSSCs.

While an electrochemical deposition has been developed for ssDSSCs, there have been no reports of a VPP method. VPP heats the monomer into the gas phase and uses an oxidant to initiate the polymerization as shown in Figure 2-3. VPP PEDOT has been shown to have the highest order and crystallinity in forming PEDOT thin films without post processing treatments.[10] These properties are desirable to have a highly conductive PEDOT layer. The higher ordering can potentially lead to more efficient solar cells by decreasing the defects and trap sites in the HTL.[21] VPP PEDOT films have been reported to have conductivities greater than 1000 S/cm with transparency greater than 90% in the visible region.[10] The reaction conditions for VPP uses low temperature processing that should not degrade the dye. Based on the mild conditions, high conductivities and transparencies, VPP PEDOT could be an important material for the advancement of the ssDSSC.

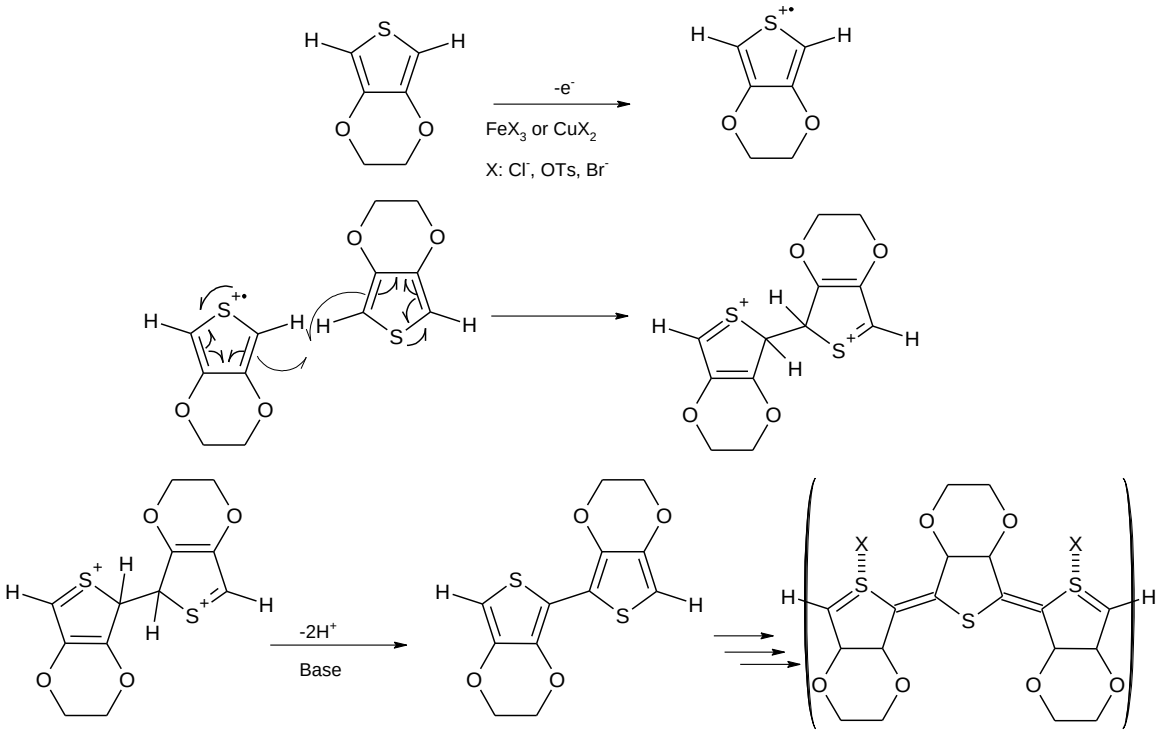


Figure 2-3: Mechanism for the vapor phase polymerization of PEDOT using an oxidant as an initiator.

Previous work in the group has focused on the development of procedures to produce highly conductive, transparent VPP PEDOT thin films. It was found that iron(III) p-toluenesulfonate (FePTs) was the best oxidant, producing films with conductivities exceeding 1000 S/cm.[22] The VPP PEDOT procedure was used to fabricate ssDSSCs but the efficiencies were 0%. X-ray photoelectron spectroscopy (XPS) showed FePTs could reduce the titanium in the mesoporous layer. Even after switching to copper (II) chloride, efficiencies did not improve.[23] It was proposed the indium tin oxide (ITO) on the poly(ethylene terephthalate) (PET) substrate would crack upon flexing during fabrication, decreasing the conductivity of the electrode. This chapter focuses on the fabrication of ssDSSCs using VPP PEDOT as a HTL using a glass substrate.

## 2.2 Experimental

### 2.2.1 Materials and Methods

Glass coated with 10 Ω FTO was purchased from Pilkington Group Limited. $TiO_2$ nanoparticles, 75% wt. titanium diisopropoxide bis(acetylacetonoate), $TiO_2$ paste, N3 dye, EDOT, terpineol ethylcellulose, and $Fe(PTS)_3$ were purchased from Sigma-Aldrich. Isopropanol and pyridine were purchase from Fisher. $CuCl_2$ was purchase from J.T. Baker. 200 proof ethanol was purchased from KOPTEC. Clevios™ SV3 PEDOT:PSS was purchased from Heraeus Kulzer. Gold shots were purchased from Kurt J. Lesker.

### 2.2.2 General Methods

For characterization methods, a Titan Solar Simulator was used for producing IV curves, along with obtaining resistances, fill factors, and efficiencies. FESEM Supra 55 VP from Zeiss was used for characterizing thicknesses of layers of the solar cells and qualitatively investigating the structure of the cells. The CHA Evaporator was used to evaporate gold.

### 2.2.3 Preparation of Substrate

Float glass was cut into pieces approximately 2 cm x 2 cm. ITO was sputtered onto the substrates giving a thickness of approximately 120 nm. Following the ITO deposition, a blocking layer of ZnO was sputtered, giving a thickness of approximately 70 nm.

FTO coated glass was cleaned using soap, rinsed with DI water before being sonicated in acetone followed by ethanol. The substrates were then treated with ozone for 6 minutes to help with adhesion of the $TiO_2$ blocking layer. 75% weight percent titanium

diisopropoxide bis(acetylacetonoate) was diluted to 50 mM with isopropanol by combining 1 mL titanium diisopropoxide bis(acetylacetonoate) to 41.2 isopropanol. The solution was left to stir until adequately dispersed.[24] FTO sputtered substrates were placed on a hot plate and about 0.5 cm of the top of the glass was covered with masks to allow contact with the anode. The hotplate was set to 450°C and the samples were allowed to heat up for 10 minutes to reach the setting temperature. Samples were sprayed at a rate of 0.318 mL/s using dry air at 15 psi. This was done at 5 second bursts while waiting 30 seconds to repeat each time. A total of 45 seconds of active spraying was performed to produce a thickness of about 70 nm. The samples were annealed for 30 minutes at this temperature, followed by cooling to room temperature.[24]

### 2.2.4 Preparation of Mesoprous$TiO_2$ Layer

The $TiO_2$ paste prepared for doctor blading contained all of: $TiO_2$ nanoparticles, oxidant (either $Fe(PTS)_3$ and pyridine, or $CuCl_2$), and N3 dye. Into a 20 mL glass vial, 1.0 g of $TiO_2$ nanoparticles (MW=79.866 g/mol), and 0.0028 g N3 dye (MW=705.641 g/mol) were added, followed by 10 ml isopropanol. Depending on the oxidant used, 0.949g $Fe(PTS)_3$ (MW=677.51 g/mol) and 60 µL pyridine, or 0.2367g $CuCl_2$ (MW= 134.45 g/mol) were also added. The vial was wrapped in aluminum foil and left stirring for 24 hours.

Approximately 0.5 cm of the ITO/ZnO sputtered substrate was masked with tape and placed on a flat surface. The doctor blade was set to the desired height and a glass pipet was used to drop the $TiO_2$ paste onto the substrate, covering the entire substrate with the mixture. The doctor blade was then used to scrape off excess $TiO_2$ mixture as shown in

Figure 5 below and set in a vacuum oven at 100°C for 10 minutes to dry. The resulting thickness was 4-60 μm depending on height of doctor blade used.

3.0 g of $TiO_2$ paste, 3.802 mL ethanol, 114 μL terpinol, and 114 μL ethylcellulose solution (10 percent weight in ethanol) were combined, sonicated, and put under heat to achieve a homogenous mixture. The ratio of $TiO_2$ to ethanol can be changed to produce different viscosities and therefore different thicknesses when depositing the layer. The solution was sonicated using an ultra-sonication bath for 10 minutes before spin coating to reduce aggregation of the nanoparticles.[24]

The FTO was masked with tape to allow for contact to the anode and the substrate was centered on the spinning block. Approximately 100 μL of the paste from 3.4 was dropped onto the glass. Using a 2 step process, the substrates were spun at 600 rpm for 20 seconds with an acceleration of 480 rpm/s, followed by 1500 rpm for 6 seconds at an acceleration of 810 rpm/s. The spin speeds can also be altered to achieve different thicknesses of thin films. The tape was removed and the substrates were heating using the follow temperature program: 100°C for 10 minutes, 150°C for 10 minutes, 325°C for 30 minutes, 450°C for 5 minutes, and 500°C for 40 minutes.[24] After the substrates had cooled to room temperature, they were placed standing up vertically in a beaker containing 25 mL of $1.4x10^{-4}$M N3 dye in ethanol. The beaker was wrapped in Parafilm M® and aluminum foil to prevent evaporation of the solvent and degradation of the dye. The substrates were allowed to soak for 24 hours before removal and to dry at 100°C for 10 minutes.

### 2.2.5 Vapor Phase Polymerization of PEDOT

For films prepared via Dr. Blading, the oxidant was preloaded in the solution applied to the substrate while the spin-coated $TiO_2$ needed to have an oxidant added. A solution of $CuCl_2$ or FePTs was prepared by adding 0.2367g $CuCl_2$ or 0.600 g FePTs to 10 ml isopropanol (60 µL of pyridine was added to the FePTs solution). This was allowed to stir until all solids dissolved. The substrate was then placed on the spin coater and masked at the top. A glass pipet was used to apply oxidant, covering the entire surface of the substrate, and the spin coater was then run at 720 rpm for 10 seconds. The substrates were removed and allowed to dry in a vacuum oven for 10 minutes at 100°C.

For the VPP process, 100 µL of EDOT was placed in the center of the petri dish inside a vacuum desiccator oven. The substrate was then suspended over the monomer at 55°C as shown in Figure 2-4. The polymerization was performed for 40 minutes, and upon removal the cells were rinsed with ethanol to remove excess oxidant. The cells were dried in an oven for 10 minutes at 100°C.

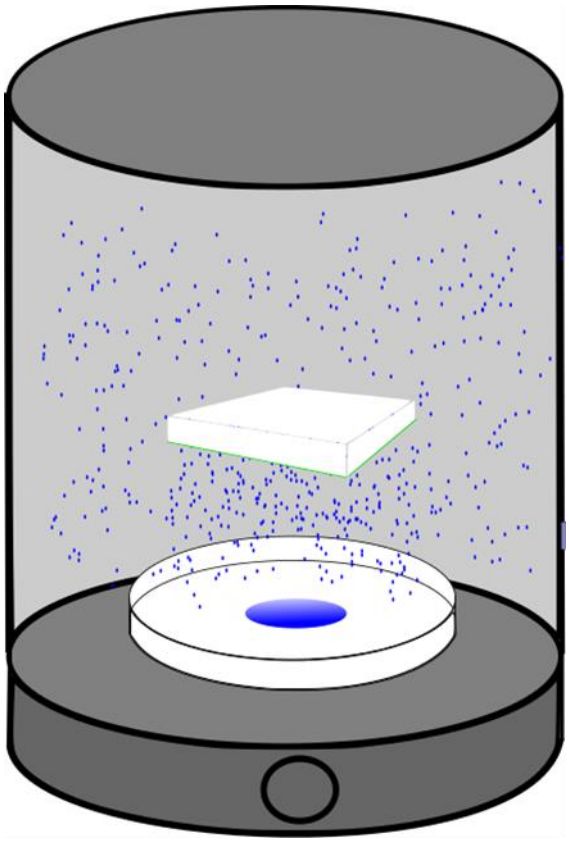

Figure 2-4 Schematic showing the EDOT monomer heated to the gas phase in an oven desiccator with an oxidant coated substrate suspended above the dish.

### 2.2.6 Application of PEDOT:PSS Layer

A solution of PEDOT:PSS was prepared by adding 5 mL PEDOT:PSS to 5 mL isopropanol and stirring for 1 hour. The solution was then applied using the spin coating method at varied RPMs depending on the desired thickness. The cells were removed and dried for 10 minutes at 100°C using an oven.

### 2.2.7 Counter Electrode Deposition

For solar cells with a silver electrode, the Magnetron Sputtering System from Torr International with a silver target was used to produce a 130 nm thick film of silver.

When gold was used as a counter electrode, a shadow mask was used to apply a 2 x 2 mm gold electrode using an evaporation method. The gold electrode thickness ranged from 65-80 nm.

## 2.3 Results and Discussion

### 2.3.1 Solar Cells Using Dr. Blade Method

Solar cells were prepared using the general experimental procedure listed above. The final stack for the first generation of solar cells use glass as a substrate with an ITO transparent conducting electrode (TCE), ZnO blocking layer, mesoporous $TiO_2$ layer, mono layer of N3 dye, VPP PEDOT and silver counter electrode as shown in Figure 2-5.

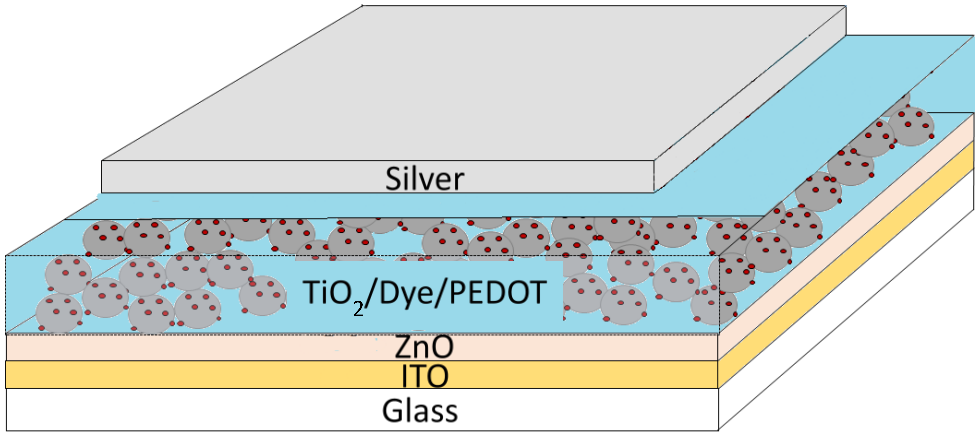


Figure 2-5: The stack of layers used in the doctor blade method of fabricating DSSCs.

Before the procedure in the experimental section for the preparation of mesoporous $TiO_2$ layer was used, others were attempted. When a $TiO_2$ nanoparticle solution was applied without the oxidant present, the film contained visible defects and had poor adhesion to the substrate. The image in Figure 2-6 using optical microscopy for characterization shows the large pin holes and defects of the $TiO_2$ layer. The presence of

defects was found to increase the shorting in the solar cell which might reduce the overall efficiency. To improve the uniformity of the $TiO_2$ layer, the oxidant was added to the solution. The films produced were more uniform so this method was used for the following experiments.

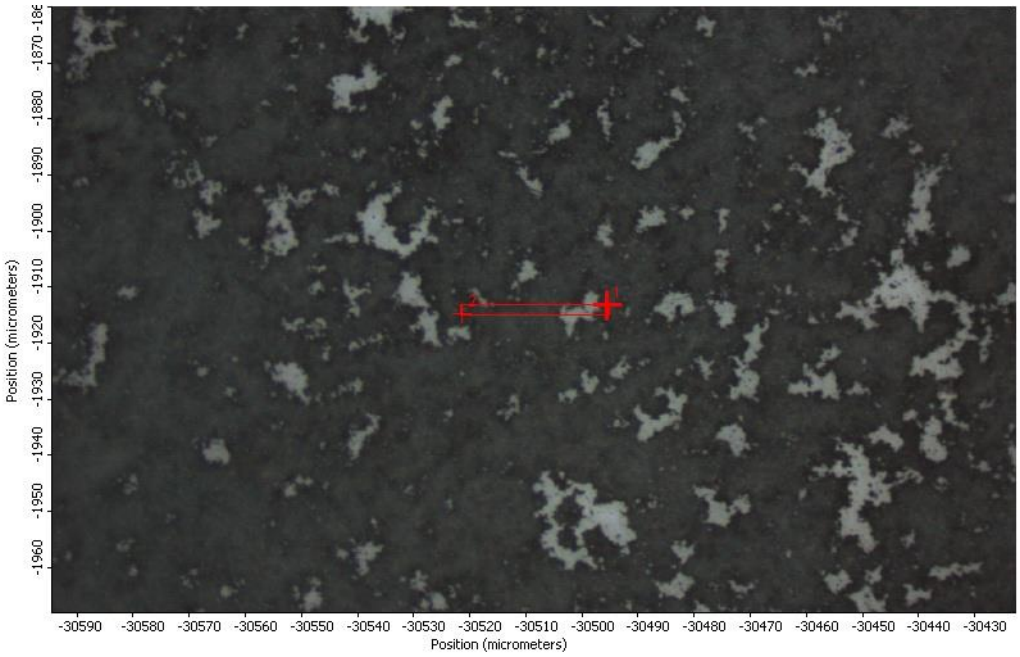


Figure 2-6: Image from optical microcopy of the $TiO_2$ layer produced from doctor blading a solution without oxidant.

The IV curve and relevant data for the solar cell with $TiO_2$ prepared by the doctor blade method shown in Figure 2-7. The overall efficiency of the cell was 0.24% even with a relatively low fill factor of 0.242. The low fill factor is a result of the series resistance being on the kΩ scale, reducing the $I_{sc.}$ The series resistance can be improved by improving the conductivity of the PEDOT or by decreasing the thickness of the $TiO_2$ layer.

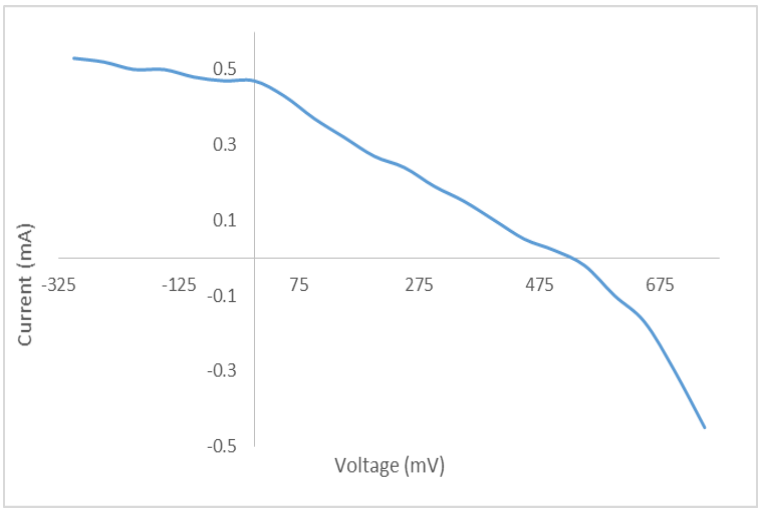


| | | |
|---|---|---|
| $V_{oc}$ | 0.524 | (V) |
| $I_{Sc}$ | 472.80 | (μA) |
| FF | 0.242 | |
| η | 0.24 | (%) |
| $R_s$ | 1.10 | (kΩ) |
| $R_{sh}$ | 7.21 | (kΩ) |

Figure 2-7*:* IV Curve for cell 5 with $CuCl_2$ as the oxidant, along with the parameters

SEM of the cross section for the solar cell above is shown in Figure 2-8. From the SEM image, the thickness of the $TiO_2$ layer was determined to be 56 μm. The average DSSC in the literature uses a thickness of 8-10 μm. A thicker layer provides a longer pathway for electrons to travel before reaching the electrode. This would explain the large series resistance which causes the low fill factor observed. To improve the solar cell efficiency a thinner mesoporous layer is needed. This can be achieved by decreasing the height of the blade for doctor blade method.

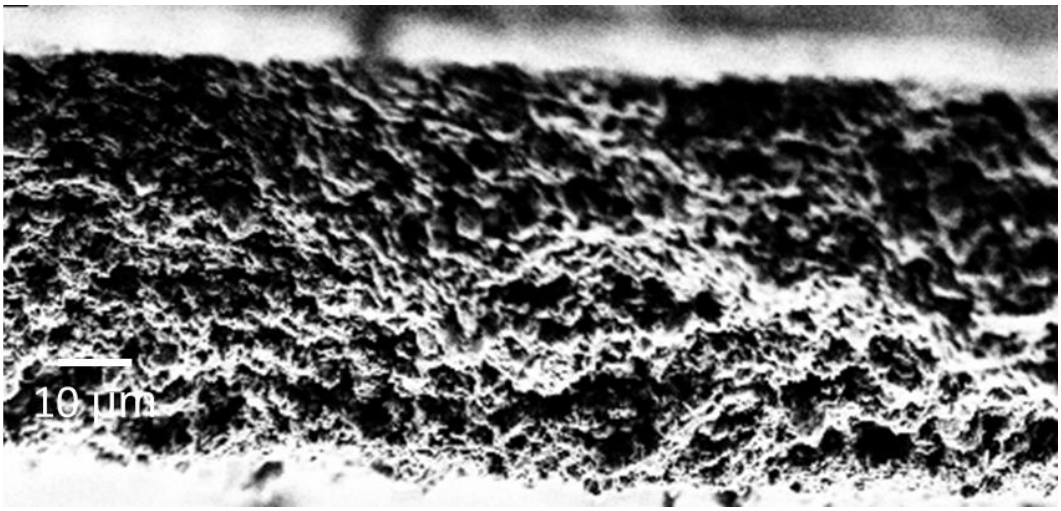


Figure 2-8: SEM image of the above cell 5, showing thickness and structure

A series of solar cells were fabricated, systematically decreasing the height of the blade for the doctor blade method with films ranging from 56-4.4 µm based on SEM cross sections. The data from IV curves based on the $TiO_2$ thicknesses is shown in Table 2-1. The results show the optimal thickness of the $TiO_2$ layer was 14.3 µm. This produced the largest $V_{oc}$ and $I_{sc}$ of the thicknesses studied. The films were thin enough to allow electron transport through the $TiO_2$ without being too thin to limit dye loading. None of the solar cells were able to be reproduced, including the 0.24% from earlier. To better understand this, SEM images were taken of the cross-sections of the solar cells.

Table 2-1: Results from IV curves when changing the thickness of the $TiO_2$ layer.

| | **4.4µm thick $TiO_2$** | | **7.6µm thick $TiO_2$** | | **9.2µm thick $TiO_2$** | | **14.3µm thick $TiO_2$** | |
|---|---|---|---|---|---|---|---|---|
| | **Avg** | **SD** | **Avg** | **SD** | **Avg** | **SD** | **Avg** | **SD** |
| Voc (V) | 0.0009 | 0.0007 | 0.0342 | 0.0224 | 0.0254 | 0.0158 | 0.3779 | 0.1806 |
| Isc (µA) | 2.09 | 2.27 | 2.46 | 0.48 | 2.39 | 1.63 | 3.07 | 0.21 |
| FF | 0.081 | 0.125 | 0.306 | 0.059 | 0.172 | 0.120 | 0.392 | 0.051 |
| Rs (kΩ) | 0.38 | 0.23 | 11 | 6 | 8 | 5 | 51 | 9 |
| Rsh (kΩ) | 0.37 | 0.23 | 13 | 9 | 7 | 4 | 178 | 124 |
| | **23µm thick $TiO_2$** | | **36µm thick $TiO_2$** | | **40µm thick $TiO_2$** | | **52µm thick $TiO_2$** | |
| | **Avg** | **SD** | **Avg** | **SD** | **Avg** | **SD** | **Avg** | **SD** |
| Voc (V) | 0.0487 | 0.0494 | 0.0534 | 0.0436 | 0.0006 | 0.0004 | 0.1694 | 0.2118 |
| Isc (µA) | 2.19 | 1.02 | 2.28 | 1.02 | 2.65 | 1.24 | 2.83 | 0.31 |
| FF | 0.381 | 0.131 | 0.249 | 0.142 | 0.028 | 0.040 | 0.334 | 0.070 |
| Rs (kΩ) | 13 | 12 | 15 | 12 | 253 | 156 | 24 | 18 |
| Rsh (kΩ) | 19 | 21 | 53 | 91 | 248 | 149 | 16 | 8 |

From the SEM images in Figure 2-9, it was observed as the films became thinner, the uniformity also decreased. When the $TiO_2$ layer was 36 and 40 µm thick as shown in Figure 2-7 e and f respectively, the films appeared to be continuous. The thickness of these films though would slow down the transfer of the electron from the n-type material to the

electrode based on the long path length. Decreasing the thickness of the $TiO_2$ layer would result in a shorter pathway however the films produced this way became less uniform resulting in more defects. Increasing the number of defects presented more opportunities for shorting in the solar cell which was likely the cause of the low efficiencies. Although the reproducibility of the solar cells was poor, there was evidence to suggest VPP PEDOT can be used as a HTL. The limitation of the solar cells produced was the mesoporous $TiO_2$ which led to using a spin coating method for the application of the $TiO_2$ layer.

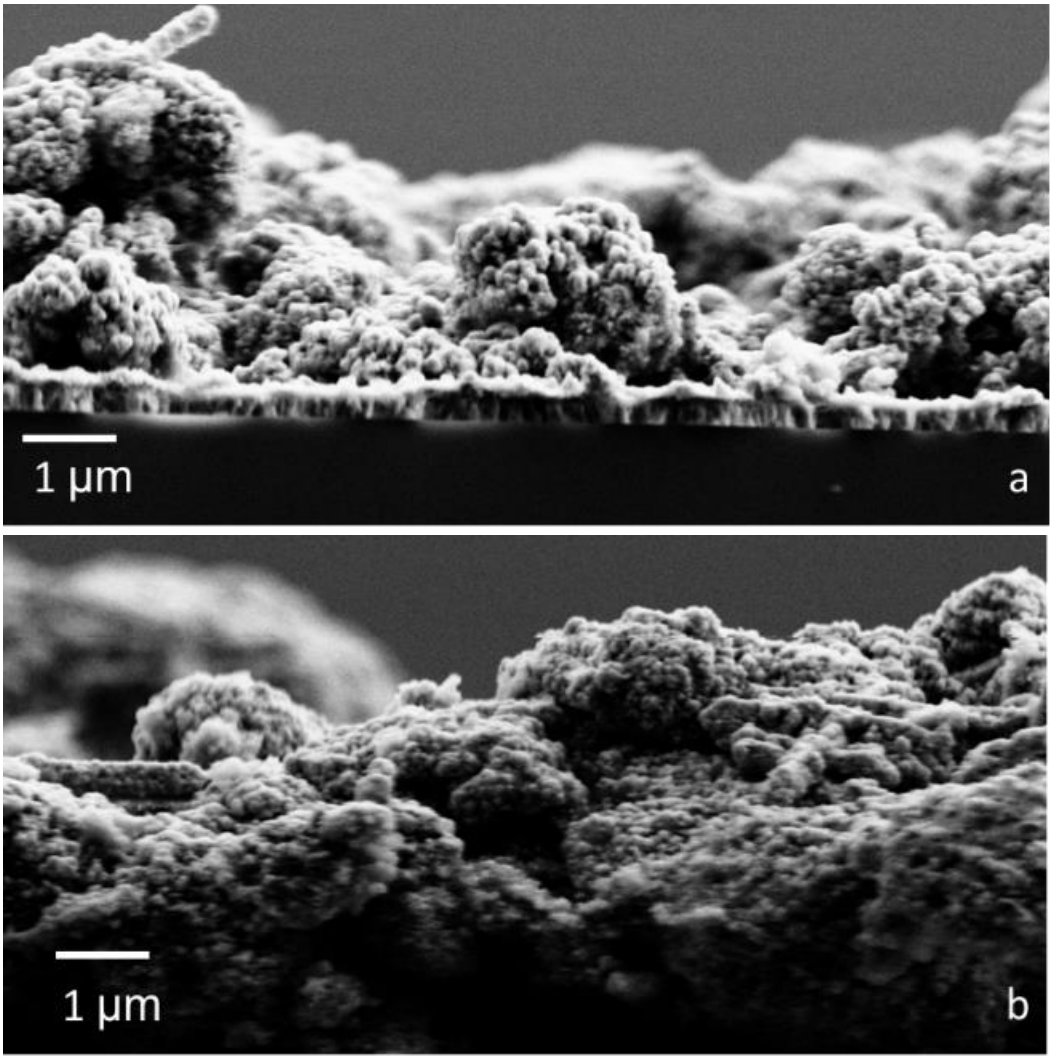

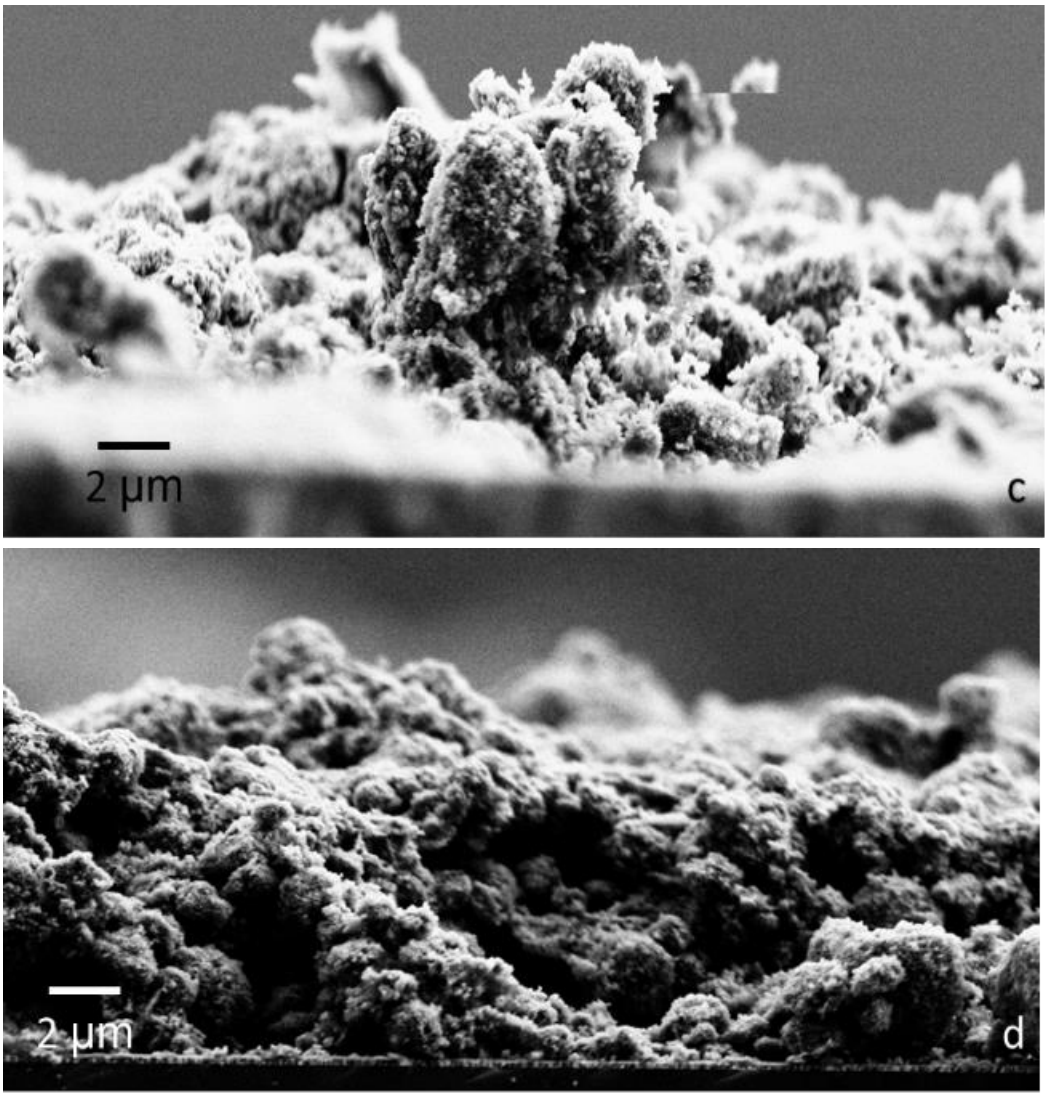
2 µm
c
2 µm
d

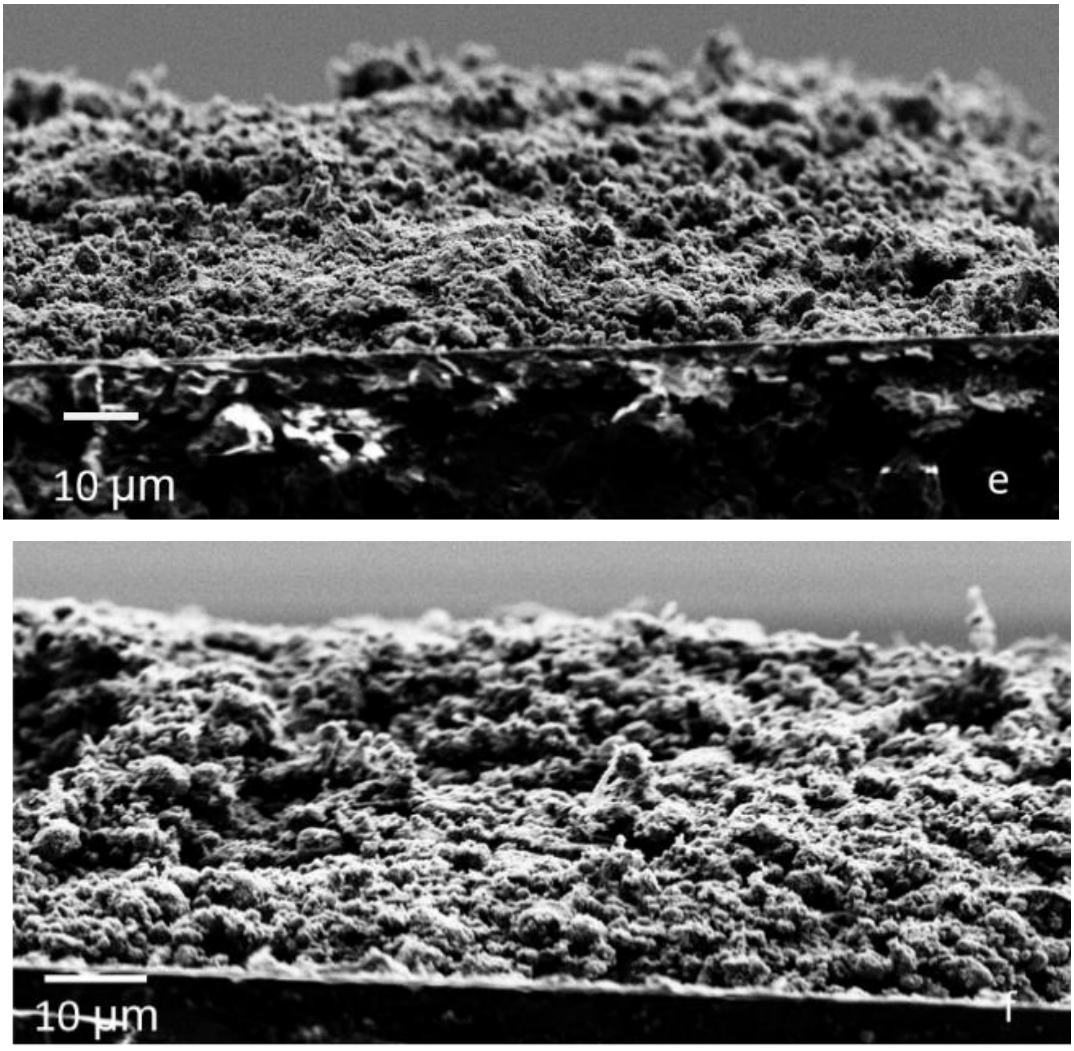


Figure 2-9: SEM images of the cross section for ssDSSCs with $TiO_2$ thickness of a) 4.4 µm b) 7.6 µm c) 9.2 µm d) 14.3 µm e) 36 µm f) 40 µm

### 2.3.2 Solar Cells Using the Spin Coating Method

Based on the poor uniformity of the mesoporous layer, a new procedure was needed for the fabrication of the solar cells. This led to the next generation of solar cells produced using a glass substrate with a FTO TCE, $TiO_2$ blocking and mesoporous layer, N3 dye, PEDOT and gold counter electrode. The final stack is shown in Figure 2-10. FTO is known to be more conducting compared to ITO which makes it a better TCE. $TiO_2$ has shown to reduce the rate of recombination when compared to ZnO.[25] The mesoporous $TiO_2$ layer was prepared using a spin coating method which can allow for more uniform

thin films compared to the Dr. Blade method. To improve the connectivity between the nanoparticles, a heating step was added to sinter the $TiO_2$ layer. The counter electrode was switched from sputtered silver to evaporated gold. Evaporation is a milder method of depositing the electrode than silver which can reduce the penetration of the electrode into the solar cell causing shorting.

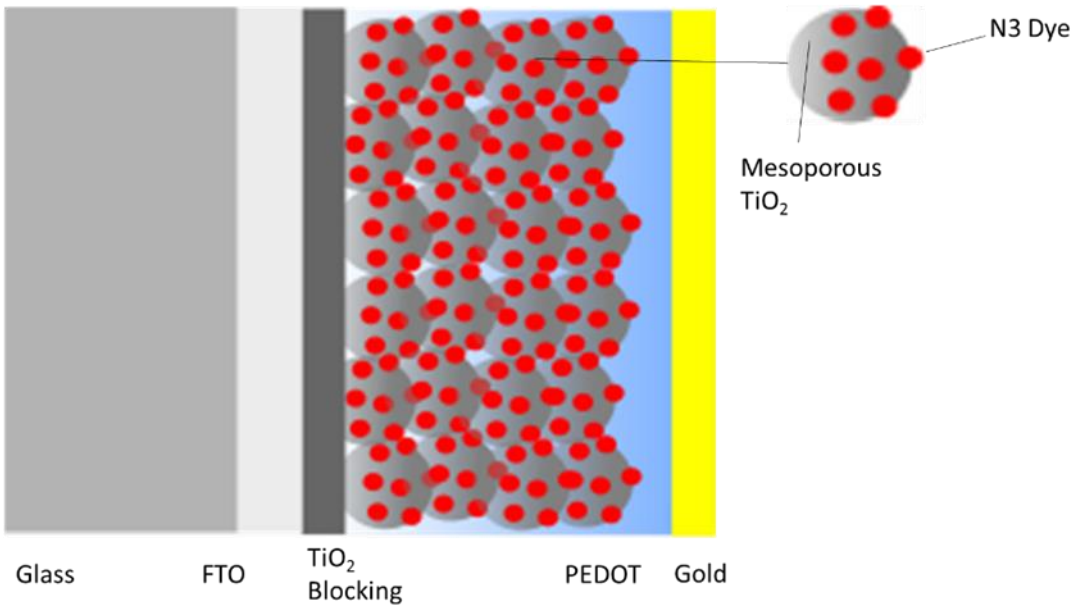


Figure 2-10: The stack of layers used in spin coating method of fabricating DSSCs.

To determine if VPP was a better method of applying PEDOT compared to PEDOT:PSS a solar cell was fabricated with a 700 nm PEDOT:PSS HTL using a spin coating method. When tested with the solar simulator, the solar cell had a short circuit current density ($I_{SC}$) of 2.36 µA , open circuit voltage ($V_{OC}$) of 0.481 V, and fill factor (FF) of 0.449, resulting in an efficiency of 0.006%. The low efficiency was likely due to the low $I_{SC}$ value, generally a result of having a high series resistance. As stated previously and shown in the SEM in Figure 2-11, the PEDOT:PSS did not fill the pores of the mesoporous $TiO_2$ layer. This produced a void between the dye layer and the HTL,

decreasing the rate of hole injection. The slow hole injection was able to increase the series resistance, resulting in a low $I_{SC}$ as observed.

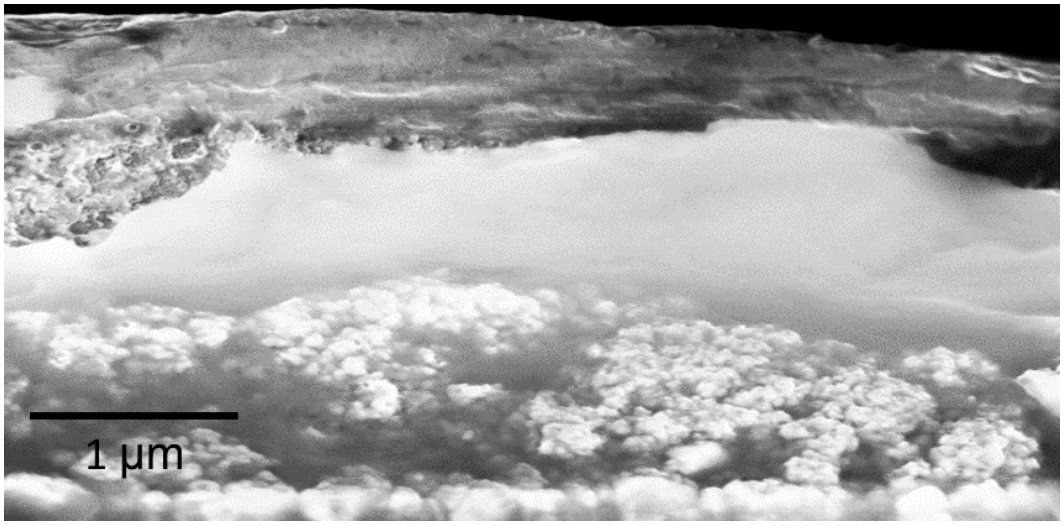


Figure 2-11: Cross-section SEM image of solar cell using PEDOT:PSS as a HTL.

To improve the filling of the mesoporous $TiO_2$ layer, a solar cells was fabricated with a VPP layer and tested using a solar simulator. The solar cell had an $I_{SC}$ of 20 µA , $V_{OC}$ of 0.016 V, and a FF of 0.235. The low $V_{OC}$ could be attributed to a low shunt resistance which would cause the cell to short circuit. A cross-section SEM of the solar cell, shown in Figure 2-12 showed there was no visible separation between the $TiO_2$ layer and the gold electrode. To prevent recombination from occurring, the separation of the electrode and $TiO_2$ needed to be increased.

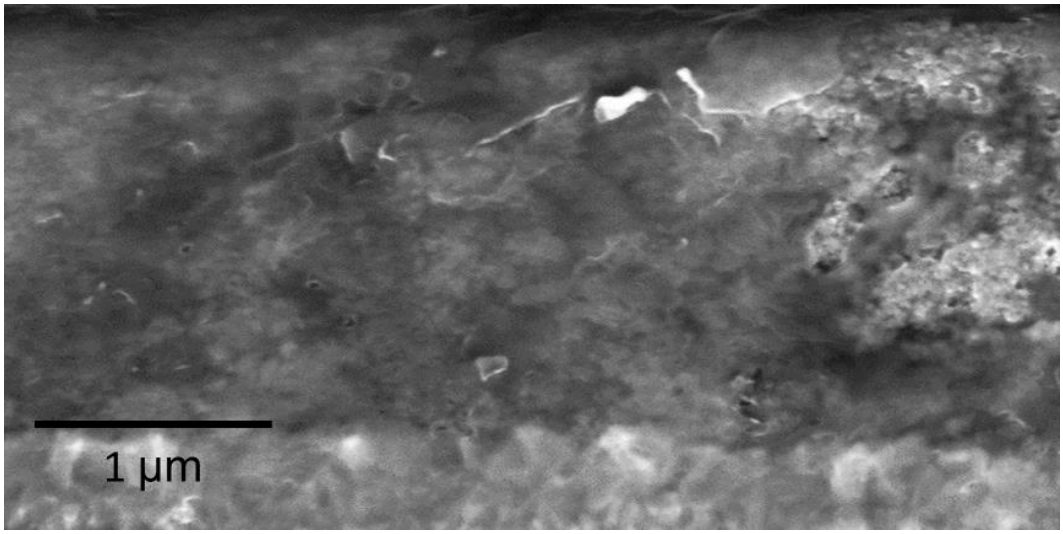


Figure 2-12: Cross-section SEM image of solar cell using VPP PEDOT as a HTL.

To improve the separation of the $TiO_2$ layer and the gold electrode, a solar cell was fabricated using both the VPP PEDOT and a 750 nm PEDOT:PSS layers before a gold electrode was evaporated on top shown in Figure 2-13. Using both layers, produced a $I_{SC}$ 342 µA, a $V_{OC}$ of 0.0591V and a FF of 0.358 producing a solar cell with a 0.18% efficiency. It is proposed the VPP layer of PEDOT produced a high $I_{SC}$ since it could fill the pores of the $TiO_2$ creating a good contact between the dye and the HTL. The addition of the PEDOT:PSS layer on top, helped create a barrier between the $TiO_2$ layer and the gold electrode. This separation could help prevent shorting of the cell, increasing the $V_{OC}$.

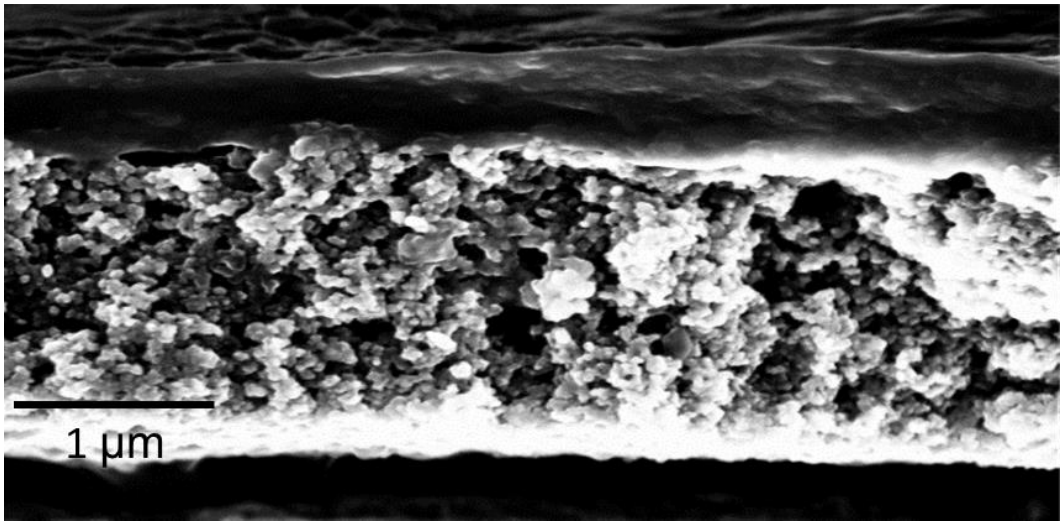


Figure 2-13: SEM of the cross-section for the VPP DSSC with 500 nm layer PEDOT:PSS layer.

The results of the solar simulator for the different ssDSSCs are summarized in Table 2-2. Based on the efficiencies, it is important to add a layer of PEDOT:PSS on top of the VPP PEDOT layer. This could help prevent the gold from interacting with the $TiO_2$ layer, shorting the solar cell. This was supported by the series resistance ($R_s$) and the shunt resistance ($R_{sh}$) of the cells in Table 2-2. For a solar cell, it was important to have a low series resistance and a large shunt resistance to maximize the efficiency. When no PEDOT:PSS was added, the series resistance was greater than the shunt resistance, meaning the solar cell was shorting. When there was a 700 nm layer of PEDOT:PSS, the shunt resistance was higher than the series, meaning it was less likely to short. Even though this was the case, there was still a need to improve the fill factor which was explored using different thicknesses of the PEDOT:PSS layer.

Table 2-2: Influence of PEDOT:PSS and VPP layer on I-V curve characteristics.

| | Only PEDOT:PSS | | Only VPP | | VPP and PEDOT:PSS | |
|---|---|---|---|---|---|---|
| | Average | St. Dev | Average | St. Dev | Average | St. Dev |
| $V_{OC}$ (V) | 0.481 | 0.173 | 0.016 | 0.013 | 0.059 | 0.003 |
| $I_{SC}$ (μA) | 2.36 | 0.13 | 20 | 10 | 342 | 75 |
| FF | 0.449 | 0.123 | 0.235 | 0.097 | 0.358 | 0.097 |
| η (%) | 0.006 | 0.003 | 0.002 | 0.001 | 0.18 | 0.03 |
| $R_S$ (Ω) | 6664 | 670 | 1092 | 1044 | 123 | 29 |
| $R_{Sh}$ (Ω) | 512584 | 344146 | 1056 | 1030.8 | 135 | 34 |

Since the thickness of the PEDOT:PSS layer could play a role in the series and shunt resistance, solar cells were prepared using different thicknesses as shown in Table 2-3. Comparing 0, 550, 700 and 1400 nm thick PEDOT:PSS layer, the cell with the best performance was the 700 nm thick PEDOT:PSS layer. Having too thick of a layer decreased the $V_{OC}$ and $I_{SC}$ of the cell since PEDOT:PSS was less conductive than VPP PEDOT. If the PEDOT:PSS layer was not thick enough, shorting could still occur between the gold and $TiO_2$ layer.

Table 2-3 Solar cell efficiency based on PEDOT:PSS thickness with VPP PEDOT.

| PEDOT:PSS Thickness | $V_{OC}$ (V) | $I_{SC}$ (µA) | FF | η (%) |
|---|---|---|---|---|
| 0 nm | 0.016 ± 0.016 | 20 ± 10 | 0.235 ± 0.097 | 0.002 ± 0.001 |
| 550 ± 20 nm | 0.037 ± 0.004 | 172 ± 49 | 0.401 ± 0.06 | 0.06 ± 0.02 |
| 700 ± 30 nm | 0.059 ± 0.003 | 342 ± 75 | 0.358 ± 0.097 | 0.18 ± 0.03 |
| 1400 ± 150 nm | 0.020 ± 0.003 | 134 ± 35 | 0.484 ± 0.171 | 0.03 ± 0.02 |

The previous cells discussed have had a mesoporous $TiO_2$ thickness of 2.5 µm, much thinner than the optimal thickness found in the literature. To achieve a thickness of 8 µm, the ratio of $TiO_2$ paste to ethanol was changed to 3:2. Decreasing the ethanol ratio resulted in thicker films and only required one layer from spin coating. The 8 µm thick mesoporous layer was used for the following experiments.

When the mesoporous layer was increased to 8 µm and the previous method of applying VPP PEDOT was used, the resulting cells produced no photo voltage. The thicker mesoporous layer increases the surface area available for PEDOT to grow. This could result in a thicker PEDOT layer that would filter light from the photoactive dye layer. To reduce the thickness of PEDOT, the spin speed for the oxidant was increased to 800 RPM for 10 seconds followed by1200 RPM for 2 seconds. The duration of the VPP was reduced from 40 minutes to 5, 10, and 15 minutes to produce thinner VPP PEDOT layers. The results in Table 2-4 show that 10 minute VPP produced the most efficient solar cell. This was likely from having a long enough polymerization time to have generated enough PEDOT to be conductive but thin enough layer to increase the transparency of the film.

Table 2-4 Solar cell efficiencies based on different VPP durations using $CuCl_2$ as an oxidant.

| VPP Duration | $V_{OC}$ (V) | $I_{SC}$ (μA) | FF | η (%) |
|---|---|---|---|---|
| 5 min | 0.200 ± 0.07 | 106 ± 100 | 0.125 ± 0.05 | 0.05 ± 0.04 |
| 10 min | 0.178 ± 0.07 | 147 ± 128 | 0.128 ± 0.07 | 0.09 ± 0.06 |
| 15 min | 0.180 ± 0.06 | 92 ± 46 | 0.044 ± 0.02 | 0.013 ± 0.006 |

Previous research has shown that $CuCl_2$ was a better oxidant for ssDSSCs than FePTs because the FePTs reduced the titanium, thereby reducing the overall efficiency of the cell. These experiments were done with more oxidant for longer polymerization times compared to the results in Table 2-5. A series of cells were fabricated with a VPP PEDOT using FePTs as an oxidant for 5, 10 and 15 minutes to determine if the change in polymerization conditions could improve solar cell performance. The cells followed the same pattern as the cells produced with $CuCl_2$ where the 10 minute polymerization was the optimal however the overall efficiencies of the cells were greater than the $CuCl_2$ VPP cells. It has been well reported in the literature VPP PEDOT thin films have the highest conductivity when using FePTs as an oxidant. The decrease in polymerization time could limit the interaction between the oxidant and the titanium. This combined with the increase in conductivity of the HTL has given the highest efficiency solar cells using a VPP PEDOT HTL.

Table 2-5 Solar cell efficiencies based on different VPP durations using FePTs as an oxidant.

| VPP Duration | $V_{OC}$ (V) | $I_{SC}$ (μA) | FF | η (%) |
|---|---|---|---|---|
| 5 min | 0.173 ± 0.03 | 216 ± 86 | 0.244 ± 0.09 | 0.18 ± 0.01 |
| 10 min | 0.335 ± 0.03 | 114 ± 22 | 0.248 ± 0.10 | 0.20 ± 0.01 |
| 15 min | 0.161 ± 0.06 | 108 ± 23 | 0.155 ± 0.03 | 0.06 ± 0.03 |

Based on the results from Tables 2-4 and 2-5, the 10 minute polymerization duration produced the most efficient solar cells. It is proposed the 10 minute polymerization allows for the thinnest film of PEDOT that is still conductive enough to act as a HTL. This is important in minimizing the series resistance as well as the filter effect which reduces the voltage of the cell. It was also determined that oxidants containing iron can still be used for the VPP method where it was previously reported to not be viable.

## 2.4 Conclusions

Based on the results, the spin coating method produced the most uniform thin films of $TiO_2$ for the n-type material in the DSSCs. The uniformity of the $TiO_2$ layer is important in reducing the shorting of the DSSC as well as in the reproducibility. The spin coating method can be used to produce films of varying thicknesses which may still need to be optimized.

The addition of a PEDOT:PSS layer prior to the electrode also plays an important role in the efficiency of the DSSCs reported. When PEDOT:PSS was used as a HTL, the lack of penetration into the mesoporous layer limited the number of active dye molecules.

When VPP was used as a HTL, the thin layer allowed for contact between the gold electrode and the $TiO_2$ layer, resulting in the solar cell shorting. The combination of the VPP PEDOT and PEDOT:PSS layer greatly increased the efficiency by allowing penetration of the mesoporous layer and forming a blocking layer between the $TiO_2$ and gold which prevented shorting. The thickness of the VPP and PEDOT:PPSS layers both play a roles in the series resistance and the transparency of the films.

Previously it was reported that FePTs could not be used as an oxidant for initiating VPP in DSSCs because it reduced the $TiO_2$ resulting in 0% efficiencies. By decreasing the amount of oxidant solution and reducing the time of the VPP, FePTs produced the highest reported ssDSSC using VPP PEDOT as a HTL. It is possible that changing the concentration and spin speed for the application of the oxidant can produce higher efficiencies. More work needs to be done in exploring post polymerization treatments as reported in the literature and other oxidants such as $FeCl_3$.

## 2.5 References


1. Grätzel, M., Recent Advances in Sensitized Mesoscopic Solar Cells. *Accounts of Chemical Research* **2009,** *42* (11), 1788-1798.

2. Hagfeldt, A.; Gratzel, M., Molecular Photovoltaics. *Accounts of Chemical Research* **2000,** *33* (5), 269-277.

3. Wu, J.; Lan, Z.; Lin, J.; Huang, M.; Huang, Y.; Fan, L.; Luo, G., Electrolytes in Dye-Sensitized Solar Cells. *Chemical Reviews* **2015,** *115* (5), 2136-2173.

4. Antila, L. J.; Myllyperkiö, P.; Mustalahti, S.; Lehtivuori, H.; Korppi-Tommola, J., Injection and Ultrafast Regeneration in Dye-Sensitized Solar Cells. *The Journal of Physical Chemistry C* **2014,** *118* (15), 7772-7780.

5. Listorti, A.; O'Regan, B.; Durrant, J. R., Electron Transfer Dynamics in Dye-Sensitized Solar Cells. *Chemistry of Materials* **2011,** *23* (15), 3381-3399.

6. Clifford, J. N.; Palomares, E.; Nazeeruddin, M. K.; Gratzel, M.; Durrant, J. R., Dye Dependent Regeneration Dynamics in Dye Sensitized Nanocrystalline Solar Cells: Evidence for the Formation of a Ruthenium Bipyridyl Cation/Iodide Intermediate. *The Journal of Physical Chemistry C* **2007,** *111* (17), 6561-6567.

7. Yanagida, S.; Yu, Y. H.; Manseki, K., Iodine/Iodide-Free Dye-Sensitized Solar Cells. *Accounts of Chemical Research* **2009,** *42* (11), 1827-1838.

8. Li, B.; Wang, L.; Kang, B.; Wang, P.; Qiu, Y., Review of recent progress in solid-state dye-sensitized solar cells. *Solar Energy Materials and Solar Cells* **2006,** *90* (5), 549 - 573.

9. Yue, G. T.; Wu, J. H.; Huang, Y. F.; Xiao, Y.; Lan, Z., Iodine/Iodide-Free and Polymer Heterojunction-Sensitized Hybrid Solar Cell. *Functional Materials Letters* **2012,** *5* (2), 4.

10. Martin, D. C.; Wu, J. H.; Shaw, C. M.; King, Z.; Spanninga, S. A.; Richardson-Burns, S.; Hendricks, J.; Yang, J. Y., The Morphology of Poly(3,4-Ethylenedioxythiophene). *Polymer Reviews* **2010,** *50* (3), 340-384.

11. Saito, Y.; Kitamura, T.; Wada, Y.; Yanagida, S., Poly(3,4-ethylenedioxythiophene) as a hole conductor in solid state dye sensitized solar cells. *Synthetic Metals* **2002,** *131* (1-3), 185-187.

12. Zhang, J. B.; Vlachopoulos, N.; Jouini, M.; Johansson, M. B.; Zhang, X. L.; Nazeeruddin, M. K.; Boschloo, G.; Johansson, E. M. J.; Hagfeldt, A., Efficient solid-state dye sensitized solar cells: The influence of dye molecular structures for the in-situ

photoelectrochemically polymerized PEDOT as hole transporting material. *Nano Energy* **2016,** *19*, 455-470.

13. Lei, Y.; Zhang, J.; Shen, Y.; Park, B.-W.; Bi, D.; Haggman, L.; Johansson, E. M.; Boschloo, G.; Anders, H.; Vlachopoulos, N.; Snedden, A.; Kloo, L.; Jarboui, A.; Chams, A.; Perruchot, C.; Jouini, M., New Approach for Preparation of Efficient Solid-State Dye-Sensitized Solar Cells by Photoelectrochemical Polymerization in Aqueous Micellar Solution. *The Journal of Physical Chemistry Letters* **2013,** *4* (23), 4026-4031.

14. Zhang, J. B.; Jarboui, A.; Vlachopoulos, N.; Jouini, M.; Boschloo, G.; Hagfeldt, A., Photoelectrochemical Polymerization of EDOT for Solid State Dye Sensitized Solar Cells: Role of Dye and Solvent. *Electrochimica Acta* **2015,** *179*, 220-227.

15. Reig-i-Plessis, D.; Panaitescu, E.; Baskaran, A.; Menon, L., A Simple Chemical Vapor Deposition Method for the Production of Highly Conductive Polymer Poly(3,4-ethylenedioxythiophene). *Journal of Nanoscience and Nanotechnology* **2013,** *13* (6), 4045-4051.

16. Vlachopoulos, N.; Zhang, J.; Hagfelt, A., Dye-sensitized Solar Cells: New Approaches with Organic Solid-state Hole Conductors. *CHIMIA International Journal for Chemistry* **2015,** *69*, 41-51.

17. Fukuri, N.; Saito, Y.; Kubo, W.; Senadeera, G. K. R.; Kitamura, T.; Wada, Y.; Yanagida, S., Performance improvement of solid-state dye-sensitized solar cells fabricated using poly(3,4-ethylenedioxythiophene) and amphiphilic sensitizing dye. *Journal of the Electrochemical Society* **2004,** *151* (10), A1745-A1748.

18. Kim, J.; Koh, J. K.; Kim, B.; Ahn, S. H.; Ahn, H.; Ryu, D. Y.; Kim, J. H.; Kim, E., Enhanced Performance of I2-Free Solid-State Dye-Sensitized Solar Cells with Conductive Polymer up to 6.8%. *Advanced Functional Materials* **2011,** *21* (24), 4633-4639.

19. Xia, J. B.; Masaki, N.; Lira-Cantu, M.; Kim, Y.; Jiang, K. J.; Yanagida, S., Influence of doped anions on poly(3,4-ethylenedioxythiophene) as hole conductors for iodine-free solid-state dye-sensitized solar cells. *Journal of the American Chemical Society* **2008,** *130* (4), 1258-1263.

20. Saito, Y.; Azechi, T.; Kitamura, T.; Hasegawa, Y.; Wada, Y.; Yanagida, S., Photo-sensitizing ruthenium complexes for solid state dye solar cells in combination with conducting polymers as hole conductors. *Coordination Chemistry Reviews* **2004,** *248* (13-14), 1469-1478.

21. Choi, Y. C.; Lee, D. U.; Noh, J. H.; Kim, E. K.; Seok, S. I., Highly Improved Sb2S3 Sensitized-Inorganic-Organic Heterojunction Solar Cells and Quantification of Traps by Deep-Level Transient Spectroscopy. *Advanced Functional Materials* **2014,** *24* (23), 3587-3592.

22. Skorenko, K. H.; Faucett, A. C.; Liu, J.; Ravvin, N. A.; Bernier, W. E.; Mativetsky, J. M.; Jones Jr, W. E., Vapor phase polymerization and mechanical testing of highly electrically conductive poly(3,4-ethylenedioxythiophene) for flexible devices. *Synthetic Metals* **2015,** *209*, 297 - 303.

23. Skorenko, K. H. Fabrication of solid state dye sensitized solar cells utilizing vapor phase polymerized poly (3,4-ethylenedioxythiopene) hole conducting layer. Binghamton Univeristy, State University of New York at Binghamton, Department of Chemistry, 2015.

24. Jeon, N. J.; Noh, J. H.; Yang, W. S.; Kim, Y. C.; Ryu, S.; Seo, J.; Seok, S. I., Compositional engineering of perovskite materials for high-performance solar cells. *Nature* **2015,** *517* (7535), 476-+.

25. Chandiran, A. K.; Abdi-Jalebi, M.; Nazeeruddin, M. K.; Gratzel, M., Analysis of Electron Transfer Properties of ZnO and TiO2 Photoanodes for Dye-Sensitized Solar Cells. *Acs Nano* **2014,** *8* (3), 2261-2268.

# Chapter 3:

# Design and Synthesis of Thiophene Containing Ligands for the Polymerization of Ruthenium Dyes with PEDOT in Solid State Dye-Sensitized Solar Cells

## 3.1 Introduction

There has been interest in transitioning from a liquid electrolyte to a solid electrolyte in DSSCs.[1-5] This could improve the overall stability and rate of electron transfer by removing the corrosive liquid and providing a tunneling or hopping mechanism of electron transfer.[3] One of the challenges with moving to a solid electrolyte is finding a material that can provide a close interaction between the sensitizer and HTL. An *in-situ* polymerization of PEDOT could allow for the filling of the mesoporous layer but it does not guarantee a close interaction with the dye. The interaction between the dye and n-type semiconductor material has been achieved through anchoring groups such as carboxylates.[6, 7] The carboxylate plays an important role in adhering the dye to the semiconductor but has also been shown to promote electron transfer from the dye to the n-type semiconductor.[8] To further enhance the regeneration of the dye, it is important to find a method of binding the photosensitizer to the hole transport material.

When looking at PEP PEDOT DSSCs, it has been shown the choice of photosensitizer is important for the fabrication of efficient solid state DSSCs. Using a dye that contains thiophene functional groups improved the overall efficiency of the solar cell. This was attributed to the more favorable interaction between the PEDOT and the dye

based on the thiophenes interacting through a physical bond. To further enhance the interaction like in the dye/semiconductor transition, a chemical bond would be needed.

As discussed previously, VPP PEDOT has shown to work as a hole transport material in solid state DSSCs. One reason is the ability of VPP PEDOT to fill the mesoporous layer of the mesoporous $TiO_2$ during the *in-situ* polymerization. The polymerization of PEDOT occurs through a carbon-carbon coupling of the $C_\alpha$-carbon of the thiophene. A ligand of interest is 4′-[4-(thiophen-3-yl-methoxymethyl)phenyl]-2,2′:6′,2″-terpyridine or ttp that has been used as a receptor in a fluorescent conjugated polymer chemosensor as shown in Figure 3-1.[9] The terpyridine would allow for binding to the ruthenium metal center while the thiophene could allow for polymerization with EDOT. The bromine bound to the $C_\alpha$ position should not prevent polymerization as PEDOT can be polymerized from a brominated EDOT monomer.[10, 11]

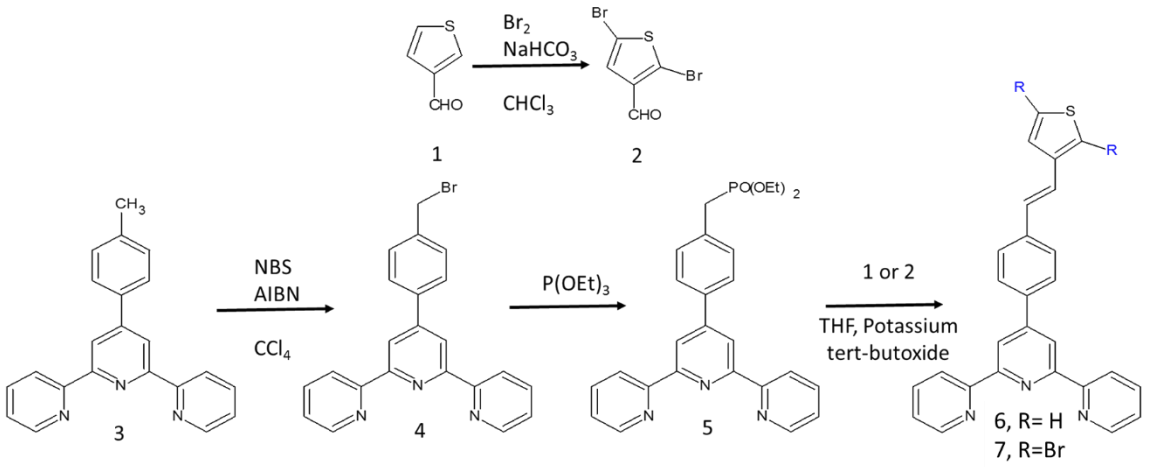


Figure 3-1: Reaction scheme for the synthesis of molecules 6 and 7 to be used as ligands.

For this study, an oxidant initiated solution polymerization of PEDOT was used instead of a VPP method. The solution method allows for thicker films to be synthesized

than the VPP method which allows for easier characterization since thin film methods are required. As discussed earlier, PEDOT like other polythiophenes is insoluble so methods such as Raman, UV-Vis and conductivity measurements can be used to show polymerization. While the oxidant initiated solution polymerization of PEDOT utilizes a different setup, the mechanism for the polymerization is the same. This means that if polymerization occurs in solution, it should also occur when transitioned to the VPP method which would be used is DSSCs.

## 3.2 Experimental

### 3.2.1 Materials and Methods

3,4-ethylenedioxythiophene (EDOT), iron (III) p-toluenesulfonate hexahydrate ($Fe(pTS)_3$, 4'-(4-methylphenyl)-2,2':6'2"-terpyridine, 3-thiophenecarboxaldehyde, 2,2'-azobis(2-methylpropionitrile), *N*-Bromosuccinimide, carbon tetrachloride and nitric acid were purchased from Sigma-Aldrich. pyridine and 30% hydrogen peroxide was purchased from Fisher Scientific. Ethanol was obtained from Pharmco-Aaper. Chloroform was purchased from spectrum chemicals and pre-cleaned plain glass microslides were obtained from VWR Scientific. All chemicals were used without further purification except the recrystallization of 2,2'-azobis(2-methylpropionitrile) and *N*-Bromosuccinimide. Prior to vapor-phase polymerization of PEDOT, the glass slides were treated with piranha acid, washed with ethanol and dried.

### 3.2.2 Material Characterization

The monomers were analyzed with a Bruker Advance III 600 MHz NMR. The chemical composition of the materials were studied with a Raman spectroscopy and spatial

Raman mapping were performed using a Thermo Scientific DXR Raman microscope. The wavelength of the excitation laser was 532nm and the power of the laser was kept at 5mW without any sample damage. The laser spot size was about 0.7μm with an x50 objective lens. Each spectrum has an average of 200 acquisitions. UV-Vis absorption measurements were taken with a Perkin Elmer Lambda 2S UV- 52 vis spectrometer using a clean glass side as a reference. Film thicknesses were measured with an SPM (STM/AFM) AFM. Conductivity measurements were taken with a 4-point probe set up.

### 3.2.3 Monomer Synthesis

**Synthesis of 4′-[4-(thiophen-3-yl-methoxymethyl)phenyl]-2,2′: 6′,2′′-terpyridine monomer (6):** A mixture of 4′-(4-bromomethylphenyl)-2,2′:6′,2′′-terpyridine (0.2153 g, 0.55 mmol) and triethyl phosphite (3 mL) was heated slowly to 120 °C for 1 h. Excess triethyl phosphite was removed from the reaction mixture by vacuum distillation to give a faint yellow oil. The residue was dissolved in 6 mL THF; 3-thiophenecarboxaldehyde (0.2 mL) was added. When dissolution was complete, KOBut (0.8 mL, 1 M in THF) was added. The mixture was stirred at room temperature for 2 h. The product mixture was poured into ethanol and filtered, yielding a tan powder (yield 25%). $^{1}$H NMR (600 MHz, $CDCl_3$) δ 8.78 (s, 2H), 8.76 (d, 2H), 8.70 (d, 2H), 7.94 (d, 2H), 7.91 (td, 2H), 7.64 (d, 2H), 7.40 (m, 5H), 7.26 (dd, 2H, trans-vinyl-H).

**Synthesis of 4′-{4-[2-(2,5-Dibromothiophen-3-yl)-vinyl]phenyl}-2,2′:6′,2′′-terpyridine monomer (7):** Was synthesized using the same method as described for 6 above. 1H NMR (600 MHz, CDCl3): δ 8.75 (s, 2H), 8.73 (d, 2H), 8.67 (d, 2H), 7.92 (d, 2H), 7.86 (td, 2H), 7.62 (d, 2H), 7.35 (td, 2H), 7.24 (s, 1H, 4-pyrrole-H), 7.02 (dd, 2H, trans-vinyl-H).

### 3.2.4 Polymer Synthesis

**Synthesis of poly( 3,4-ethylenedioxythiophene) (PEDOT)**

Two solutions were prepared by mixing 0.035 mL EDOT in 5 mL 1:1 ratio ethanol and chloroform and dissolving 0.4962 g FePTs in 10 mL of 1:1 ratio ethanol and chloroform with 6 μL pyridine. A glass slide was placed in a Petri dish within an oven at 60°C. The films was prepared by placing 1 mL of the EDOT solution and 2mL of the oxidant solution onto the glass slide and allowed to react for 40 minutes. The slides were then rinsed with ethanol to removed excess oxidant and dried at 100 °C for 10 minutes.

**Synthesis of poly (4′-[4-(thiophen-3-yl-methoxymethyl)phenyl]-2,2′: 6′,2′′-terpyridine) (pttp)**

Two solutions were prepared by mixing 0.0476 g molecule 6 or 0.0317 g molecules 7 in 5 mL 1:1 ratio ethanol and chloroform and dissolving 0.4962 g FePTs in 10 mL of 1:1 ratio ethanol and chloroform with 6 μL pyridine. A glass slide was placed in a Petri dish within an oven at 60°C. The films was prepared by placing 1 mL of the ligand solution and 2mL of the oxidant solution onto the glass slide and allowed to react for 40 minutes. The slides were then rinsed with ethanol to removed excess oxidant and dried at 100 °C for 10 minutes.

**Synthesis of 3,4-ethylenedioxythiophene, 4′-[4-(thiophen-3-yl-methoxymethyl)phenyl]-2,2′: 6′,2′′-terpyridine copolymer**

Solutions used in the synthesis of PEDOT and pttp were mixed in ratios of 1:3, 1:1, and 3:1. A glass slide was placed in a Petri dish within an oven at 60°C. The films was prepared by placing a total of 1 mL of monomer solution and 2mL of the oxidant solution onto the

glass slide and allowed to react for 40 minutes. The slides were then rinsed with ethanol to removed excess oxidant and dried at 100 °C for 10 minutes.

### 3.2.5 Ruthenium Dye Synthesis

**Synthesis of (iso-thiocyanato) (2,2-bipyridyl-4,4-di-carboxylato) (4′-[4-(thiophen-3-yl-methoxymethyl)phenyl]-2,2′: 6′,2′′-terpyridine) ruthenium (II) Ru(ttp-H)(dcbpy)(SCN)**

In a round bottom flask, 0.2374 g (6) and 0.1037 g $RuCl_3$ was purged under nitrogen for 15 minutes. Anhydrous DMF (20 mL) was added to the round bottom under nitrogen and heated at 130 °C for 4.5 hours. After 4.5 hours, 0.173 g 2,2-bipyridyl-4,4-d-carboxylic acid was added and heated at 130 °C for 4 hours. The temperature was then decreased to 100 °C and 2.4191 g ammoniumthiocyanate was added and allowed to reflux overnight. After cooling, the product was recovered through removing solvent under heated vacuum, before being acidified with 1 M HCl. And filtered. The product was then purified with a sephadex column using methanol as a solvent.

**Synthesis of (iso-thiocyanato) (2,2-bipyridyl-4,4-di-carboxylato) (4′-{4-[2-(2,5-Dibromothiophen-3-yl)-vinyl]phenyl}-2,2′:6′,2′′- terpyridine) ruthenium (II) Ru(ttp-Br)(dcbpy)(SCN)**

Was synthesized using the procedure described above using (7).

### 3.3 Results and Discussion

The monomers were synthesized by bromonating 4’-(4-methylphenyl)-2,2’:6’2”-terpyridine using a free radical reaction with NBS followed by a Wittig reaction. The two

monomers were used in the oxidant initiated polymerization reactions discussed in the experimental section.

Molecules 6 and 7 were confirmed using $^{1}H$ NMR with the resulting spectrum shown in Figure 3-2. The formation of the doublet of doublets around 7 ppm in each spectrum represent the alkene formation from the Wittig reaction, confirming the formation of the final product. No other peaks appear in the NMR spectrum showing a high purity of the final product was recovered.

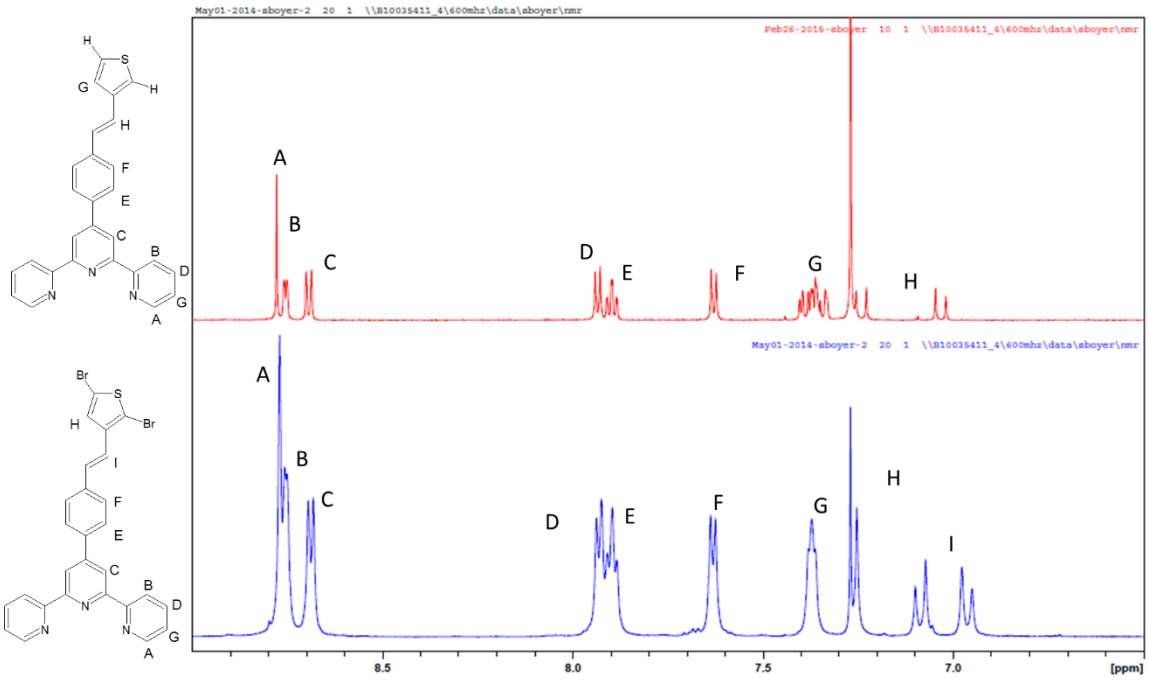


Figure 3-2: $^{1}H$ NMR spectrum of monomers 6 and 7 showing the doublet of doublets at ~7 ppm showing alkene from the Wittig reaction.

Polymers were synthesized using different ratios of EDOT and monomers 6/7. The resulting polymers could not be characterized using solution based NMR because they were insoluble. Solid state $C^{13}$ NMR was used to characterize the material as shown in Figure 3-3. The top spectrum is of the ttp-Br monomer using a cross-polymerization (CP-

MAS) shows aromatic carbon between 110 and 160 ppm as expected. A CP-MAS spin-echo experiment was used to produce the bottom spectrum of the copolymer between EDOT and ttp. The signal to noise ratio is poor and while there is a broad peak around 50 ppm which could be from $CH_2$, it is not definitive. For this reason, other methods need to be used to determine if the ttp monomer is polymerizing with EDOT.

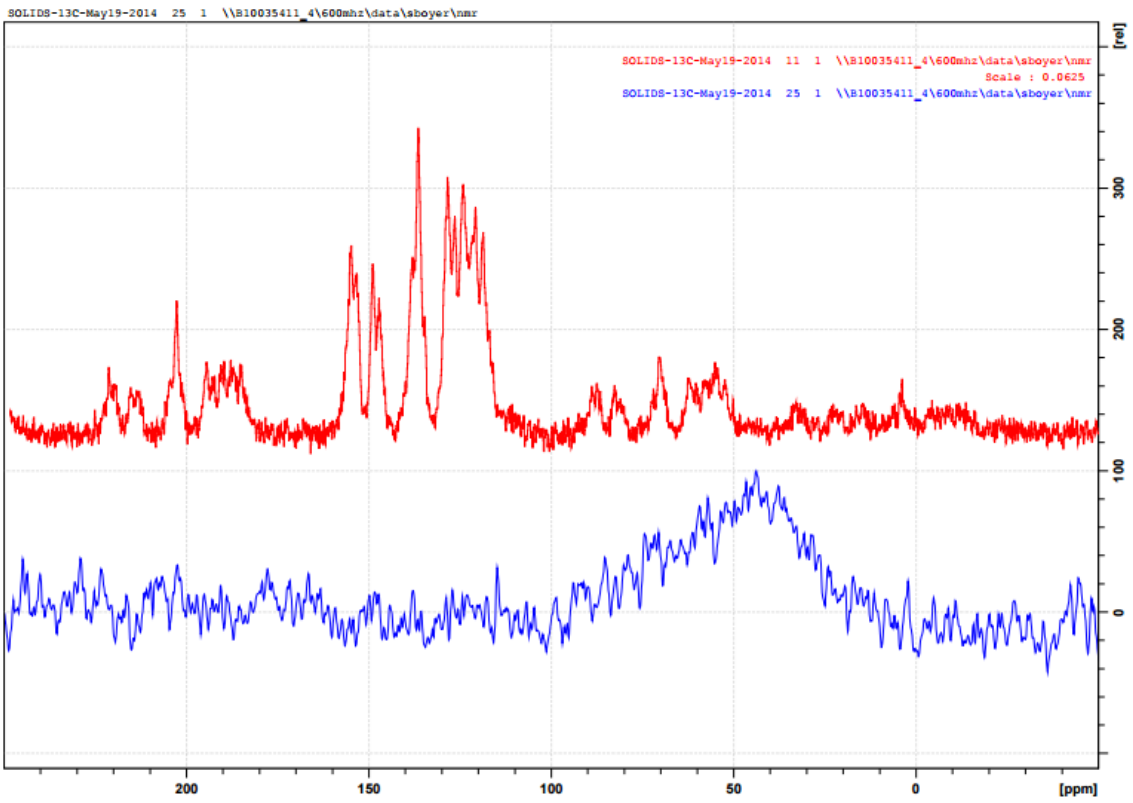


Figure 3-3: Solid state NMR spectrum for ttp-Br monomer and product of ttp-EDOT copolymerization reaction.

A common method of characterizing PEDOT thin films is using Raman. The resulting Raman spectrum from the different polymers are shown in Figure 3-4 a and b. In Figure 3-4a the R= H. All the spectrum show the characteristic Raman stretch between 1400 and 1500 $cm^{-1}$ corresponding to the $C_\alpha$-$C_\beta$ stretch of the thiophene ring.[12, 13] As the

concentration of EDOT monomer is added to the reaction, the maximum red shifts and narrows as shown in Figure 3-4b. The broader peaks toward the poly-ligand suggests an increase in vibrational modes which can be different phases of the copolymer.[13] Films were also prepared with monomer 7 and EDOT with the resulting Raman spectrum shown in Figure 3-4c. As more monomer is added, the peak at 1425 $cm^{-1}$ decreases, suggesting a lack of polymerization between monomer 7 and EDOT. Based on this, monomer 7 is not polymerizing with EDOT and would not be an option as a ligand for a sensitizer. This could be a result of the difference in kinetics between the two monomers when one contains bromine and the other does not. The oxidant initiated solution polymerization is rapid and is one of the reasons for the relatively low conductivities from films made using this method.[10] When the bromine is present, the group needs to be removed from the thiophene before polymerization occurs, adding a step.

a) .

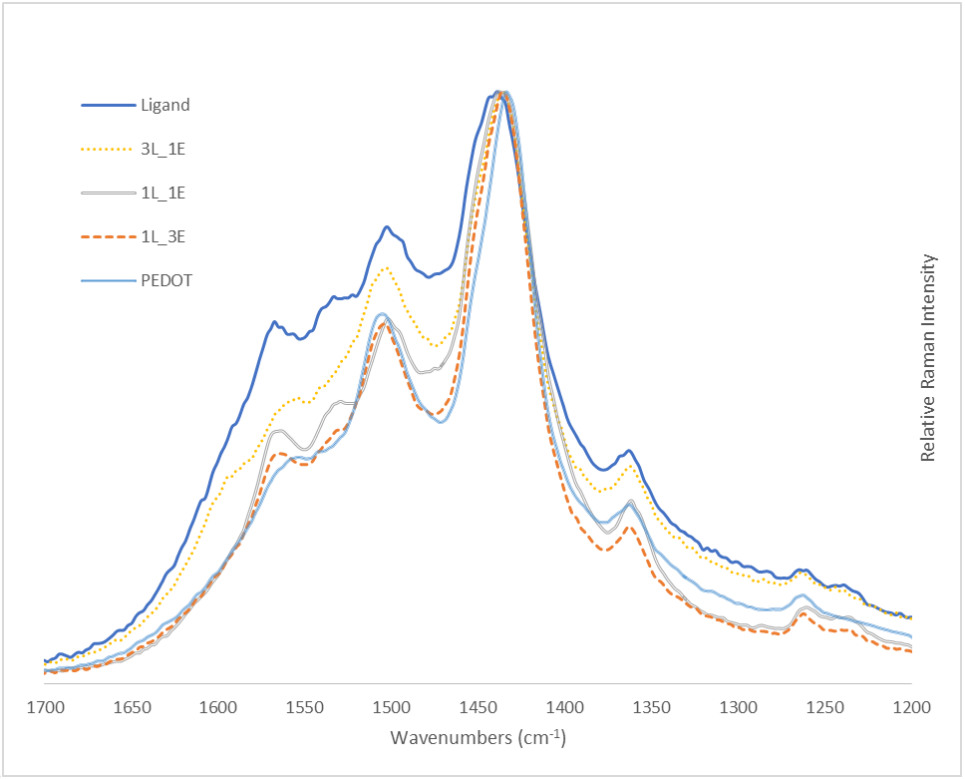

b)

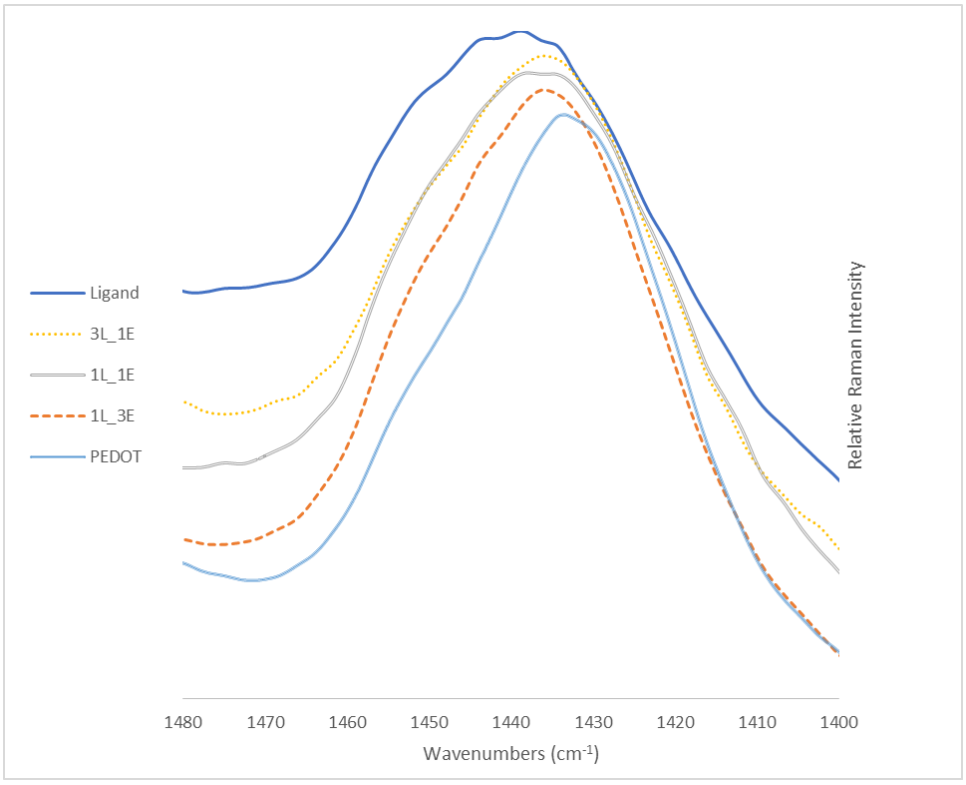


c)

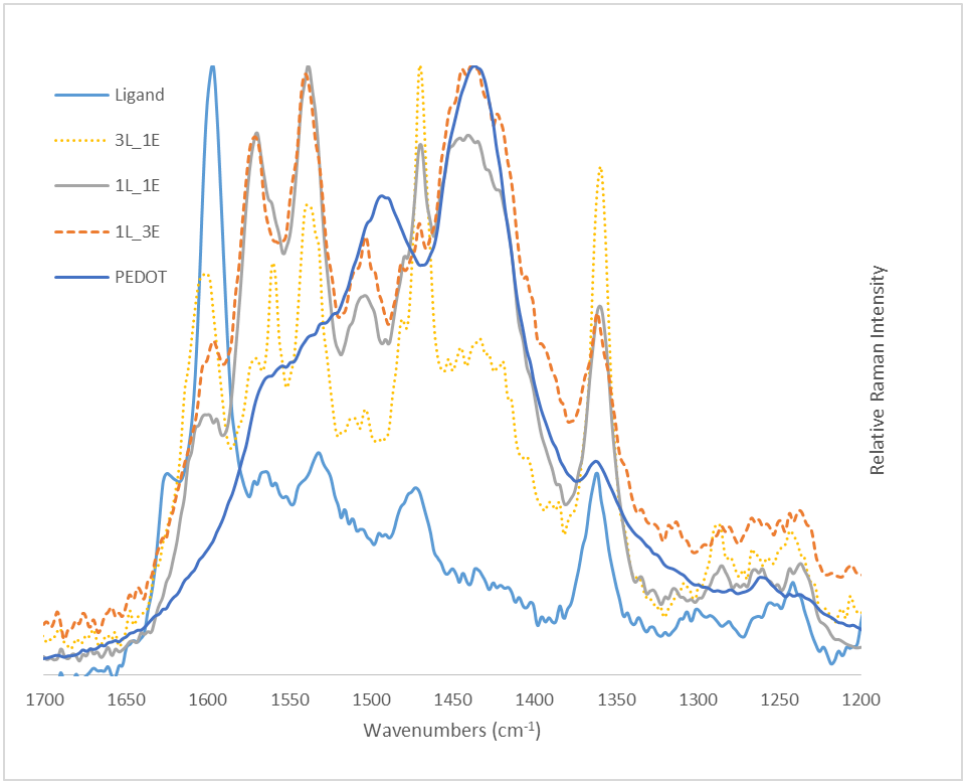


Figure 3-4: Raman spectrum of thin film products with a) ttp-H and EDOT, b)ttp-H and EDOT focused on thiophene region, and c) ttp-Br and EDOT.

UV-Vis of the polymer films prepared using the monomer where R=H shown in Figure 3-5 shows a broadening of the peak at 325 nm and an increase in absorbance in the near IR as the concentration of EDOT is increased. This suggests copolymerization occurs and as the EDOT concentration increase, the absorbance in the near IR also increases.[13] The absorbance in the IR corresponds to the bipolaron state of PEDOT which indicated anion doping and an extended polymer chain conformation.[14]

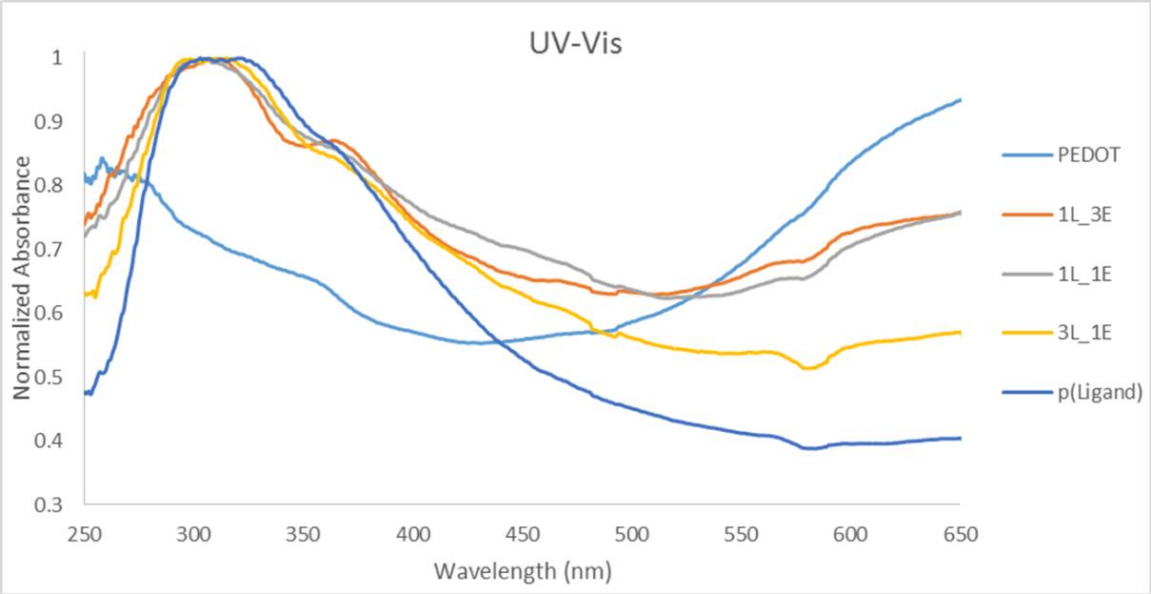


Figure 3-5: UV-vis spectrum of thin films produced from ttp-H and EDOT at different ratios.

Conductivity measurements were done using a 4-point probe for the sheet resistance and AFM to determine the thickness of the films. The conductivity of the in situ PEDOT is relatively low compared to the literature but is attributed to using a glass substrate which has poor adhesion compared to PET. The conductivity decreases as the concentration or ligand is increased, the poly-ligand no measurable conductivity. PEDOT has a high conductivity compared to other polythiophenes because the structure prevents cross-linking from polymerization of the $C_\beta$. The synthesized monomers have an open $C_\beta$

which could allow cross-linking to occur, reducing the conductivity of the films. This is supported with the broadening observed in the Raman spectrum.

Table 3-1: Conductivity for polymer films synthesized with different ratios of EDOT to monomer.

| Polymer | Conductivity (S/cm) |
|---|---|
| PEDOT | 1.13E-04 |
| 1 Ligand:3 EDOT | 7.92E-06 |
| 1 Ligand:1 EDOT | 6.25E-06 |
| 3 Ligand:1 EDOT | 3.24E-06 |
| Poly(Ligand) | 0 |

Based on the Raman, UV-Vis and conductivity results, monomer 6 would be a potential ligand for a sensitizer in a ssDSSC with VPP PEDOT as a HTL. Dyes were synthesized based on a one-pot reflux as described in the experimental section with proposed structures in Figure 3-6. The actual structure of the dyes has yet to be determined because a single crystal for x-ray diffraction has not been successfully obtained. Because ruthenium is paramagnetic, NMR cannot be used to determine the structure of the molecules.

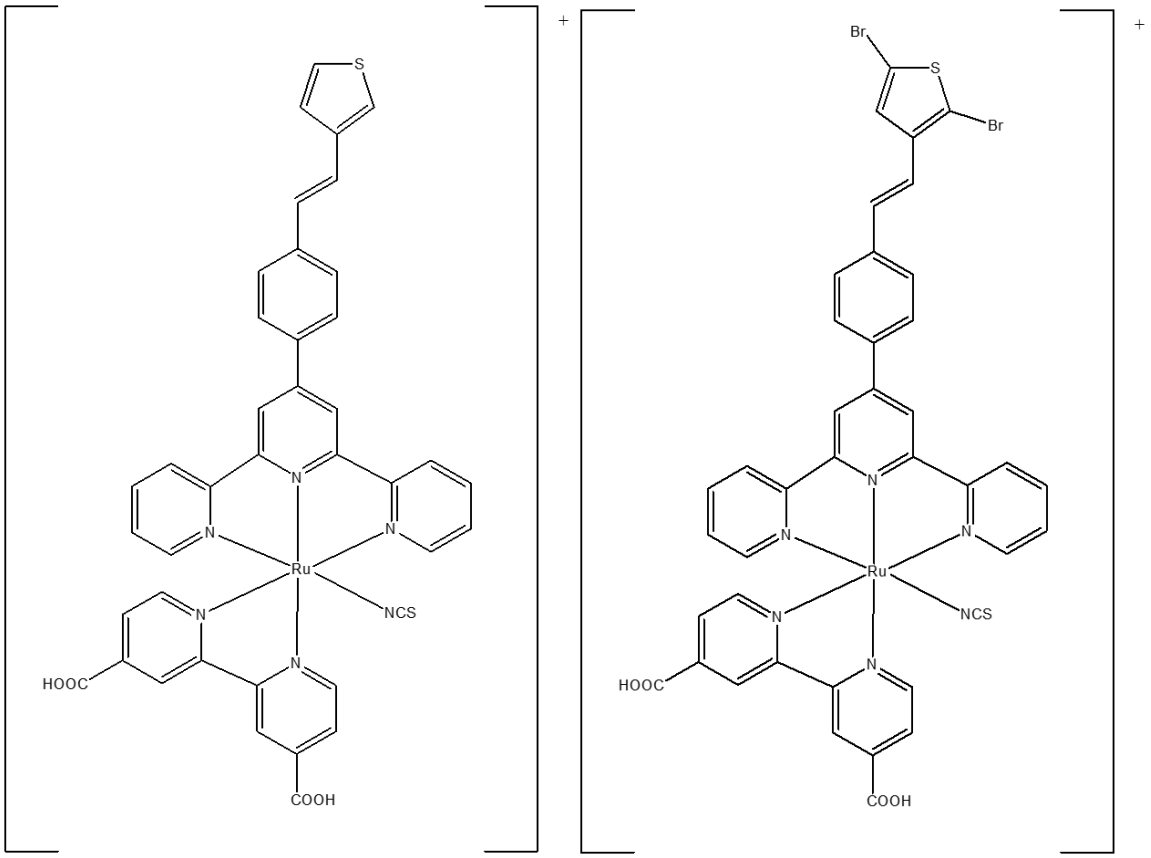


Figure: 3-6 Proposed structure of dyes with (left) ttp-H ligand and (right) ttp-Br ligand.

The dyes were characterized using UV-Vis spectroscopy and the molar extinction coefficient was plotted based on wavelength as shown in Figure 3-7. The dyes were plotted with N3 dye as a comparison to a dye commonly used in the literature. The terpyridine ligand absorbs more broadly than the bipyridine peak evident by the broadening of the $\pi$-$\pi^*$ transition from ~250 nm-400 nm. Both dyes contain MLCT at 500 and 575 nm which is characteristic of ruthenium polypyridyl dyes. Based on the UV-Vis, the new dyes are comparable to the N3 dye in terms of absorptivity.

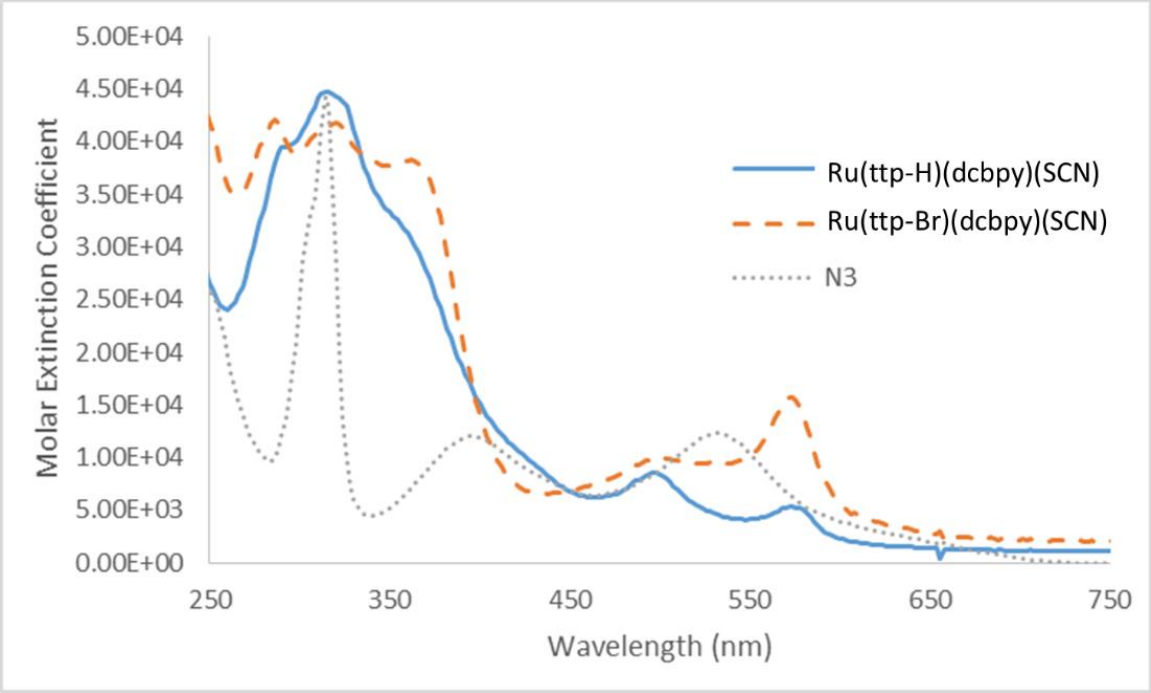


Figure 3-7: Wavelength versus molar extinction coefficient for ruthenium polypyridyl complexes with ttp ligands and N3 dye.

### 3.4 Conclusion

Based on the results, the ttp-H can be polymerized with EDOT to form a copolymer while ttp-Br cannot. Dyes were synthesizes with either the ttp-H or ttp-Br ligands and compare favorably to N3 dye in terms of absorption of visible light. The resulting dyes can be used to compare the effects in solar cells when the dye is polymerized into PEDOT or isn't based on the ligand of choice. This could provide great insight as to the important of the rate of dye regeneration from the solid state electrolyte VPP PEDOT.

## 3.5 References


1. Li, B.; Wang, L.; Kang, B.; Wang, P.; Qiu, Y., Review of recent progress in solid-state dye-sensitized solar cells. *Solar Energy Materials and Solar Cells* **2006,** *90* (5), 549 - 573.

2. Vlachopoulos, N.; Zhang, J.; Hagfelt, A., Dye-sensitized Solar Cells: New Approaches with Organic Solid-state Hole Conductors. *CHIMIA International Journal for Chemistry* **2015,** *69*, 41-51.

3. Wu, J.; Lan, Z.; Lin, J.; Huang, M.; Huang, Y.; Fan, L.; Luo, G., Electrolytes in Dye-Sensitized Solar Cells. *Chemical Reviews* **2015,** *115* (5), 2136-2173.

4. Yanagida, S.; Yu, Y. H.; Manseki, K., Iodine/Iodide-Free Dye-Sensitized Solar Cells. *Accounts of Chemical Research* **2009,** *42* (11), 1827-1838.

5. Yuan, H. L.; Li, J. P.; Wang, M. K., Recent progress in research on solid organic-inorganic hybrid solar cells. *Acta Physica Sinica* **2015,** *64* (3), 10.

6. Murakoshi, K.; Kano, G.; Wada, Y.; Yanagida, S.; Miyazaki, H.; Matsumoto, M.; Murasawa, S., Importance of binding states between photosensitizing molecules and the $TiO_2$ surface for efficiency in a dye-sensitized solar-cell. *Journal of Electroanalytical Chemistry* **1995,** *396* (1-2), 27-34.

7. Li, J. R.; Nilsing, M.; Kondov, I.; Wang, H. B.; Persson, P.; Lunell, S.; Thoss, M., Dynamical simulation of photoinduced electron transfer reactions in dye-semiconductor systems with different anchor groups. *Journal of Physical Chemistry C* **2008,** *112* (32), 12326-12333.

8. She, C. X.; Guo, J. C.; Irle, S.; Morokuma, K.; Mohler, D. L.; Zabri, H.; Odobel, F.; Youm, K. T.; Liu, F.; Hupp, J. T.; Lian, T., Comparison of interfacial electron transfer through carboxylate and phosphonate anchoring Groups. *Journal of Physical Chemistry A* **2007,** *111* (29), 6832-6842.

9. Zhang, Y.; Murphy, C. B.; Jones, W. E., Poly p-(phenyleneethynylene)-alt-(thienyleneethynylene) polymers with oligopyridine pendant groups: Highly sensitive chemosensors for transition metal ions. *Macromolecules* **2002,** *35* (3), 630-636.

10. Martin, D. C.; Wu, J. H.; Shaw, C. M.; King, Z.; Spanninga, S. A.; Richardson-Burns, S.; Hendricks, J.; Yang, J. Y., The Morphology of Poly(3,4-Ethylenedioxythiophene). *Polymer Reviews* **2010,** *50* (3), 340-384.

11. Kim, J.; Koh, J. K.; Kim, B.; Ahn, S. H.; Ahn, H.; Ryu, D. Y.; Kim, J. H.; Kim, E., Enhanced Performance of I2-Free Solid-State Dye-Sensitized Solar Cells with Conductive Polymer up to 6.8%. *Advanced Functional Materials* **2011,** *21* (24), 4633-4639.

12. Selvaganesh, S. V.; Mathiyarasu, J.; Phani, K. L. N.; Yegnaraman, V., Chemical synthesis of PEDOT-Au nanocomposite. *Nanoscale Research Letters* **2007,** *2* (11), 546-549.

13. Ouyang, J.; Xu, Q. F.; Chu, C. W.; Yang, Y.; Li, G.; Shinar, J., On the mechanism of conductivity enhancement in poly (3,4-ethylenedioxythiophene): poly(styrene sulfonate) film through solvent treatment. *Polymer* **2004,** *45* (25), 8443-8450.

14. Cho, M. S.; Kim, S. Y.; Nam, J. D.; Lee, Y., Preparation of PEDOT/Cu composite film by in situ redox reaction between EDOT and copper(II) chloride. *Synthetic Metals* **2008,** *158* (21-24), 865-869.

# Chapter 4

## The Role of Ruthenium Photosensitizers in the Degradation of Phenazopyridine with $TiO_2$ Electrospun Fibers

### 4.1 Introduction

Semiconducting oxides are a promising class of materials for the photodegradation of organic pollutants.[1-5] Titanium dioxide ($TiO_2$) has been thoroughly investigated as a photooxidizer that is stable, low cost, and environmentally friendly. However, its wide band gap (~3.0 eV) requires UV radiation, which is not optimal for environmental applications, particularly in remote settings, that rely on visible solar radiation. In order for $TiO_2$ to be more feasible photocatalyst, it must be able to absorb more of the solar spectrum in the visible and near IR irradiation from 400-800 nm, making up 43% and 52% of the solar spectrum respectively. To improve the effectiveness of these photocatalysts in the visible region, $TiO_2$ can be modified with metal nanoparticle loading, metal ion doping, dye sensitization, composite semiconductor and anion doping.[2-6] One issue with doping is the introduction of trap sites decreases the efficiency of the electron/hole transfer to the surface, reducing the number of radicals present in solution.[3] For this reason, our focus is to modify the surface to expand the region of absorption into that commonly used in dye sensitized solar cells (DSSCs).[7]

Ruthenium polypyridyl complexes are common sensitizers used in $TiO_2$ based DSSCs due to their strong visible absorption and efficient electron injection into

semiconductor layers.[7-12] Here, the dye studied was *cis*-dichlorobis(2,2'-bipyridyl-4,4'-dicarboxylic acid)ruthenium (II) ($Ru(dcbpyH_2)_2Cl_2$), shown in Figure 4-1a. The dye is a strong electron injector due to of the covalent interactions with the metal oxide through the carboxylic acid anchoring groups and the close energy of the LUMO compared to the conduction band of $TiO_2$ as shown in Figure 4-1b, resulting in electron injection rates on the sub-picosecond timescale.[9 13, 14]

a.

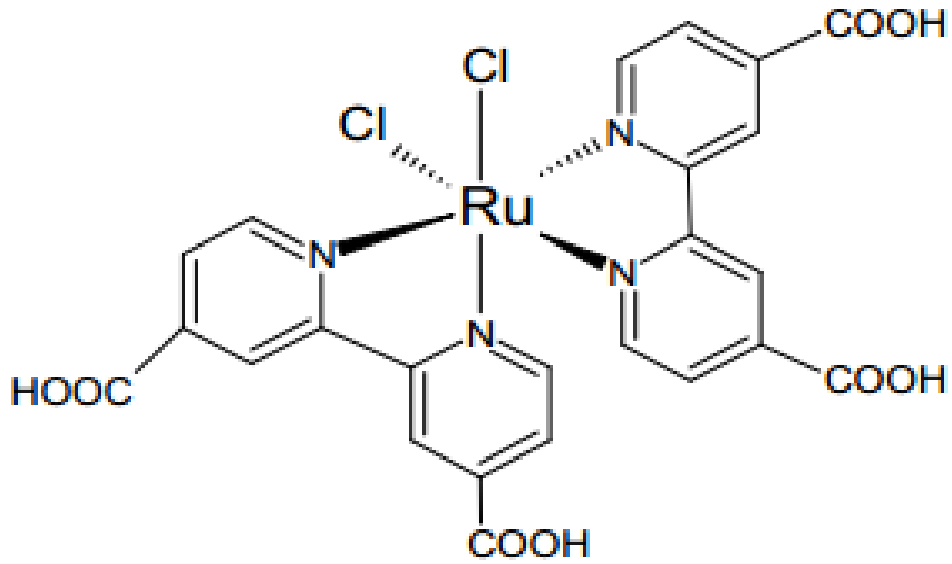


b.

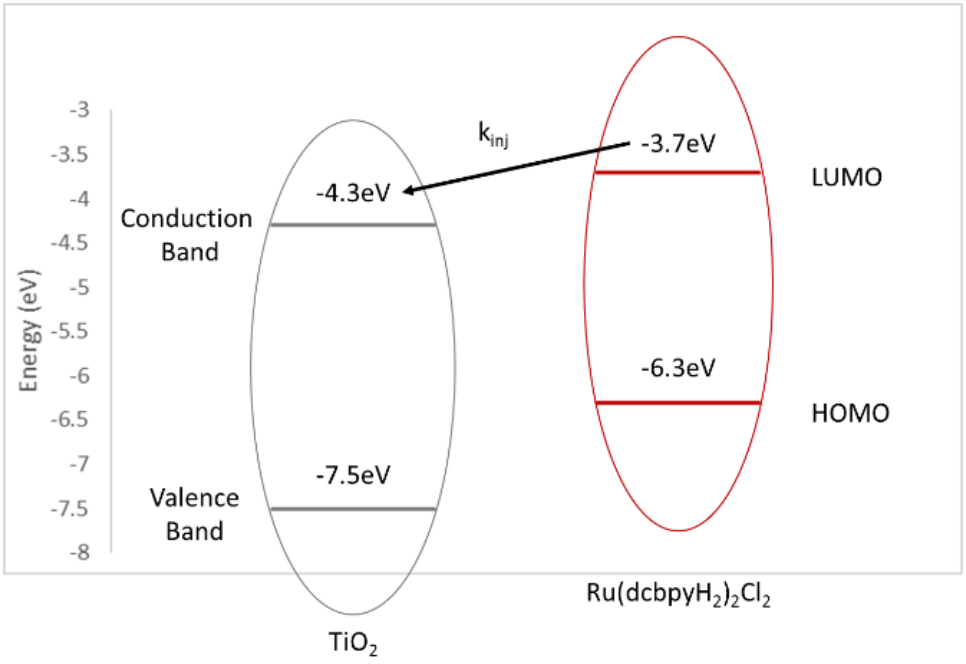


Figure 4-1: a) Molecular structure of $Ru(dcbpyH_2)_2Cl_2$. b) Energy level diagram for $TiO_2$ and $Ru(dcbpyH_2)_2Cl_2$.

Our group has previously studied the degradation of the biopharmaceutical pyridinediamine,3-(phenylazo) monohydrochloride, or phenazopyridine (PAP), shown in Figure 4-2.[15] PAP is commonly used as an analgesic and anesthetic drug to reduce pain

from urinary tract infections. PAP serves as a model pollutant due to its structural similarity to other known organic toxins found in biomedical waste water.[16] The presence of its azo-group, amines, and phenyl ring are similar to functional groups present on many toxic organic pollutants and other antibiotics like amoxicillin and tetracycline. These products can build up in biomedical waste streams and lead to contamination of environmental waters.

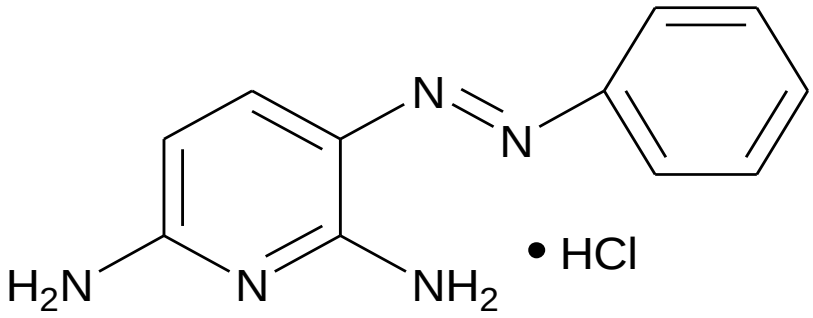


Figure 4-2: Chemical structure of the environmental pollutant phenazopyridine.

Here we exhibit the feasibility of using $TiO_2$ as a photocatalyst under environmental conditions for the degradation of organic pollutants by expanding the dye sensitized absorption into the visible region. This was accomplished using the same concept as DSSCs using a dye as a photosensitizer, injecting electrons into the electron conducting $TiO_2$ layer as shown in Figure 4-3. Cis-dichlorobis(2,2'-bipyridyl-4,4'-dicarboxylic acid)ruthenium(II) is a known electron injecting dye that will be used to sensitize $TiO_2$ electrospun fibers. Prior studies have shown that excited electrons in the conduction band favor the formation of peroxide radical anions in the presence of adsorbed oxygen on the surface. The generation of these radicals in the presence of visible light is expected to improve the effectiveness of the $TiO_2$ catalyst, increasing the rate of PAP degradation.

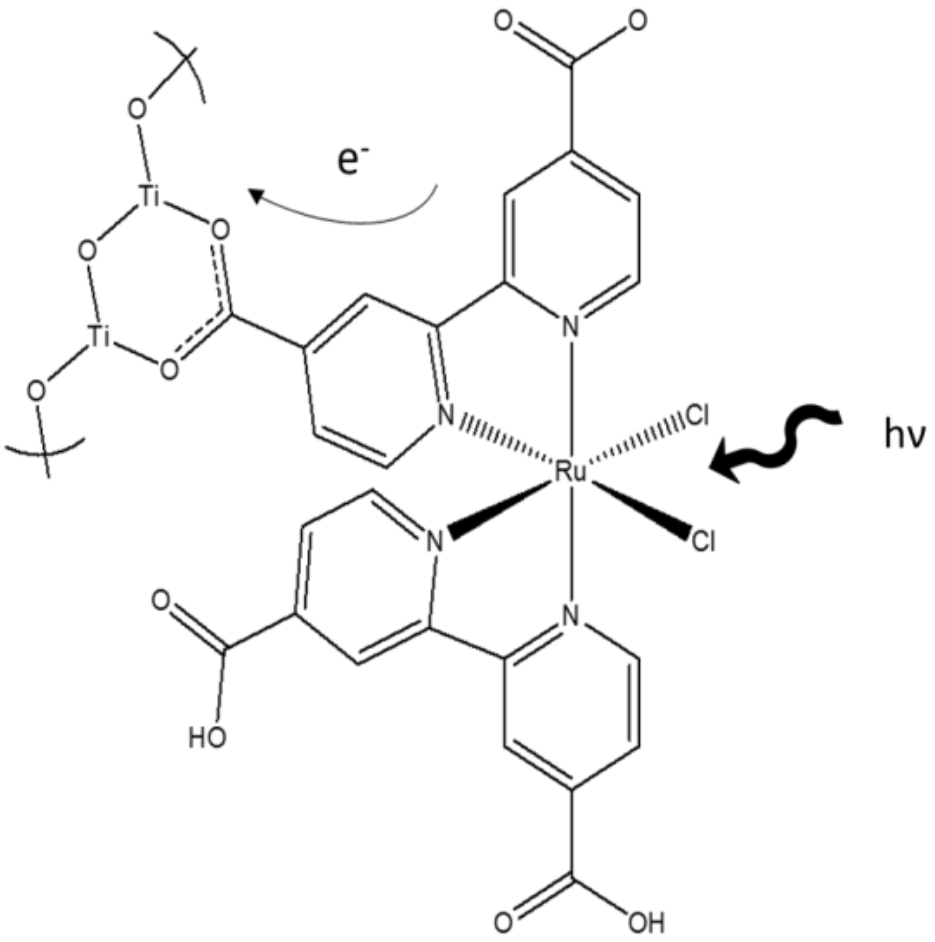


Figure 4-3: The absorption of a photon promotes the excitation and injection of an electron for the photosensitizer to the semiconductor.

## 4.2 Experimental

### 4.2.1 Materials

All materials were purchased commercially and used as received unless otherwise indicated. Poly(methyl methacrylate) (PMMA), 4,4-dimethyl-2,2'-bipyridine, $RuCl_3(H_2O)_3$, titanium isopropoxide (TTIP), anhydrous dimethylformamide (DMF), and ethanol were purchased from Sigma-Aldrich. Chloroform, diethyl ether, acetone, and sodium dichromate were purchased from Fisher. The solvents hydrochloric acid and sulfuric acid were purchased from JT Baker. Cis-dichlorobis(2,2'-bipyridyl-4,4'-dicarboxylic acid)ruthenium(II) ($Ru(dcbpyH_2)_2(Cl)_2$) was synthesized using a procedure

from the literature under nitrogen and was used without further purification.[17] Reactions that were light sensitive were conducted in the dark and the reaction apparatus was covered with aluminum foil.

### 4.2.2 Characterization

The pre-calcined $TiO_2$ polymer fibers were fabricated using a high voltage Spellman SL 30 generator. The photodegradation experiments were performed using an Oriel 66001 UV lamp (100-400 nm range) with Oriel 68805 40-200 Watt universal Arc lamp power supply. UV-Vis measurements of aliquots of PAP were made on a Hewlett Packard 8452A Diode Array spectrophotometer to track concentration change during the photodegradation experiment. Fourier transform infrared spectra (FTIR) of $Ru(dcbpyH_2)_2Cl_2$ and $Ru(dcbpyH_2)_2Cl_2$-sensitized $TiO_2$ fibers were obtained using a Bruker Equinox 55. Scanning electron microscopy (SEM) images were obtained on a FESEM, Supra 55 VP from Zeiss. X-ray diffraction(XRD) of the calcined fibered was obtained using, PANalytical's X'Pert PRO Materials Research Diffractometer with Cu Kα X-radiation ($\lambda$ = 1.5418 Å).

### 4.2.3 Synthesis of $TiO_2$ Electrospun Fibers

$TiO_2$ fibers were prepared by a using a sol-gel synthesis, followed by electrospinning of polymer sol-gel, and calcination treatment of polymer fibers.[18, 19] A polymeric sol-gel was generated by stirring and ambient hydrolysis of TTIP using 1:2 mass ratio of PMMA:TTIP, where 320 mg of PMMA (MW = 35,000 g/mol) was completely dissolved in 2 mL of chloroform followed by drop wise addition of 640 mg of TTIP with

continuous stirring for 30 min. 2 mL of DMF was then added and stirred for 2 h to increase the dielectric constant of the composite solution which aids in the electrospinning process.

The high voltage (25 kV) pulled the precursor sol-gel from the syringe onto the conductive Al collector forming polymer fibers. The resulting polymer fibers were left overnight to allow for complete hydrolysis of TTIP to $Ti(OH)_4$ and further condensation to amorphous $TiO_2$ followed by calcination treatment of 360°C for 4h in air to create mixed $TiO_2$ crystal phase fibers.

### 4.2.4 Preparation of $Ru(dcbpyH_2)_2(Cl)_2$- sensitized $TiO_2$ Fibers

0.7 mg of $Ru(dcbpyH_2)_2(Cl)_2$ was added to 33.2 µL of 0.1 M NaOH solution, 20 mL of ethanol was added and the solution allowed to stir in the dark for ~0.5 h. To the solution, 12.2 mg $TiO_2$ fibers was added and stirred for 24 h. The resulting solution was washed with ethanol to remove any excess dye. For the washing process, the solution was centrifuged and the supernatant fluid was decanted and dried under vacuum.

### 4.2.5 Photodegradation Procedure

To a quartz vial or glass beaker, 12.0 mL of 144 µM PAP/water solution, 14.0 mg of photocatalyst (either $Ru(dcbpyH_2)_2Cl_2$, $TiO_2$ fibers or $Ru(dcbpyH_2)_2Cl_2$ - sensitized fibers) was added. To determine the stability of PAP, 12.0 mL of 144 µM PAP/water solution was used without the addition of a catalyst. This solution was allowed to stir in the dark for 1 h. At 15 min time intervals, 1.0 mL aliquots were taken with a syringe during a 2 h time period. The 1.0 mL aliquot was centrifuged for 5 min and then 0.5 mL of the upper solution was obtained for concentration measurements using a UV-Vis diode array spectrophotometer monitoring the absorbance at 424 nm. The remainder of the solution

from the 1.0 mL aliquot was not put back into the reaction cell. The solution in the reaction cell was stirred in the dark for 1 h and then irradiated with a UV lamp for another hour to perform degradation.

### 4.3 Results and Discussion

Electrospun $TiO_2$ fibers were prepared from a sol-gel precursor solution as described in the procedure and shown in Scheme 4-1. The solution was electrospun at 25 kV with an 11 cm working distance from copper tip to aluminum collector. The fibers formed under these conditions at room temperature had an average diameter of 500 nm and a smooth morphology. The fibers were calcined at 360 ℃ for 4 hours under an ambient atmosphere to form crystalline $TiO_2$ fibers. These fibers were used as the control group for all subsequent testing. The preformed, calcined fibers were soaked in a 5.29 M $Ru(dcbpyH_2)_2Cl_2$ dye solution to promote binding of the dye at the surface of the fiber. After soaking, the fibers were rinsed with ethanol to wash any unbound dye, leaving a uniform mono layer of dye.[20] Prior studies with derivatives of $Ru(dcbpyH_2)_2Cl_2$ have shown strong binding through the carboxylic acid function group to the surface of $TiO_2$ particles and thin films.[21] All of the samples were allowed to dry prior to further studies.

Scheme 4-1: Schematic procedure for the process of the fabrication of the $TiO_2$ fibers and dye sensitized fibers including sol-gel preparation, electrospinning of polymer sol-gel solution, calcination treatment of polymer fibers, and soaking in dye solution.

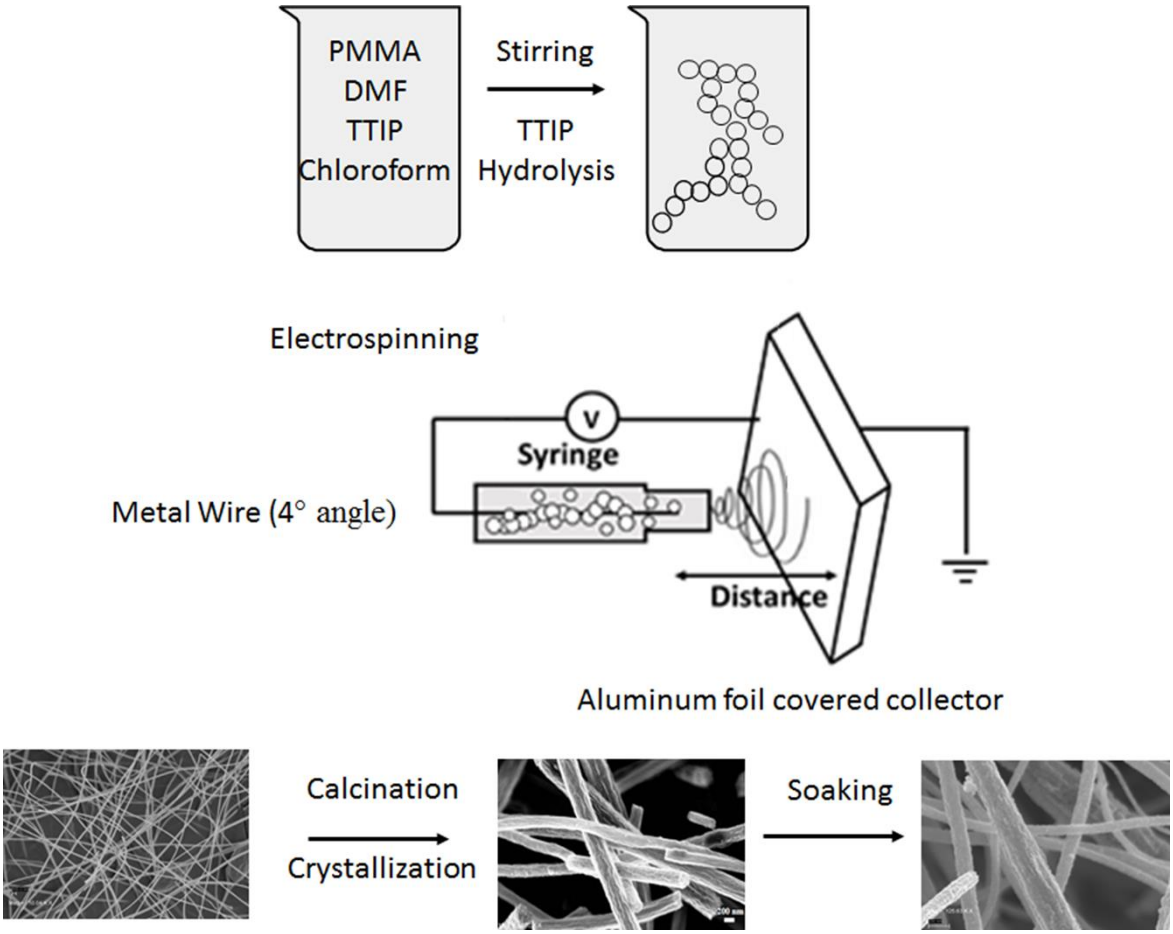


SEM images were obtained of the electrospun TTIP polymer fibers, post-calcined $TiO_2$ fibers and the $Ru(dcbpyH_2)_2Cl_2$-$TiO_2$ sensitized fibers. Figure 4-4a shows an SEM image of $TiO_2$ polymer fibers after electrospinning the sol-gel solution. The fibers are long with a smooth surface morphology. The average diameter of the polymer fiber was approximately 500 nm. Figure 4-4b shows an SEM image of $TiO_2$ fibers after calcination. Compared to 4-4a, the fibers in 4-4b are shorter and more rod like with a folded surface morphology. The lengths of the fibers are shorter due to breakage during the calcination process. The loss of carbon from the PMMA polymer during calcination also results in a

reduced average diameter to approximately 200 nm. Figure 4-4c shows the dye substituted $TiO_2$ to have a similar diameter and structure to those in 4-4b. However, there appears to be less of the folded morphology and a rougher surface morphology in this case.

a) 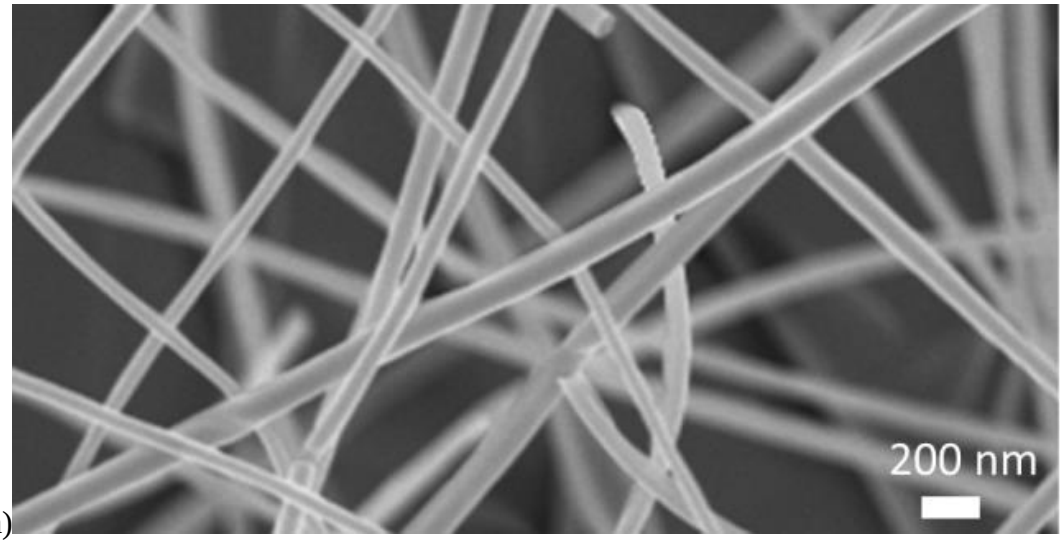


b) 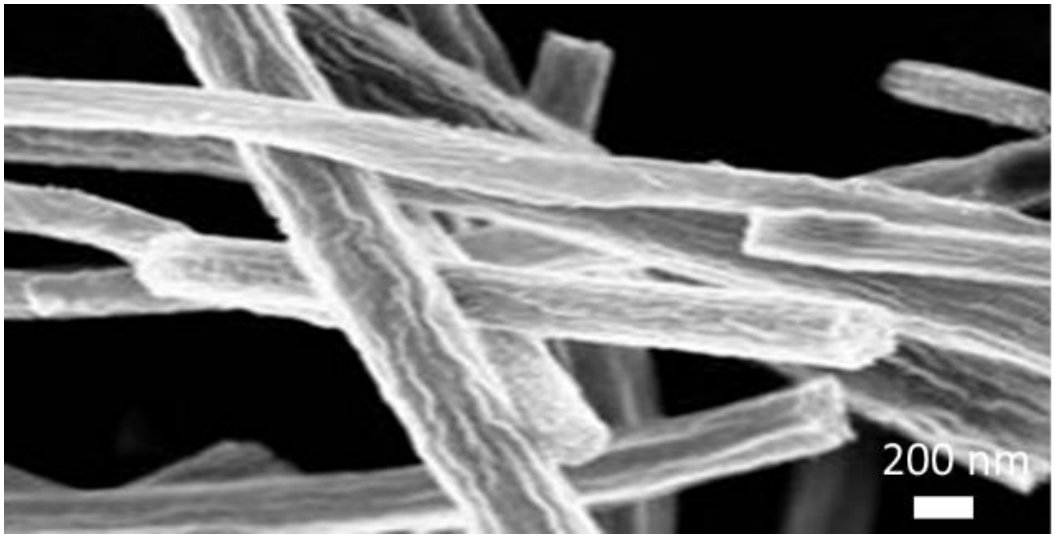

c) 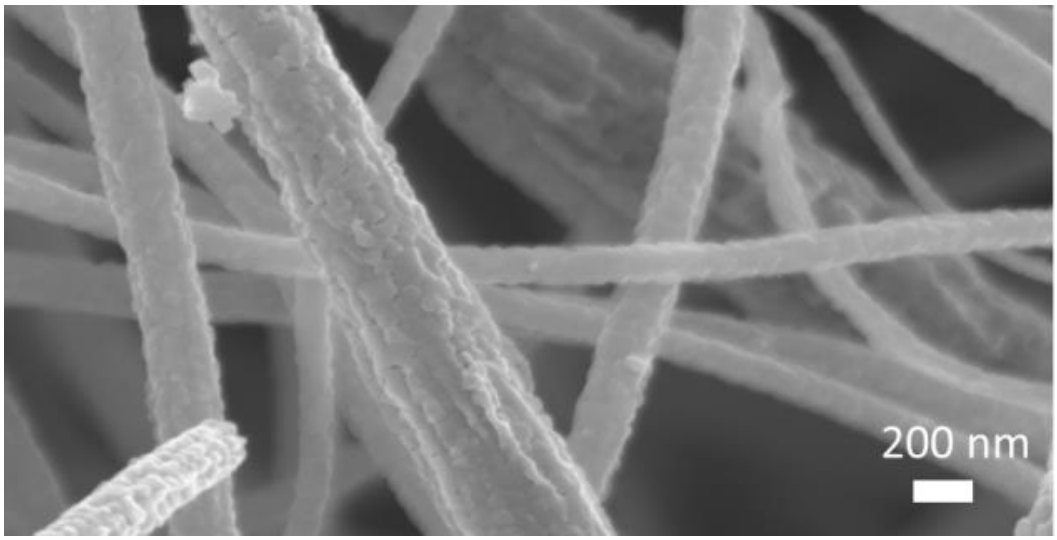


Figure 4-4. SEM image of a) $TiO_2$ polymer fibers after electrospinning b) $TiO_2$ fibers after calcination at 360 ℃ for 4 hours under ambient atmosphere and c) $Ru(dcbpyH_2)_2Cl_2$-$TiO_2$ fibers.

X-ray Diffraction (XRD) was used to confirm the formation of post calcination crystalline $TiO_2$ fibers prior to adding dye. For the anatase phase, the major peaks were obtained at 2θ values of 25.2, 37.9, 48.1, 54.0, and 55.0° representing the Miller indices of (101), (104), (200), (105), and (211) planes, respectively. For the rutile phase, peaks were observed at 2θ values of 27.4, 36.1, 41.3, and 54.4°, respectively, representing the Miller indices of (110), (101), (111), and (211) planes, respectively. The weight fraction of anatase-to-rutile transformation in the post-calcined $TiO_2$ fibers can be calculated from the equation of $W_R=1/[1+0.8(I_A/I_R)]$, where $I_A$ is the X-ray integrated intensities of the (101) reflection of anatase at 2θ of 25.2° and $I_R$ is that of the (110) reflection of rutile at 2θ of 27.4°.[22, 23] The $TiO_2$ fibers were determined to be 18% rutile based on the XRD in Figure 4-5. This anatase-to-rutile fraction was chosen because it is close to the fraction of Degussa P25 (25% rutile), which has been found to have better photocatalytic properties than pure anatase phase $TiO_2$.[24]

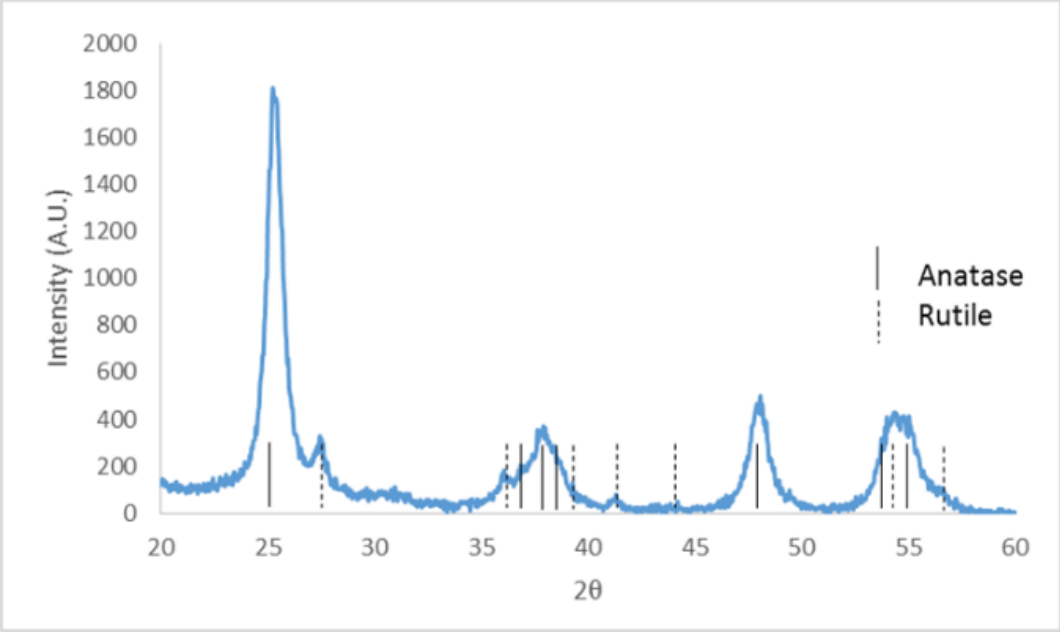


Figure 4-5: XRD data for post-calcined fibers showing an 18% rutile fraction. The solid vertical lines and dashed vertical lines represent pure anatase and rutile phase $TiO_2$ respectively.

FTIR spectroscopy was used to examine the binding of the $Ru(dcbpyH_2)_2Cl_2$ on the $TiO_2$ by comparing the pre and post soaked $TiO_2$ fibers shown in Figure 4-6. The splitting of the carbonyl peak in the dye at 1714 and 1605 $cm^{-1}$ is a result of protonation and deprotonation of the carboxylic acid group on the dye. When looking at the dye bound to $TiO_2$ there are no peaks above 1700 $cm^{-1}$ suggesting that only deprotonated dye is bound.[21] There is an observed shift from the fibers at 1631 $cm^{-1}$ to 1619 $cm^{-1}$ in the dye sensitized fibers. This is in the region of the carboxylic acid group showing binding of the dye to the $TiO_2$. The low intensity of the dye peaks in the dye-sensitized fibers is a result of a less than 1 wt.% loading of the dye on the fibers resulting in a weak signal.

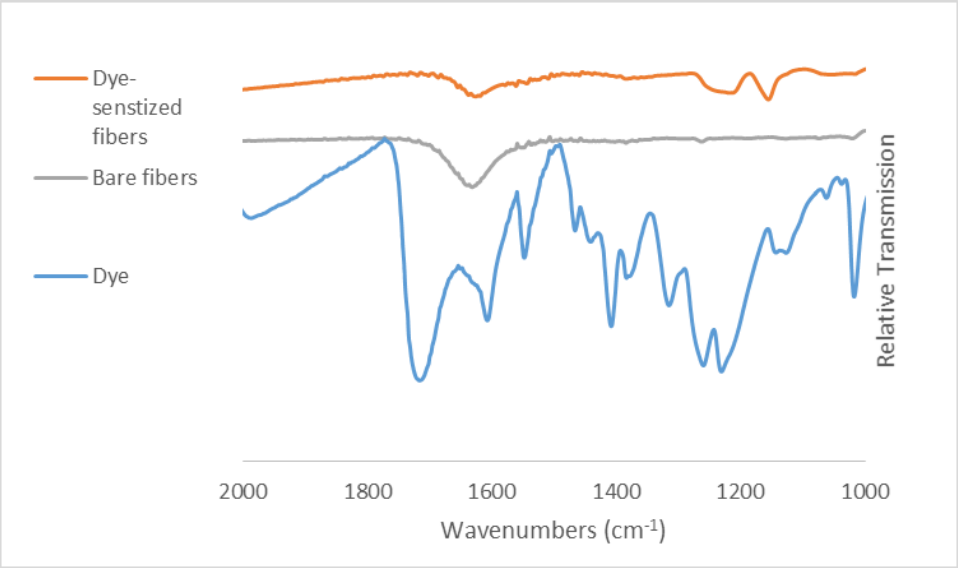


Figure 4-6: IR spectrum for the dye, $TiO_2$ fibers, and dye soaked $TiO_2$ fibers.

To explore the efficiency of the new materials as visible photocatalysts, degradations of PAP were conducted under both UV and visible irradiation in an aqueous solution. UV-Vis measurements were taken over time to monitor the changes in concentration of PAP. To determine the stability of the dye-sensitized fibers, an aqueous solution of fibers were irradiated with UV-light continuously for 53 h, showing no change in the absorbance. The dye sensitized fibers were compared to the control fibers, the dye, and samples with no catalyst under UV and visible irradiation to determine the role that the ruthenium dye plays in in the degradation process of PAP.

Two controls and two experiments were conducted in duplicate. These experiments used a quartz cell which would allow UV irradiation to penetrate to the sample. The first control used PAP solution with no catalyst. The second control used a solution containing $Ru(dcbpyH_2)_2Cl_2$ and PAP. Experiments used bare $TiO_2$ fibers or $Ru(dcbpyH_2)_2Cl_2$ – sensitized $TiO_2$ fibers as a catalyst in a PAP solution within a quartz cell. The

concentrations of PAP were tracked by measuring the absorbance at 424 nm over the course of 2 hours. The first hour (t = -60 to t =0) of the experiment was conducted in the dark to allow the adsorption of PAP to equilibrate. This allowed for the stirring of the photocatalyst and PAP and thus adsorption of PAP molecules onto the surface of $TiO_2$.[4] During the second hour of the experiment (t =0 to t = 60), the sample was irradiated with a UV lamp. While the UV lamp was on, there was no significant changes in the temperature of the reaction vessel. An aliquot of the solution was taken every 15 min which was centrifuged to remove any suspended catalyst. The sample was taken from the centrifuged solution, and diluted with deionized water before absorbance measurements were recorded.

Under the experimental conditions stated above, the UV-Vis absorption spectrum of the PAP degradation using $TiO_2$ fibers and $Ru(dcbpyH_2)_2Cl_2$ - sensitized $TiO_2$ fibers are shown in Figure 4-7. From the absorbance data, the initial rates of the reactions were determined to be first order based on the plot in Figure 4-8. Although the ratio of $TiO_2$ to PAP is 100:1, the reaction is not considered pseudo-first order. The molar ratio does not take into account only surface $TiO_2$ without dye adsorbed would be active in producing radicals, therefore no reactant is in excess. From the plot, the rate constant for the photodegradation of PAP using bare $TiO_2$ fibers and $Ru(dcbpyH_2)_2Cl_2$ - sensitized $TiO_2$ fibers were determined to be $0.032 \pm 0.003$ $min^{-1}$ and $0.012 \pm 0.002$ $min^{-1}$, respectively while the controls showed no degradation.

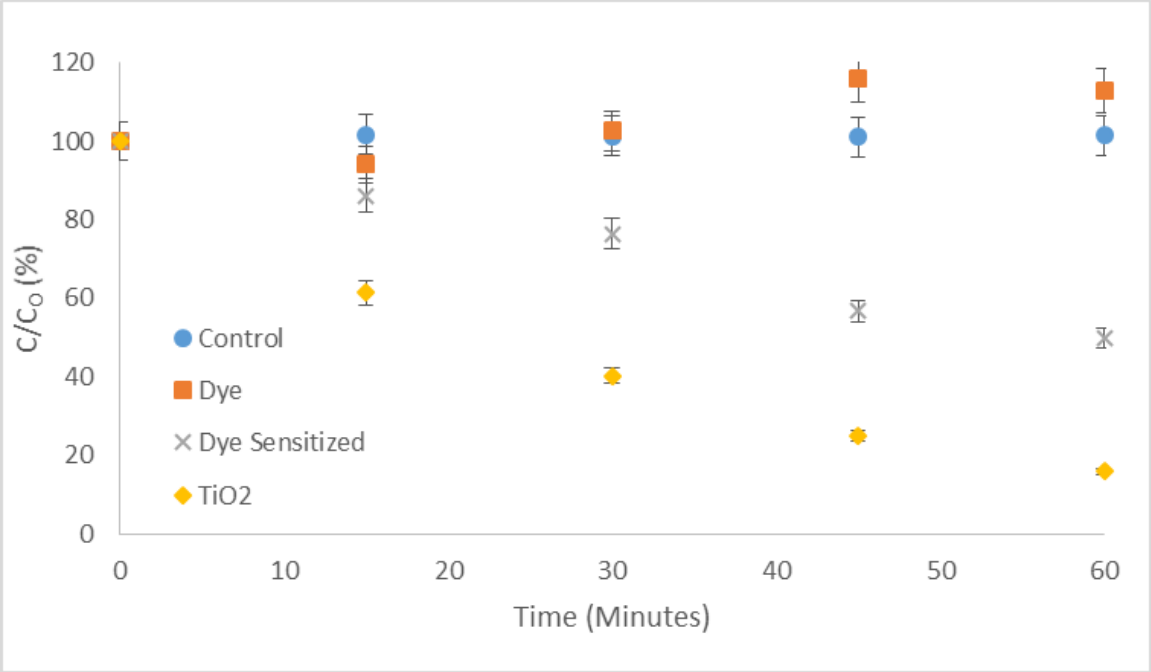


Figure 4-7. Absorption of PAP over time when exposed to no catalyst, $Ru(dcbpyH_2)_2Cl_2$ $TiO_2$ fibers and $Ru(dcbpyH_2)_2Cl_2$ - sensitized $TiO_2$ fibers in dark and under UV irradiation.

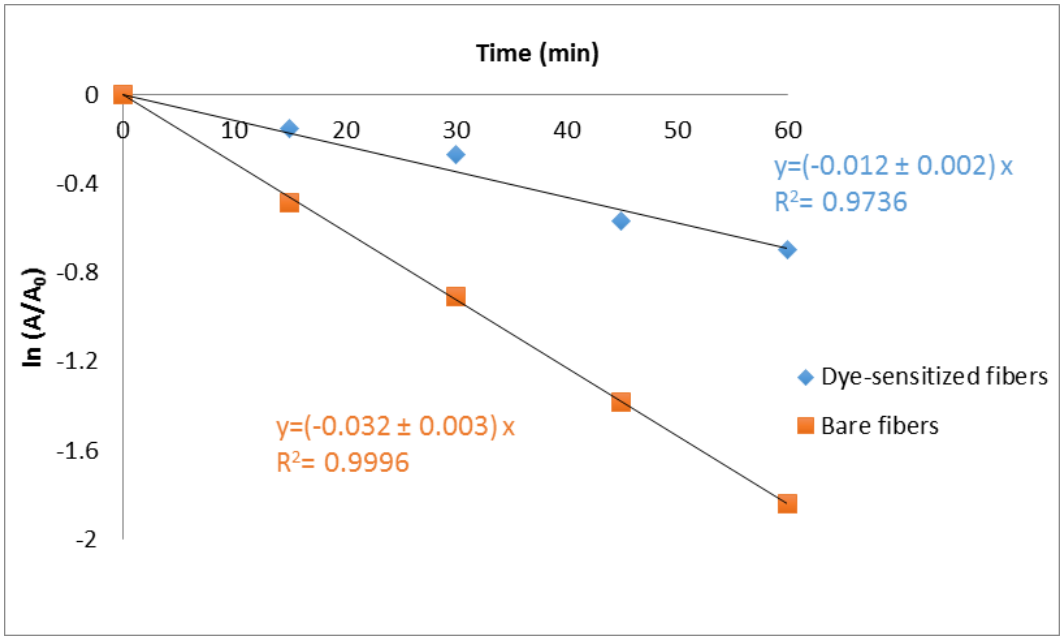


Figure 4-8: First order rate law plot for the degradation of PAP with $TiO_2$ fibers and $Ru(dcbpyH_2)_2Cl_2$ - sensitized $TiO_2$ fibers under UV/visible irradiation.

An equivalent experiment was carried out in a glass beaker which was chosen to filter light at energies higher than 320 nm, therefore blocking any UV irradiation from

being absorbed by the catalyst. Again the concentration during the reaction was monitored using UV Vis as shown in Figure 4-9. Like previously, no degradation was observed for the controls. From the absorbance data, the initial rates were again determined to be first order rate law, this time having 0.014 ± 0.001 $min^{-1}$ and 0.012 ± 0.0002 $min^{-1}$ for $TiO_2$ fibers and $Ru(dcbpyH_2)_2Cl_2$ - sensitized $TiO_2$ fibers respectfully as shown in Figure 4-10.

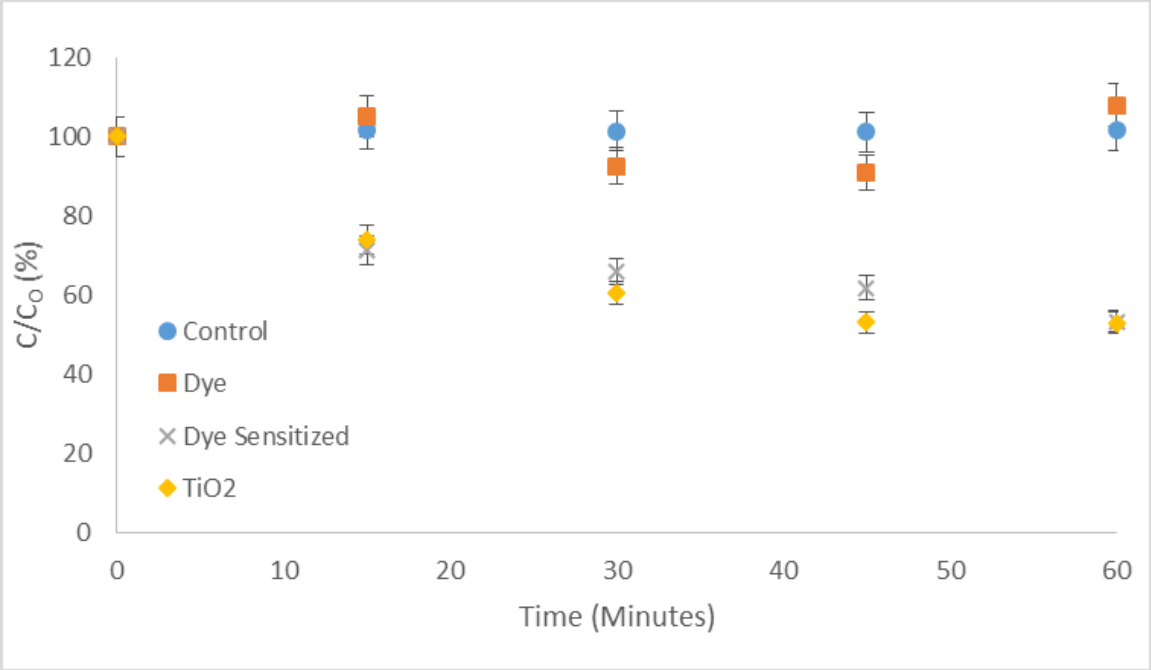


Figure 4-9: Absorption of PAP over time when exposed to no catalyst, $Ru(dcbpyH_2)_2Cl_2$, $TiO_2$ fibers and $Ru(dcbpyH_2)_2Cl_2$ - sensitized $TiO_2$ fibers in dark and under visible irradiation.

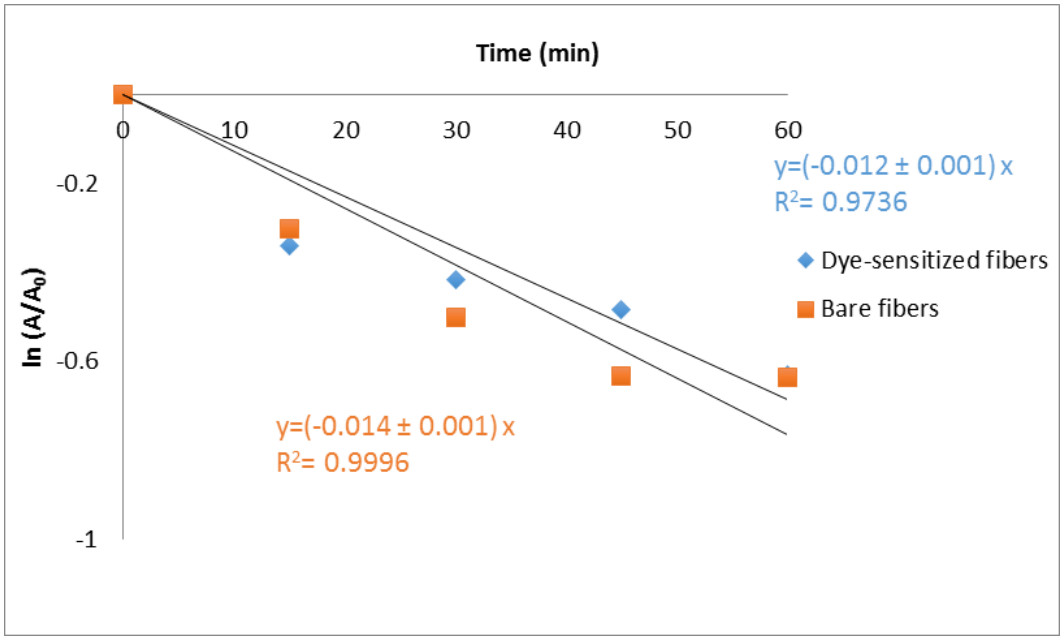


Figure 4-10. First order rate law plot for the degradation of PAP with $TiO_2$ fibers and $Ru(dcbpyH_2)_2Cl_2$ - sensitized $TiO_2$ fibers under visible irradiation.

The results in Table 4-1 show that PAP is stable in an aqueous solution both with and without the dye present when irradiated with either UV or visible light. The most efficient catalyst was found to be the bare $TiO_2$ fibers under UV irradiation. A decrease in the rate of degradation was observed when going from UV to visible irradiation with non-sensitized $TiO_2$. The band gap of $TiO_2$ is in the UV region meaning it will absorb light and create the most electron-hole pairs in the UV range. The initial rate for the $TiO_2$ fibers when exposed to visible light were similar to the $Ru(dcbpyH_2)_2Cl_2$– sensitized $TiO_2$ fibers when exposed to both UV and visible irradiation. All the fibers with similar rates were all lower in rate than the bare fibers under UV irradiation. The decrease in the initial rate going from the bare fibers under UV irradiation to the dye sensitized fibers under UV irradiation suggests there is a charge transfer from the dye, resulting in a decrease in efficiency.

Table 4-1. Initial rate constants of PAP degradation using $TiO_2$ fibers and $Ru(dcbpyH_2)_2Cl_2$– sensitized $TiO_2$ fibers in quartz vial and glass beaker.

| Photocatalyst | Quartz vial (UV/Visible Irradiation) | Glass beaker (Visible Irradiation) |
|---|---|---|
| No Catalyst | No degradation | No degradation |
| $Ru(dcbpyH_2)_2Cl_2$ | No degradation | No degradation |
| $TiO_2$ Fibers | $0.032 \pm 0.003$ $min^{-1}$ | $0.014 \pm 0.001$ $min^{-1}$ |
| $Ru(dcbpyH_2)_2Cl_2$– sensitized $TiO_2$ Fibers | $0.012 \pm 0.002$ $min^{-1}$ | $0.012 \pm 0.001$ $min^{-1}$ |

The role of the dye was to absorb light in the visible region through a metal to ligand charge transfer (MLCT) transition. This has previously been shown to inject electrons into the $TiO_2$ conduction band.[7,8] This process would help expand the region of absorption and electron-hole separation following injection as shown in step 1 and 2 of Figure 4-11. There are competing pathways that decrease efficiency and electron-hole separation under visible irradiation, namely, steps 3 (back electron transfer) and 6 (electron reaction with oxygen). If the rate for the recombination is faster than the rate of radical formation, there will be a decrease in radical formation. This decrease in radical formation will be further amplified under UV irradiation because the $TiO_2$ will be populating the conduction band with electrons from the valence band. A similar mechanism has been shown with the use of 2,4,6-triphenylpyrilium hydrogen sulfate (TPPHS) as a photosensitizer.[6] It was found using TPPHS as a photosensitizer increased the rate under UV irradiation, while there was a reduction in the rate during visible irradiation compared to bare $TiO_2$. This was attributed to the increase electron hole separation under UV

irradiation. Another example uses CdS as a photosensitizer which was able to increase the rate under visible light, however the material leached $Cd^{2+}$ showing the instability of the material.[5] These examples of surface modifications showing enhancement in the degradation rate suggestions binding to the $TiO_2$ surface can still improve degradation. This supports the observed decrease in rate being a function of electron pathway over the reduction of active sites on $TiO_2$. These examples, along with the results in this paper, show three different results when using different photosensitizers, showing different mechanisms. All of this suggests surface modification of $TiO_2$ with photosensitizers is a more complex system than in a DSSC.[4-6, 25]

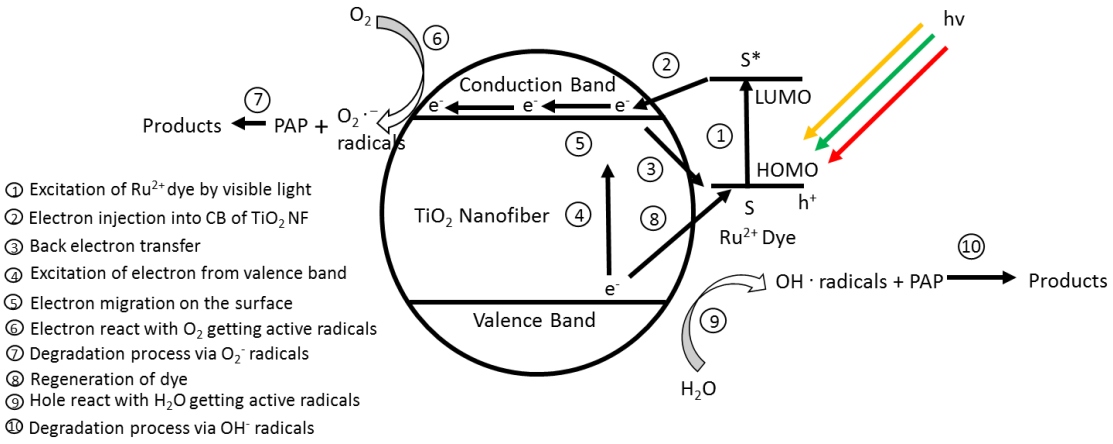


Figure 4-11: Proposed mechanism for formation of radicals from dye-sensitized $TiO_2$ fibers.

Ruthenium polypyridyl dyes are known electron injectors, increasing the population of electrons in the conduction band of the $TiO_2$.[7-12] There has been previous attempts to use ruthenium dyes to enhance the rate of degradation under visible irradiation.[26 27] These examples showed no enhancement under visible irradiation, but did not test the material under UV irradiation as presented here. The decrease in rate of

degradation under UV irradiation when dye is attached supports the preferred pathway for the degradation of PAP progressing through the formation of hydroxyl radicals.

PAP has been explored previously in the literature, examining the effect of pH, ozone, and reactive oxygen species on the degradation rate of PAP.[28] It was determined that pH and amount of ozone play a role in promoting charge separation in the $TiO_2$.[28] Gaseous oxygen showed no improvement because the electron transfer is too slow.[28 29] When a hydroxyl radical scavenger ($NaH_2PO_4$) was added, the degradation was significantly reduced, supporting the results above. Instead of using electron injecting surface modifications, hydroxyl radical formation and charge separation could be enhanced with a hole transport modification such as introduction of poly(ethylene dioxythiophene) (PEDOT). PEDOT has been shown to enhance the photocatalytic performance of different semiconductors.[30,] There are other materials which could also be explored and which are known hole transporting materials such as NiO.

### 4.4 Conclusion

The results suggest that the electron transfer from the conduction band of $TiO_2$ does not play a major role in the degradation of PAP. This is based on the decrease in rate of degradation from $TiO_2$ fibers to dye sensitized $TiO_2$ fibers under UV irradiation and the consistent rate for the dye sensitized $TiO_2$ fibers. It is possible that the degradation efficiency would be improved with the use of a hole-transport dye which would increase the radicals formed from the valence band of $TiO_2$.

## 4.5 References


1. Herrmann, J. M.; Duchamp, C.; Karkmaz, M.; Hoai, B. T.; Lachheb, H.; Puzenat, E.; Guillard, C., Environmental green chemistry as defined by photocatalysis. *Journal of Hazardous Materials* **2007,** *146* (3), 624-629.

2. Zyoud, A.; Zaatar, N.; Saadeddin, I.; Helal, M. H.; Campet, G.; Hakim, M.; Park, D.; Hilal, H. S., Alternative natural dyes in water purification: Anthocyanin as TiO2-sensitizer in methyl orange photo-degradation. *Solid State Sciences* **2011,** *13* (6), 1268-1275.

3. Carp, O.; Huisman, C. L.; Reller, A., Photoinduced reactivity of titanium dioxide. *Progress in Solid State Chemistry* **2004,** *32* (1–2), 33-177.

4. Wang, Y.; Huang, Y.; Ho, W.; Zhang, L.; Zou, Z.; Lee, S., Biomolecule-controlled hydrothermal synthesis of C–N–S-tridoped TiO2 nanocrystalline photocatalysts for NO removal under simulated solar light irradiation. *Journal of Hazardous Materials* **2009,** *169* (1–3), 77-87.

5. Zyoud, A. H.; Zaatar, N.; Saadeddin, I.; Ali, C.; Park, D.; Campet, G.; Hilal, H. S., CdS-sensitized TiO2 in phenazopyridine photo-degradation: Catalyst efficiency, stability and feasibility assessment. *Journal of Hazardous Materials* **2010,** *173* (1–3), 318-325.

6. Hilal, H. S.; Majjad, L. Z.; Zaatar, N.; El-Hamouz, A., Dye-effect in TiO2 catalyzed contaminant photo-degradation: Sensitization vs. charge-transfer formalism. *Solid State Sciences* **2007,** *9* (1), 9-15.

7. Antila, L. J.; Myllyperkiö, P.; Mustalahti, S.; Lehtivuori, H.; Korppi-Tommola, J., Injection and Ultrafast Regeneration in Dye-Sensitized Solar Cells. *The Journal of Physical Chemistry C* **2014,** *118* (15), 7772-7780.

8. Falaras, P., Synergetic effect of carboxylic acid functional groups and fractal surface characteristics for efficient dye sensitization of titanium oxide. *Solar Energy Materials and Solar Cells* **1998,** *53* (1–2), 163-175.

9. Listorti, A.; O'Regan, B.; Durrant, J. R., Electron Transfer Dynamics in Dye-Sensitized Solar Cells. *Chemistry of Materials* **2011,** *23* (15), 3381-3399.

10. Pastore, M.; De Angelis, F., Intermolecular Interactions in Dye-Sensitized Solar Cells: A Computational Modeling Perspective. *The Journal of Physical Chemistry Letters* **2013,** *4* (6), 956-974.

11. Mukherjee, K.; Teng, T.-H.; Jose, R.; Ramakrishna, S., Electron transport in electrospun TiO2 nanofiber dye-sensitized solar cells. *Applied Physics Letters* **2009,** *95*, 012101.

12. Yang, L.; Woon-Fong Leung, W., Application of a Bilayer TiO2 Nanofiber Photoanode for Optimization of Dye-Sensitized Solar Cells. *Advanced Materials* **2011,** *23* (39), 4559--4562.

13. De Angelis, F.; Fantacci, S.; Selloni, A.; Nazeeruddin, M. K., Time dependent density functional theory study of the absorption spectrum of the [Ru(4,4′-COO−-2,2′-bpy)2(X)2]4− (X = NCS, Cl) dyes in water solution. *Chemical Physics Letters* **2005,** *415* (1–3), 115-120.

14. De Angelis, F.; Fantacci, S.; Selloni, A., Alignment of the dye's molecular levels with the TiO2 band edges in dye-sensitized solar cells: a DFT–TDDFT study. *Nanotechnology* **2008,** *19* (42), 424002.

15. Liu, J.; McCarthy, D. E.; Cowan, M. J.; Obuya, E. A.; Decoste, J. B.; Skorenko, K. H.; Tong, L.; Boyer, S. M.; Bernier, W. E.; Jones Jr, W. E., Photocatalytic activity of TiO2 polycrystalline sub-micron fibers with variable rutile fraction. *Applied Catalysis B: Environmental* **2016,** *187*, 154-162.

16. Chatzitakis, A.; Berberidou, C.; Paspaltsis, I.; Kyriakou, G.; Sklaviadis, T.; Poulios, I., Photocatalytic degradation and drug activity reduction of Chloramphenicol. *Water Research* **2008,** *42* (1–2), 386 - 394.

17. Nazeeruddin, M. K.; Kay, A.; Rodicio, I.; Humphry-Baker, R.; Mueller, E.; Liska, P.; Vlachopoulos, N.; Graetzel, M., Conversion of light to electricity by cis-X2bis(2,2'-bipyridyl-4,4'-dicarboxylate)ruthenium(II) charge-transfer sensitizers (X = Cl-, Br-, I-, CN-, and SCN-) on nanocrystalline titanium dioxide electrodes. *Journal of the American Chemical Society* **1993,** *115* (14), 6382-6390.

18. Obuya, E. A.; Harrigan, W.; Andala, D. M.; Lippens, J.; Keane, T. C.; Jones Jr, W. E., Photodeposited Pd nanoparticle catalysts supported on photoactivated TiO2 nanofibers. *Journal of Molecular Catalysis A: Chemical* **2011,** *340* (1–2), 89-98.

19. Obuya, E. A.; Joshi, P. C.; Gray, T. A.; Keane, T. C.; Jones Jr., W. E., *Application of Pt.TiO2 Nanofibers in Photosensitized Degradation of Rhodamine B*. 2013; Vol. 6.

20. O'Regan, B. C.; Durrant, J. R., Kinetic and Energetic Paradigms for Dye-Sensitized Solar Cells: Moving from the Ideal to the Real. *Accounts of Chemical Research* **2009,** *42* (11), 1799-1808.

21. Finnie, K. S.; Bartlett, J. R.; Woolfrey, J. L., Vibrational Spectroscopic Study of the Coordination of (2,2‘-Bipyridyl-4,4‘-dicarboxylic acid)ruthenium(II) Complexes to the Surface of Nanocrystalline Titania. *Langmuir* **1998,** *14* (10), 2744-2749.

22. Su, R.; Bechstein, R.; Sø, L.; Vang, R. T.; Sillassen, M.; Esbjörnsson, B.; Palmqvist, A.; Besenbacher, F., How the Anatase-to-Rutile Ratio Influences the Photoreactivity of TiO2. *The Journal of Physical Chemistry C* **2011,** *115* (49), 24287-24292.

23. Zachariah, A.; Baiju, K. V.; Shukla, S.; Deepa, K. S.; James, J.; Warrier, G. K., Synergistic Effect in Photocatalysis As Observed for Mixed-Phase Nanocrystalline Titania

Processed via Sol−Gel Solvent Mixing and Calcination. *Journal of Physical Chemistry C* **2008,** *112* (30), 11345-11356.

24. Hurum, D. C.; Agrios, A. G.; Gray, K. A.; Rajh, T.; Thurnauer, M. C., Explaining the Enhanced Photocatalytic Activity of Degussa P25 Mixed-Phase TiO2 Using EPR. *The Journal of Physical Chemistry B* **2003,** *107* (19), 4545-4549.

25. Hodak, J.; Quinteros, C.; Litter, M. I.; San Roman, E., Sensitization of $TiO_2$ with phthalocyanines. Part 1.—Photo-oxidations using hydroxoaluminium tricarboxymonoamidephthalocyanine adsorbed on TiO2. *Journal of the Chemical Society, Faraday Transactions* **1996,** *92* (24), 5081-5088.

26. Cho, Y.; Choi, W.; Lee, C.-H.; Hyeon, T.; Lee, H.-I., Visible Light-Induced Degradation of Carbon Tetrachloride on Dye-Sensitized TiO2. *Environmental Science \& Technology* **2001,** *35* (5), 966-970.

27. Bae, E.; Choi, W., Highly Enhanced Photoreductive Degradation of Perchlorinated Compounds on Dye-Sensitized Metal/TiO2 under Visible Light. *Environmental Science \& Technology* **2003,** *37* (1), 147-152.

28. Fathinia, M.; Khataee, A., Photocatalytic ozonation of phenazopyridine using TiO2 nanoparticles coated on ceramic plates: mechanistic studies, degradation intermediates and ecotoxicological assessments. *Applied Catalysis A: General* **2015,** *491*, 136 - 154.

29. Gilbert, E., Influence of Ozone on the Photocatalytic Oxidation of Organic Compounds. *Ozone: Science \& Engineering* **2002,** *24* (2), 75-82.

30. Liu, J. Fabrication, Optimization and Functionalization of Electrospun $TiO_2$ Nanofiberous Materials for use in Photodegradation of Environmental Toxins. Binghamton University, Binghamton, NY, 2015.

# Chapter 5

# Fabrication and Characterization of Electrospun Conducting Fibers for Piezoelectric Materials

## 5.1 Introduction

Intrinsically conducting polymers (ICP) or "synthetic metals" are polymers that that have electrical, magnetic and optical properties common of metals and semiconductors.[1] ICPs have been explored for their applications in flexible organic electronic devices including photovoltaics, light-emitting diodes, sensors, actuators and thin-film transistors.[2] Polymer nano fibers have drawn interest based on the large surface area to volume ratio achieved when fibers become sub-micron in diameter.[3] Nanofibers have been found to have superior mechanical properties and flexibility in surface functionalities compared to other forms of the same material.[3] This has led to conducting nanofibers being developed for controlled drug release, membranes for ultrafast lasers, liquid separation, solar cells and as chemical sensors.[1, 4-7] The range of applications of conducting fibers makes it important to continue to develop better materials.

A popular method of fabricating conductive fibers is the electrospinning method.[1, 3, 8] Electrospinning uses an electric field to create a jet of polymer solution. As the solution travels through the air, the solvent evaporates leaving behind a charged fiber that is collected on a conducting collector as shown in Figure 5-1.[9] Electrospinning is a versatile method that can be tuned to produce a broad range of materials because of the range of

solvents and materials that can be incorporated into the precursor solution allowing for composite materials.[3] The properties of the materials can further be changed by changing the viscosity, conductivity and surface tension of the solution or the electric potential and distance between the collector and tip.[9]

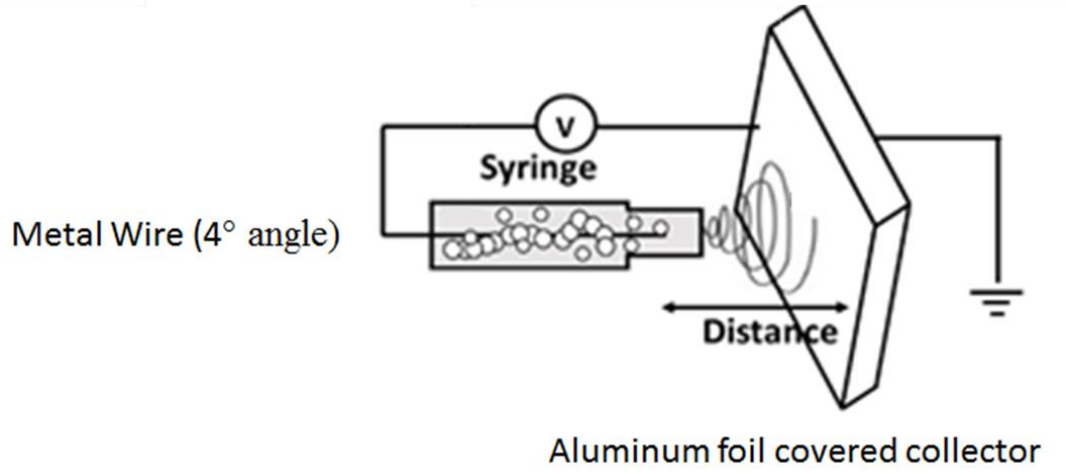


Figure 5-1: Electrospinning method using a copper wire tip and an aluminum collector.

Electrospinning solutions use high molecular weight polymers to increase the interactions of the polymers in solution to increase the viscosity of the solution.[10] Since most conductive polymers are either low molecular weight or insoluble presenting challenges for electrospinning. To overcome this, a high molecular weight polymer can be used as a template polymer. There are several different template polymers that have been used including Poly(methyl methacrylate) (PMMA), shown in Figure 5-2. PMMA is a polymer that has been well studied in electrospinning because of the control of the fiber diameter based on the electrospinning conditions.[11] PMMA has also been a popular choice in the literature for forming composites with carbon based materials or the fabrication of $TiO_2$ nano fibers.[4, 12-14] The ability to use PMMA in a range of composite materials makes

it an attractive candidate as a template polymer. One challenge in using PMMA as a template polymer is it is an insulator. Because of this, it is important to consider other template polymers.

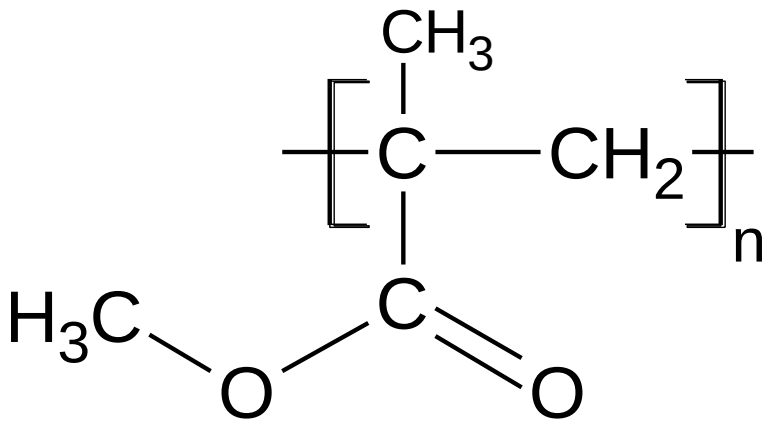


Figure 5-2: Chemical structure of the polymer PMMA.

Another option of a template polymer is polyvinylidene fluoride (PVDF) shown in Figure 4-3. PVDF is a known piezoelectric polymer that has been used for actuators, drug delivery and sensors with the chemical structure shown in Figure 5-3. PVDF is commonly used as a membrane material in lithium ion batteries because it is chemically inert with the electrolyte solution.[5] This would help make the resulting device using PVDF stable, preventing ions from mixing until sensitized with an electric field. One of the unique properties of PVDF is as a piezoelectric material, it has a negative $d_{33}$ value which means when an electric field is applied, the polymer will compress instead of expand. PVDF has previously been used to prepare electrospun fibers, supporting the use as a template polymer.[15-17]

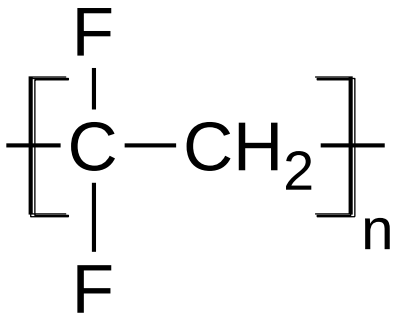


Figure 5-3: Chemical structure of the polymer PVDF

The polymer poly(vinylidene fluoride-hexafluoro propylene) (PVDF-HFP) is a copolymer based on PVDF as shown in Figure 5-4. PVDF-HFP has been used as a polymer electrolyte because of its conductivity and cycling behavior.[18] Like PVDF, PVDF-HFP has known piezoelectric properties which would increase the applications of fibers prepared using the polymer as a template polymer.[19] PVDF-HFP is also a polymer that has been electrospun, making it a candidate for a template polymer.[20, 21]

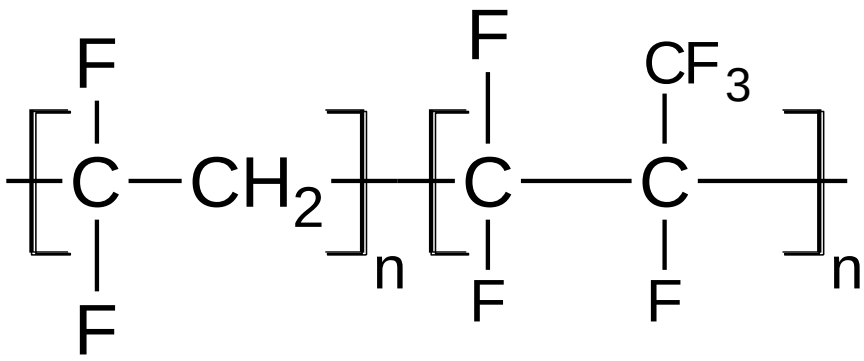


Figure 5-4: Chemical structure of the polymer PVDF-HFP

Because PVDF and PVDF-HFP are piezoelectric material, the fibers can be used to develop an electroactive material. The piezoelectric material acts as the ion in shown in Figure 5-5 and the ICP acts as the electrode. When an electric field is produced, the ions

will align, resulting in a conformational change. Electroactive polymers have particular interest in the biomedical field as an actuator or artificial muscle.[22]

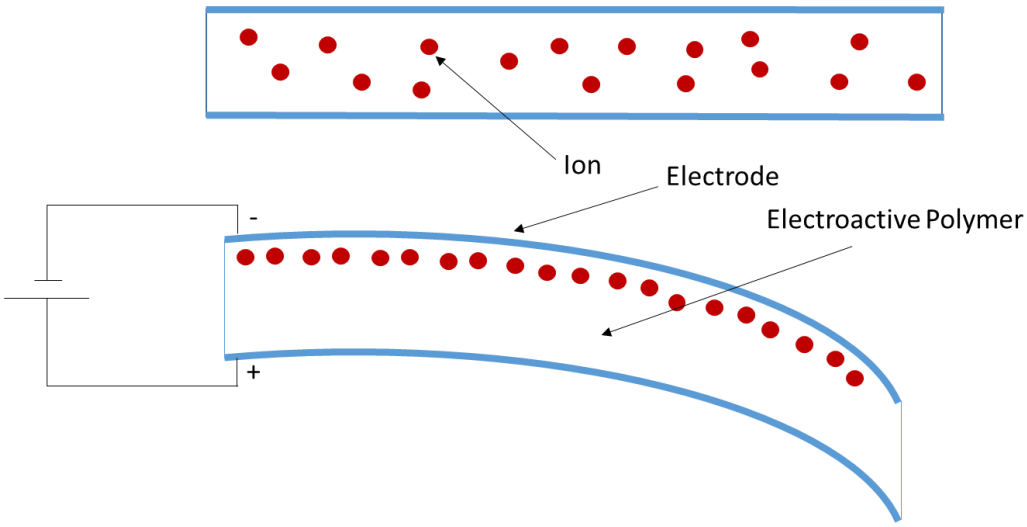


Figure 5-5: Mechanism for the conformational change that occurs in an electroactive polymer when an electric field is applied.

To make a conducting composite material, one method is incorporating a conducting material such as carbon into the fibers. Conductive fillers such as carbon black, graphene, carbon nanotubes, and expanded graphite have been used with polymers such as Nylon 6 and PMMA to increase the conductivity of composites.[4, 12, 23, 24] Graphene nano platelets (GNPs) are a class of material that has small stacks of graphene usually 1-15 nm thick.[25] GNPs can be dispersed into composites and have been shown to improve the electrical and thermal conductivity, fracture toughness and storage modulus of nano-composite materials.[25]

An alternative to using GNPs is incorporating an intrinsically conducting polymer (ICP) in the fibers. Conductive polymers have been explored for their potential as a cheaper alternative to metal based electrodes.[26-28] One conducting polymer that has received interest is poly(3,4-ethylenedioxythiophene) (PEDOT) as shown in Figure 5-6.

As discussed previously, PEDOT is an insoluble polymer so an *in situ* method of growing the polymer is required to add it to the PMMA polymer template. The *in situ* method used was a vapor phase polymerization (VPP) method which has shown to give some of the highest conductivities reported in the literature.[2, 29, 30] To use VPP, an oxidant is required to initiate the polymerization of the monomer 3,4-ethylenedioxythiophene (EDOT) which is in the vapor phase. The oxidant used is iron(III) p-toluenesulfonate (FePTs) since it has given some of the highest reported conductivity values of PEDOT films.[2, 31]

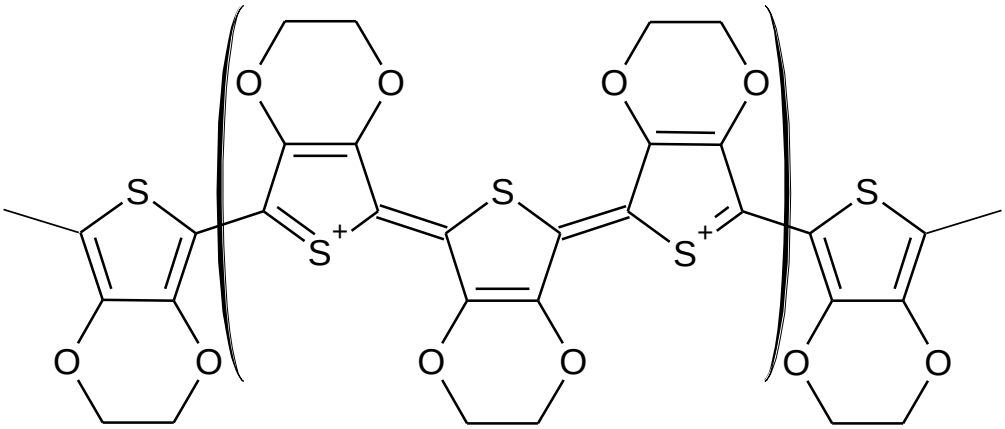


Figure 5-6: Molecular structure of the conductive polymer poly(3,4-ethylenedioxythiophene) (PEDOT).

Previous work has looked at fabricating conducting fibrous composite material using carbon or conducting polymers.[4, 7, 8, 32] The conductivity of the electrospun fibrous mats have been much lower than thin films of similar materials. For this reason, new combinations of conducting materials and template polymers need to be explored. This chapter focuses on the fabrication and characterization of fibrous mats containing either graphene nanoplatelets or PEDOT as a conductive material using PMMA, PVDF, and PDFV-HFP as a template material.

## 5.2 Experimental

### 5.2.1 Materials

All materials were purchased commercially and used as received unless otherwise indicated. Poly(methyl methacrylate) 350k g/mol (PMMA), polyvinylidene fluoride (275k g/mol), poly(vinylidene fluoride-hexafluoro propylene) (455k g/mol) anhydrous dimethylformamide (DMF), iron (III) p-toluenesulfonate hexahydrate (FePTs) and ethanol were purchased from Sigma-Aldrich. Chloroform, isopropanol, pyridine, and acetone were purchased from Fisher.

### 5.2.2 General Methods

The polymer fibers were fabricated using a high voltage Spellman SL 30 generator. Scanning electron microscopy (SEM) images were obtained on a FESEM, Supra 55 VP from Zeiss. Conductivity was measured using a two-point probe method. Two pieces of stainless steel metal electrodes (1.5 $cm^2$ surface area) were pressed with fibers between to ensure good contact. The resistance was measured with a voltmeter and the thickness was measured with a micrometer.

### 5.2.3 Preparation of Electrospun Fibers

#### Preparation of PMMA Electrospun Fibers

Generally, the PMMA fibers were fabricated using an electrospinning method as described in the overview section. The fibers were spun from a solution that contained 320 mg PMMA (350k g/mol) in 2 mL of chloroform and 2 mL of DMF. From here the process could be modified to functionalize the PMMA fibers to make them conductive.

**Preparation of PMMA-graphene Infused Electrospun Fibers**

To make the PMMA fibers conductive allowing for the aligning of ions required for a conformational change, 3, 6, and 9 wt% graphene nanoplatelets (NPs) were added to the PMMA solution prior to electrospinning. These solutions were electrospun at 25 kV and a working distance of 18 cm from the copper tip to the aluminum collector.

**Fabrication of PEDOT/PMMA Fibers**

Two methods were used for the fabrication of PEDOT/PMMA fibers. For the fabrication of the PMMA/PEDOT fibers, PMMA fibers were aquired through the electrospinning method previously discussed. The fibers were then soaked in an oxidant solution before undergoing the VPP process.

**Fabrication of PEDOT/PVDF Fibers**

A solution of 0.7345 g PVDF (275k MW) was dissolved in 4 mL DMF and 2 mL acetone which was electrospun at 15 kV and 11cm working distance. A 0.13 g sample of the resulting fibers was soaked in 3 mL of a 0.1g/1 mL solution of FePTs in ethanol with 21 µL pyridine for 1 hour. The fibers were removed and dried overnight before undergoing VPP at 60 °C for 2 hours.

For PVDF fibers fabricated with preloading of the oxidant, a solution was prepared with 0.3863 g PVDF (275, 000 g/mol) and 0.2277 FePTs in 2 mL DMF, 1 mL acetone and 14 µL pyridine. The fibers were electrospun at 20 kV and 15 cm working distance.

### Fabrication of PEDOT/PVDF-HFP Fibers

For PVDF-HFP fibers fabricated by soaking fibers prepared from a solution of 0.7808 g PVDF-HFP (455,000 MW) in 4 mL DMF and 2 mL acetone. The fibers were electrospun at 15 kV and 11 cm working distance.

## 5.3 Results and discussion

PMMA fibers were fabricated using an electrospinning method as described in the overview section. The fibers were spun from a solution that contained 320 mg PMMA (350k g/mol) in 2 mL of chloroform and 2 mL of DMF with 3, 6 and 9 wt% graphene nanoparticles added to the solution. The 9wt% was the limit for graphene loading based the dispersion of the nanoparticles in solution. Larger wt% of graphene would settle, clogging the syringe, preventing the formation of fibers. The resulting fibers were gray in color, getting darker as more graphene was added as shown in Figure 5-7.

Figure 5-7: Electrospun PMMA doped with 3, 6, and 9 wt% graphene NPs (from left to right).

The conductivity of the fibers were measured using 4-point probe showing the fibers were insulating except for the 9 wt% fibers which had a sheet resistance of 2-5 kΩ. SEM was used to look at the surface morphology of the electrospun PMMA fibers. The SEM shown in Figure 5-8 is from the 9 wt% graphene NP PMMA fiber. The SEM showed the graphene NPs aggregated on the surface of the PMMA. This would mean the graphene is not evenly dispersed throughout the fibers which would explain the low conductivity of the fibers. To have an electroactive polymer, the ions need to align throughout the entire sample. Having the aggregates would prevent this from happening, limiting the confirmation change of the material. This would mean that graphene would need to be replaced with another conducting material.

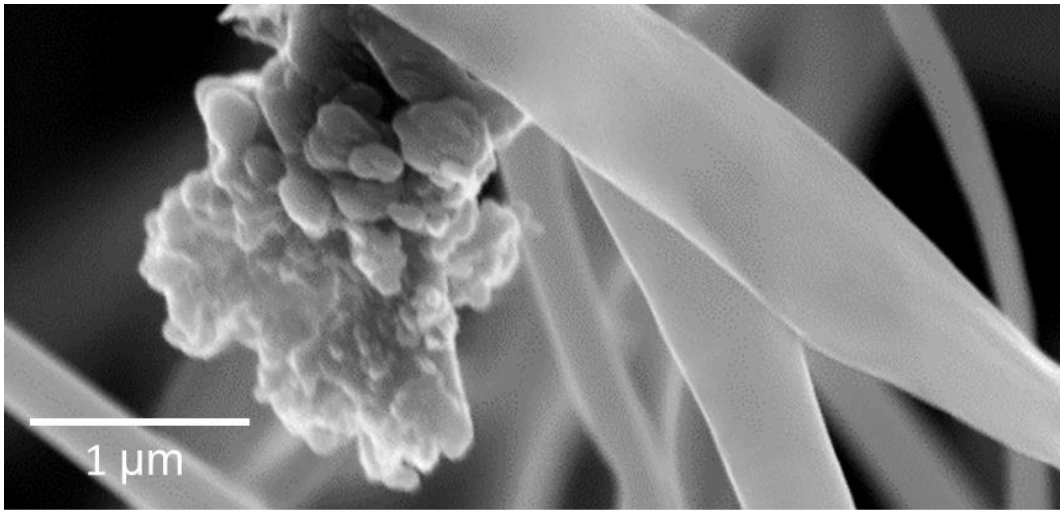


Figure 5-8: SEM image of PMMA with 9 wt% graphene nano platelets loaded.

An alternative to incorporating graphene into the polymer matrix is using a conducting polymer such as PEDOT. As previously discussed, PEDOT can be fabricated through a variety of methods including a VPP method. The oxidant for VPP can be added either prior to electrospinning or the fibers can be soaked after as shown in Scheme 5-1. After the oxidant loaded fibers have been prepared, they are placed in a vacuum oven in the presence of the monomer EDOT to form the PMMA-PEDOT fibers.

Scheme 5-1 Two methods for fabricating PMMA-PEDOT fibers depending on when the oxidant is added to the fibers.

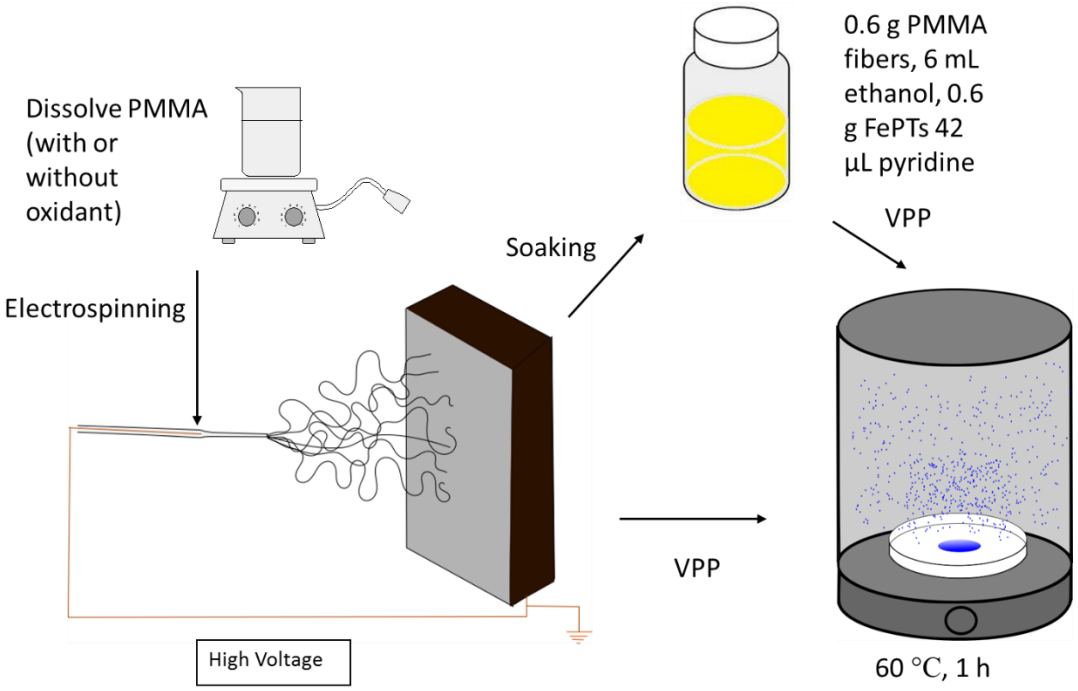


Although both methods of loading the oxidant produced PMMA-PEDOT fibers, the mechanical properties varied. The fibers that were spun with the oxidant retained the light weight, soft mechanical properties of the PMMA fibers. The fibers that were soaked in the oxidant solution became more solid and rigid. SEM of the fibers in Figure 5-9 a and b show the soaked fibers have cross-linking between the fibers likely caused by the VPP process. The fibers spun with the oxidant present in the precursor solution do not appear to have the cross-linking junctions as shown in Figure 5-9b. The presence of the polymerized junctions could be the cause of the change in mechanical propertied. To retain the properties of the template polymer, the fibers with oxidant in the precursor solution were further studied.

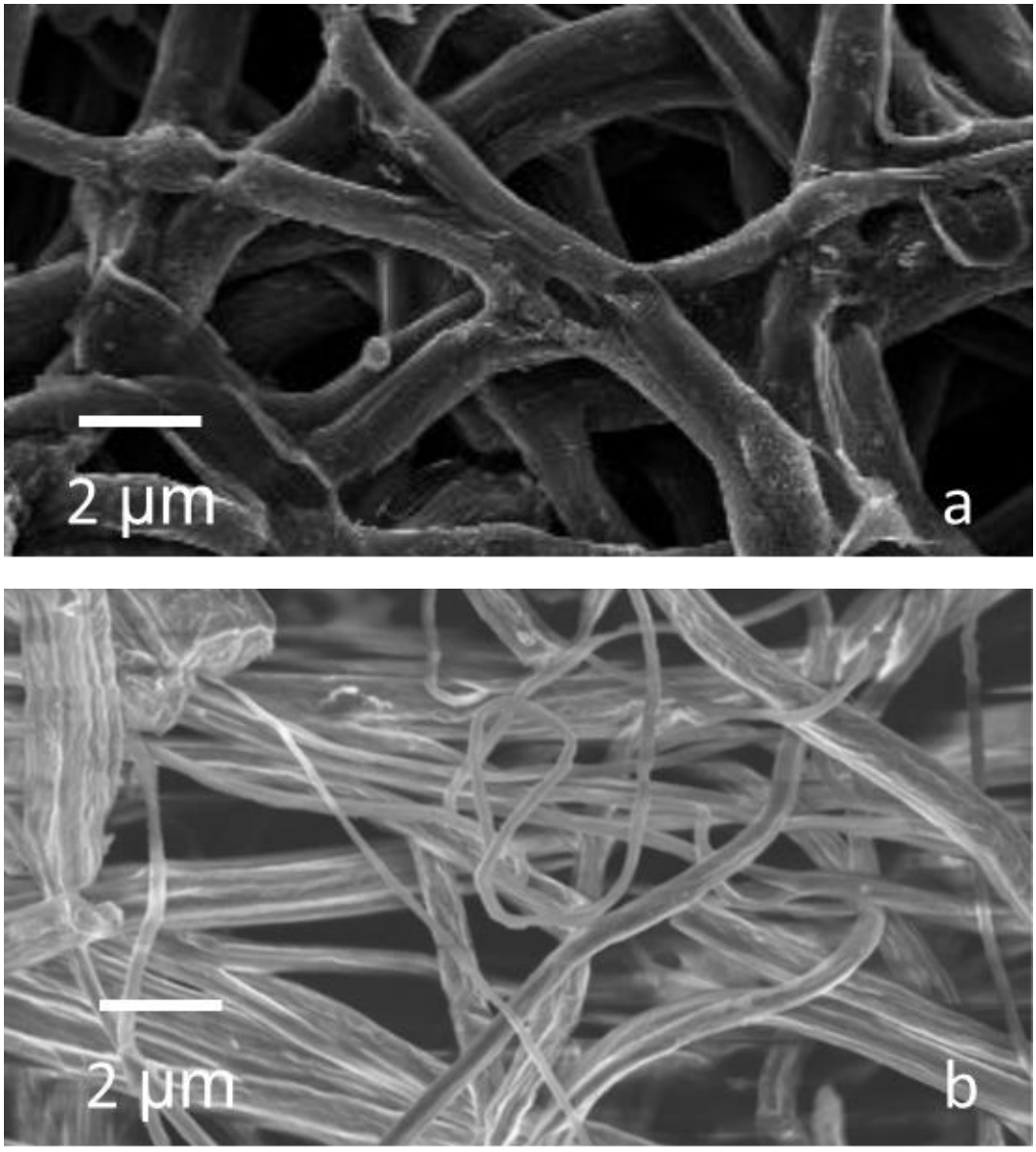


Figure 5-9: SEM images of PMMA-PEDOT fibers based on a) soaking fibers in oxidant and b) spinning fibers with oxidant.

Raman spectroscopy was used to characterize the PMMA fibers before and after VPP as shown in Figure 5-10. The PMMA fibers show the main characteristic peak around 3000 $cm^{-1}$ corresponds to the C-H stretching vibration, matching the literature. After VPP was performed, the PMMA-PEDOT fibers show a broad peak around 1500 $cm^{-1}$ corresponds to the characteristic Cα-Cβ stretch in PEDOT.[33] The C-H peak from the PMMA is still present in the fibers.

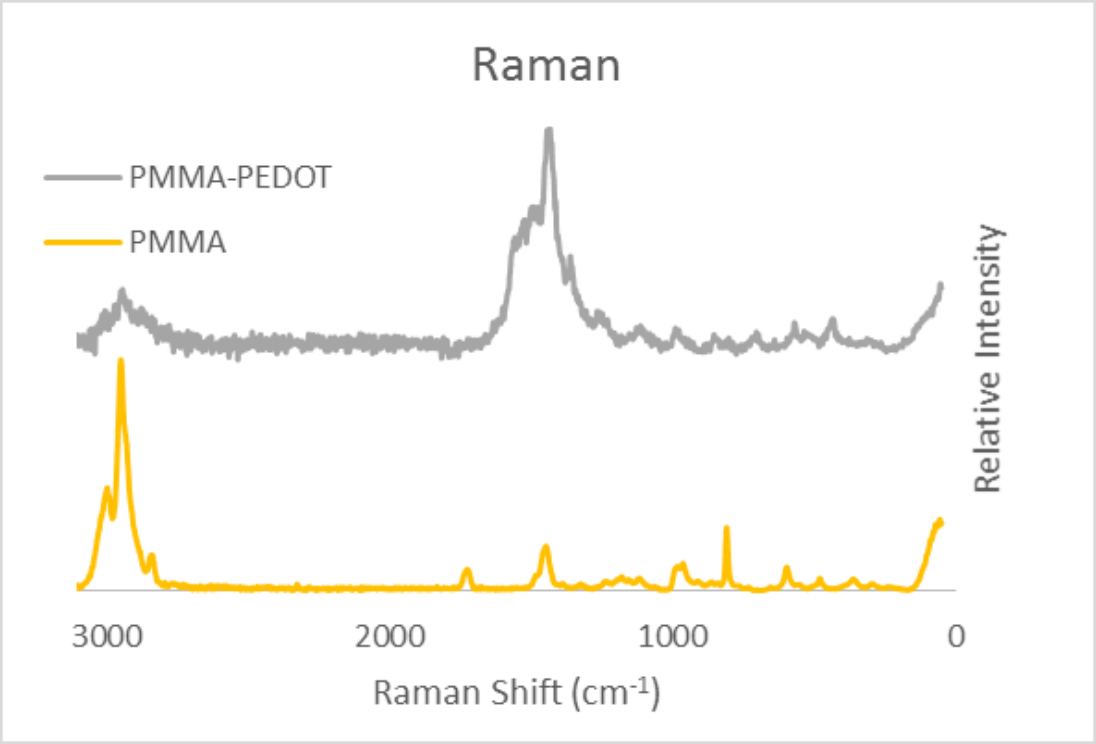


Figure 5-10: Raman spectrum of electrospun fibers before and after the VPP process.

SEM was used to characterize the PMMA fibers before and after the VPP process to see if the PEDOT was distributed evenly throughout the sample as shown in Figure 5-11. Figure 5-11a shows a smooth surface morphology for the PMMA fiber. After the VPP process, the fibers have a rougher surface with multiple folded layers as shown in Figure 5-11b. These layers are the PEDOT that was grown on the fibers surface, acting as an electrode for the electroactive polymers. Based on the Raman and the SEM, the PEDOT is present and evenly distributed on the fibers which was not observed with the graphene nano platelets.

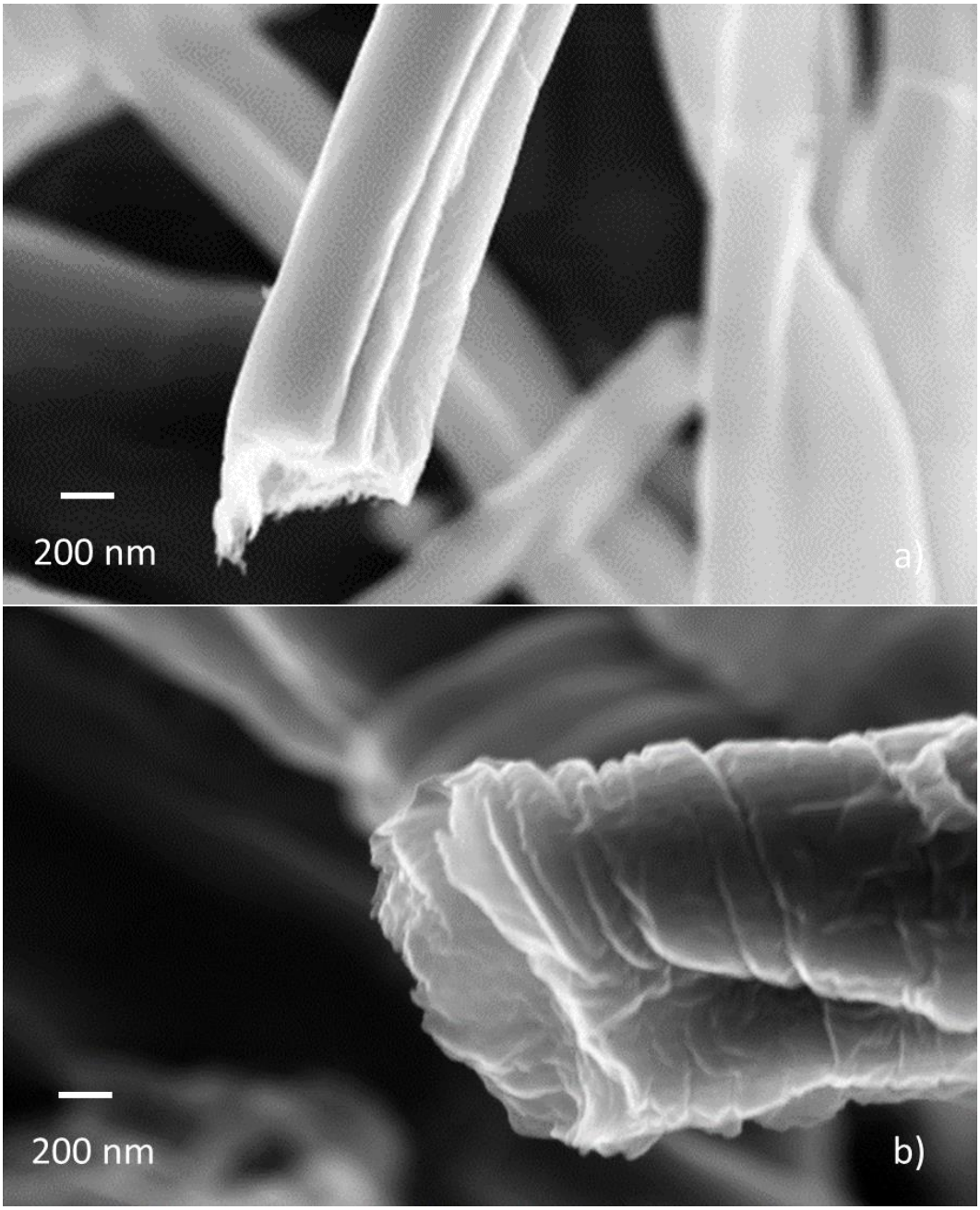


Figure 5-11: SEM images of a) PMMA fibers pre-polymerization and b) PMMA fibers post-polymerization.

To determine the amount of oxidant to use in the precursor solution, three different wt % of oxidant was fabricated. Having too much oxidant can result in rapid polymerization which will reduce the crystallinity. If not enough oxidant is used, the polymerization will be incomplete resulting in shorter chains of PEDOT which will have

lower conductivities. Three different concentrations of oxidant were used with the results shown in Table 5-1. The wt% oxidant is the amount of oxidant relative to the PMMA fibers being soaked. As the concentration of oxidant was decreased, the conductivity of the fibers also decreased. Currently the maximum concentration used was 50% due to the solubility of the oxidant in solution. Using less oxidant may prevent the polymerization from reaching completion which would reduce the conductivity.

Table 5-1: Conductivity of PEDOT-PMMA fibers based on the wt% of FePTs.

| Voltage | Distance | Wt% Oxidant | Temperature | Color | Sheet Resistance |
|---|---|---|---|---|---|
| 19 kV | 15 cm | 50% | 60 C | Blue | 121 ± 27 Ω |
| 19 kV | 15 cm | 33% | 60 C | Blue | 1175 ± 300 Ω |
| 19 kV | 15 cm | 14% | 60 C | Orange | Nonconducting |

The fibers spun with the oxidant prior to VPP were spun at different voltages and distances to determine effect on conductivity shown in Table 5-2. The diameter of the fibers was determined using SEM. From the results, there was no relationship between the electrospinning conditions and the conductivity of the fibers. One possibility is the diameter of the fiber is not the major factor for the conductivity of the fibers. The difference between the most and least conducting fibers is 0.08 S/cm while the diameters ranged from 200-600 nm. The other possibility is the template polymer is playing a larger role in the conductivity than the PEDOT. Since PMMA is an insulating polymer, it could reducing the overall conductivity of the fibers. This is supported by other

PEDOT coated fibers with greater conductivity using template polymers other than PMMA.

Table 5-2: Conductivity of PEDOT-PMMA fibers based on electrospinning voltage and working distance.

| Voltage | Distance | Conductivity | Diameter |
|---|---|---|---|
| 18 kV | 19 cm | 0.13 ± 0.1 S/cm | 284 ± 63 nm |
| 18 kV | 17 cm | 0.19 ± 0.1 S/cm | 620 ± 164 nm |
| 18 kV | 15 cm | 0.14 ± 0.2 S/cm | 462 ± 226 nm |
| 18 kV | 13 cm | 0.14 ± 0.1 S/cm | 460 ± 156 nm |
| 15 kV | 15 cm | 0.20 ± 0.1 S/cm | 486 ± 124 nm |
| 18 kV | 15 cm | 0.14 ± 0.2 S/cm | 462 ± 226 nm |
| 21 kV | 15 cm | 0.16 ± 0.2 S/cm | 230 ± 72 nm |
| 24 kV | 15 cm | 0.12 ± 0.1 S/cm | 575 ± 300 nm |

An alternative to PMMA is PVDF which is a polymer electrolyte used in membranes for batteries. Using a polymer electrolyte instead of an insulating material could increase the conductivity of the composite material. PEDOT-PVDF fibers were prepared by electrospinning fibers preloaded with oxidant solution and by soaking PVDF fibers in an oxidant solution. SEM micrographs of fibers prepared by each method are shown in Figure 5-12. Based on the SEM images, the fibers prepared by spinning the oxidant were more uniform in size and appear to be smoother than the fibers that were soaked in an oxidant solution prior to VPP. The difference in the morphology could be a difference in where the PEDOT is located. In the fibers preloaded with oxidant, the oxidant

would be incorporated into the fibers. This could result in a PEDOT infused PVDF fiber. The fibers that were soaked in the oxidant solution may have more PEDOT on the surface based on the morphology difference. If the oxidant is only present on the surface of the fibers, this could result in a PEDOT coated fiber.

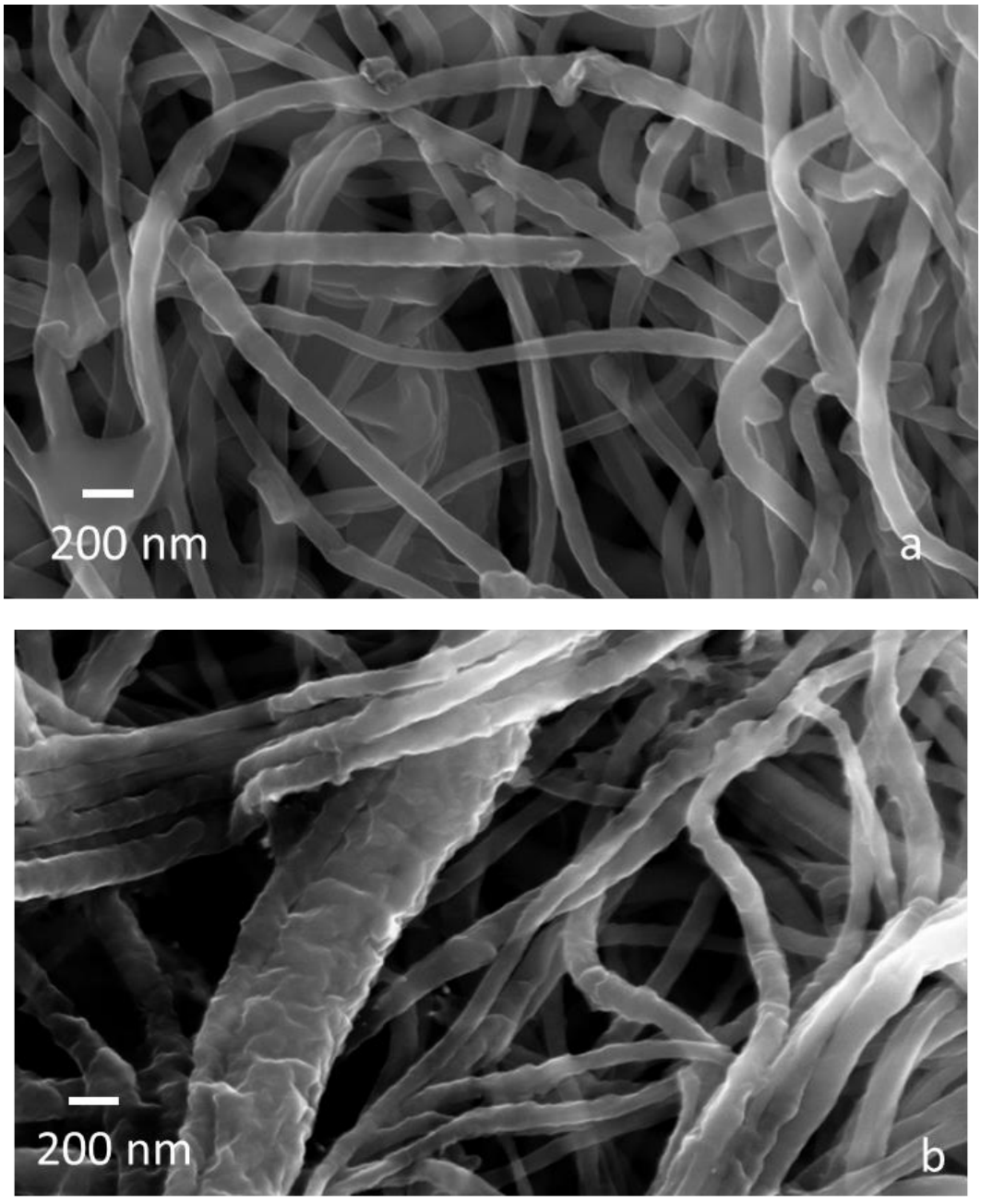


Figure 5-12 PEDOT-PVDF fibers when a) oxidant was spun with fibers and b) when fibers were soaked in an oxidant solution.

PVDF films are known to be piezoelectric if a poling step is used before the formation of the film.[5] One way to predict piezoelectric properties is looking at the phase of PVDF. Based on the literature, PVDF can be in three phases, α, β, and γ phase. The β phase is the phase that has the best piezoelectric properties based on the alignment of the dipole.[34] FTIR can be used to determine the phase of the PVDF present. The FTIR-ATR plots of the fibrous mats are shown in Figure 5-13. Focusing on the peak at 840 $cm^{-1}$ would be indicate the PVDF is β-phase however there is a shoulder around 833 $cm^{-1}$ which represents γ-phase. Based on the IR, electrospinning of PVDF fibers produced a material that is β-phase which could offer an alternative to poling.

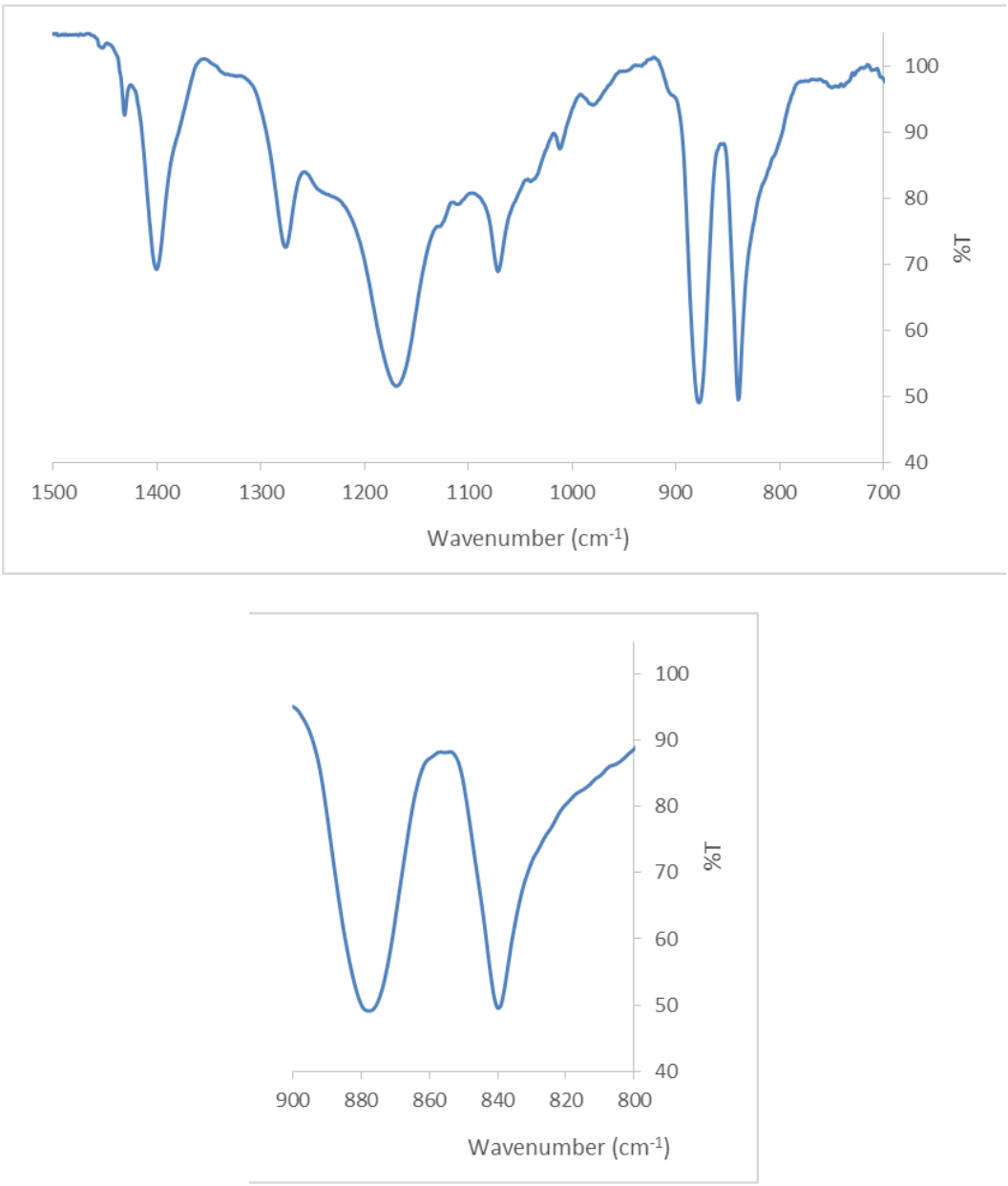


Figure 5-13: FTIR-ATR spectrum of PEDOT-PVDF fibers.

The conductivity of the PEDOT-PVDF fibers remained the same regardless of when the oxidant was added as shown in Table 5-3. If the fibers are to be used as an electroactive polymer, it is important that the PEDOT be only on the surface of the fibers. If the PEDOT is infused into the fibers, the alignment of the polymer in the electric field may not be drastic enough to induce a large conformational change. Based on the SEM

images in Figure 5-12, the soaking method could provide a surface coating of PEDOT. When comparing the conductivity of the PEDOT-PVDF and PEDOT-PVDF-HFP as shown in Table 5-3, the conductivity using PVDF-HFP was significantly greater. PVDF-HFP could be a promising template polymer in the fabrication of conductive fibrous mats as it produced the highest conductivity of the materials reported in the study. To further enhance the conductivity of the PVDF-HFP fibrous mat, different diameter fibers can be prepared and the utilization of post polymerization treatments could be explored.

Table 5-3: Comparing loading oxidant prior or post electrospinning effect on the conductivity of PEDOT-PVDF fibers and initial results of PEDOT-PVDF-HFP fibers.

| Template Polymer | Oxidant Loading Step | Voltage | Distance | Diameter | Conductivity |
|---|---|---|---|---|---|
| PVDF | Pre-spinning | 20 kV | 15 cm | 125 ± 9 nm | 0.17 ± 0.4 S/cm |
| PVDF | Post-spinning | 15 kV | 11 cm | 124 ± 35 nm | 0.16 ± 0.2 S/cm |
| PVDF-HFP | Post-spinning | 15 kV | 11 cm | 261 ± 105 nm | 0.28 ± 0.2 S/cm |

## 5.4 Conclusions

PEDOT-PMMA fibers had very little difference in conductivity regardless of the electrospinning parameters. This could be because PMMA is an insulating material which could limit the overall conductivity of the material. It was shown that increasing the wt% of oxidant increased the conductivity of the resulting fibers. This could be because more oxidant is needed for the complete polymerization of PEDOT resulting in the most conducting material. When using PMMA as a template polymer, when the oxidant is added plays a role in the mechanical properties of the resulting material. When the oxidant was added prior to electrospinning, the fibers retained the mechanical properties of PMMA.

When the fibers were soaked in an oxidant solution, the fibers became more rigid and stiff, possibly from the increased cross-linking observed in the SEM.

Using PVDF as a template polymer showed no difference in conductivity or mechanical properties based on when the oxidant was added. The fabrication of PVDF fibers using the electrospinning method produced fibers that shown to be β-phase of PVDF which is the piezoelectric phase of the polymer. This is important because the use of electrospinning showed to replace the poling which is required for the fabrication of β-phase PVDF. Preliminary results show that PVDF-HFP produced the most conductive fibers of 0.28 S/cm. Further optimization of the fibers are required based on the electrospinning parameters and the polymerization procedure.

## 5.5 References


1. Abidian, M. R.; Kim, D. H.; Martin, D. C., Conducting-polymer nanotubes for controlled drug release. *Advanced Materials* **2006,** *18* (4), 405-+.

2. Martin, D. C.; Wu, J. H.; Shaw, C. M.; King, Z.; Spanninga, S. A.; Richardson-Burns, S.; Hendricks, J.; Yang, J. Y., The Morphology of Poly(3,4-Ethylenedioxythiophene). *Polymer Reviews* **2010,** *50* (3), 340-384.

3. Huang, Z. M.; Zhang, Y. Z.; Kotaki, M.; Ramakrishna, S., A review on polymer nanofibers by electrospinning and their applications in nanocomposites. *Composites Science and Technology* **2003,** *63* (15), 2223-2253.

4. Bao, Q. L.; Zhang, H.; Yang, J. X.; Wang, S.; Tong, D. Y.; Jose, R.; Ramakrishna, S.; Lim, C. T.; Loh, K. P., Graphene-Polymer Nanofiber Membrane for Ultrafast Photonics. *Advanced Functional Materials* **2010,** *20* (5), 782-791.

5. Darestani, M. T.; Coster, H. G. L.; Chilcott, T. C.; Fleming, S.; Nagarajan, V.; An, H., Piezoelectric membranes for separation processes: Fabrication and piezoelectric properties. *Journal of Membrane Science* **2013,** *434*, 184-192.

6. Kim, Y.; Ryu, T. I.; Ok, K. H.; Kwak, M. G.; Park, S.; Park, N. G.; Han, C. J.; Kim, B. S.; Ko, M. J.; Son, H. J.; Kim, J. W., Inverted Layer-By-Layer Fabrication of an Ultraflexible and Transparent Ag Nanowire/Conductive Polymer Composite Electrode for Use in High-Performance Organic Solar Cells. *Advanced Functional Materials* **2015,** *25* (29), 4580-4589.

7. Choi, J.; Lee, J.; Choi, J.; Jung, D.; Shim, S. E., Electrospun PEDOT:PSS/PVP nanofibers as the chemiresistor in chemical vapour sensing. *Synthetic Metals* **2010,** *160* (13–14), 1415 - 1421.

8. Feng, Z. Q.; Wu, J. H.; Cho, W. R.; Leach, M. K.; Franz, E. W.; Naim, Y. I.; Gu, Z. Z.; Corey, J. M.; Martin, D. C., Highly aligned poly(3,4-ethylene dioxythiophene) (PEDOT) nano- and microscale fibers and tubes. *Polymer* **2013,** *54* (2), 702-708.

9. Doshi, J.; Reneker, D. H., Elecrospinning process and applications of electrospun fibers. *Journal of Electrostatics* **1995,** *35* (2-3), 151-160.

10. Li, Z.; Wang, C., Effects of Working Parameters on Electrospinning. In *One-Dimensional nanostructures: Electrospinning Technique and Unique Nanofibers*, Springer Berlin Heidelberg: Berlin, Heidelberg, 2013; pp 15-28.

11. Gupta, P.; Elkins, C.; Long, T. E.; Wilkes, G. L., Electrospinning of linear homopolymers of poly(methyl methacrylate): exploring relationships between fiber formation, viscosity, molecular weight and concentration in a good solvent. *Polymer* **2005,** *46* (13), 4799-4810.

12. Zeng, J. J.; Saltysiak, B.; Johnson, W. S.; Schiraldi, D. A.; Kumar, S., Processing and properties of poly(methyl methacrylate)/carbon nano fiber composites. *Composites Part B-Engineering* **2004,** *35* (2), 173-178.

13. Boyer, S. M.; Liu, J.; Zhang, S.; Ehrlich, M. I.; McCarthy, D. L.; Tong, L.; DeCoste, J. B.; Bernier, W. E.; Jones Jr., W. E., The role of ruthenium photosensitizers in the degradation of phenazopyridine with TiO2 electrospun fibers. *Journal of Photochemistry and Photobiology A: Chemistry* **2016,** *329*, 46 - 53.

14. Liu, J.; McCarthy, D. L.; Cowan, M. J.; Obuya, E. A.; DeCoste, J. B.; Skorenko, K. H.; Tong, L.; Boyer, S. M.; Bernier, W. E.; Jones Jr., W. E., Photocatalytic activity of TiO2 polycrystalline sub-micron fibers with variable rutile fraction. *Applied Catalysis B: Environmental* **2016,** *187*, 154 - 162.

15. Gopal, R.; Kaur, S.; Ma, Z. W.; Chan, C.; Ramakrishna, S.; Matsuura, T., Electrospun nanofibrous filtration membrane. *Journal of Membrane Science* **2006,** *281* (1-2), 581-586.

16. Kim, J. R.; Choi, S. W.; Jo, S. M.; Lee, W. S.; Kim, B. C., Electrospun PVdF-based fibrous polymer electrolytes for lithium ion polymer batteries. *Electrochimica Acta* **2004,** *50* (1), 69-75.

17. Yee, W. A.; Kotaki, M.; Liu, Y.; Lu, X. H., Morphology, polymorphism behavior and molecular orientation of electrospun poly(vinylidene fluoride) fibers. *Polymer* **2007,** *48* (2), 512-521.

18. Stephan, A. M., Review on gel polymer electrolytes for lithium batteries. *European Polymer Journal* **2006,** *42* (1), 21-42.

19. He, X. J.; Yao, K.; Gan, B. K., Phase transition and properties of a ferroelectric poly(vinylidene fluoride-hexafluoropropylene) copolymer. *Journal of Applied Physics* **2005,** *97* (8), 6.

20. Lalia, B. S.; Guillen-Burrieza, E.; Arafat, H. A.; Hashaikeh, R., Fabrication and characterization of polyvinylidenefluoride-co-hexafluoropropylene (PVDF-HFP) electrospun membranes for direct contact membrane distillation. *Journal of Membrane Science* **2013,** *428*, 104-115.

21. Yao, C.; Li, X. S.; Neoh, K. G.; Shi, Z. L.; Kang, E. T., Antibacterial activities of surface modified electrospun poly(vinylidene fluoride-co-hexafluoropropylene) (PVDF-HFP) fibrous membranes. *Applied Surface Science* **2009,** *255* (6), 3854-3858.

22. Smela, E., Conjugated polymer actuators for biomedical applications. *Advanced Materials* **2003,** *15* (6), 481-494.

23. Zheng, W.; Wong, S. C., Electrical conductivity and dielectric properties of PMMA/expanded graphite composites. *Composites Science and Technology* **2003,** *63* (2), 225-235.

24. Pinto, G.; Lopez-Gonzalez, C.; Jimenez-Martin, A., Polymer composites prepared by compression molding of a mixture of carbon black and nylon 6 powder. *Polymer Composites* **1999,** *20* (6), 804-808.

25. Chandrasekaran, S.; Seidel, C.; Schulte, K., Preparation and characterization of graphite nano-platelet (GNP)/epoxy nano-composite: Mechanical, electrical and thermal properties. *European Polymer Journal* **2013,** *49* (12), 3878-3888.

26. Forrest, S. R., The path to ubiquitous and low-cost organic electronic appliances on plastic. *Nature* **2004,** *428* (6986), 911-918.

27. Roncali, J., Conjugates poly(thiophenes) synthesis, functionalization, and applications. *Chemical Reviews* **1992,** *92* (4), 711-738.

28. MacDiarmid, A. G., "Synthetic metals": A novel role for organic polymers (Nobel lecture). *Angewandte Chemie-International Edition* **2001,** *40* (14), 2581-2590.

29. Cho, B.; Park, K. S.; Baek, J.; Oh, H. S.; Lee, Y. E. K.; Sung, M. M., Single-Crystal Poly(3,4-ethylenedioxythiophene) Nanowires with Ultrahigh Conductivity. *Nano Letters* **2014,** *14* (6), 3321-3327.

30. Madl, C. M.; Kariuki, P. N.; Gendron, J.; Piper, L. F. J.; Jones, W. E., Vapor phase polymerization of poly (3,4-ethylenedioxythiophene) on flexible substrates for enhanced transparent electrodes. *Synthetic Metals* **2011,** *161* (13-14), 1159-1165.

31. Skorenko, K. H.; Faucett, A. C.; Liu, J.; Ravvin, N. A.; Bernier, W. E.; Mativetsky, J. M.; Jones Jr, W. E., Vapor phase polymerization and mechanical testing of highly electrically conductive poly(3,4-ethylenedioxythiophene) for flexible devices. *Synthetic Metals* **2015,** *209*, 297 - 303.

32. Laforgue, A.; Robitaille, L., Production of Conductive PEDOT Nanofibers by the Combination of Electrospinning and Vapor-Phase Polymerization. *Macromolecules* **2010,** *43* (9), 4194-4200.

33. Selvaganesh, S. V.; Mathiyarasu, J.; Phani, K. L. N.; Yegnaraman, V., Chemical synthesis of PEDOT-Au nanocomposite. *Nanoscale Research Letters* **2007,** *2* (11), 546-549.

34. Martins, P.; Lopes, A. C.; Lanceros-Mendez, S., Electroactive phases of poly(vinylidene fluoride): Determination, processing and applications. *Progress in Polymer Science* **2014,** *39* (4), 683-706.

# Chapter 6

## Summary and Future Work

Solid state DSSCs using VPP PEDOT as a solid electrolyte and dye sensitized $TiO_2$ electrospun nanofibers for the degradation of PAP under visible irradiation was investigated. Solid state DSSC's offer a cheaper alternative to other photovoltaics and there have been great interest transitioning to solid state electrolytes. We have fabricated the first working solid state DSSC utilizing a VPP PEDOT hole conducting material with efficiencies as great as 0.2%. The work provides a foundation for future devices to be fabricated utilizing the VPP method.

In Chapter 2 we showed the fabrication of solid state DSSCs perform better using a spin-coated mesoporous $TiO_2$ layer than a Dr. Blade coated layer. It was also demonstrated that a combination of VPP PEDOT and PEDOT:PSS provide the best combination of filling of the $TiO_2$ layer and preventing shorting with the gold layer. Results show the duration of the VPP has a great effect on maximizing of the $I_{sc}$ and $V_{OC}$ and thus the efficiency. While previously reported to not be a viable oxidant, FePTs produced the highest efficiency of the solar cells fabricated.

While working solar cells were fabricated using VPP PEDOT, the efficiencies are much lower than other reported methods using PEDOT. To further improve the efficiencies, device optimization is required. Solar cells need to be fabricated with different blocking layer, mesoporous, VPP PEDOT and PEDOT:PSS thicknesses to find the optimal

conditions for fabrication. It is also possible to improve the conductivity of the VPP PEDOT and PEDOT:PSS layers using a post deposition treatment such as ion exchange. Increasing the conductivity of the hole conducting materials will improve the $I_{sc}$ which should improve the efficiency of the solar cell. It is also important to further explore FePTs as an oxidant for the VPP method. XPS studies on $TiO_2$ after the polymerization of PEDOT could determine if the Ti is being reduces at the conditions used for the device fabrication.

Chapter 3 demonstrated the successful synthesis of two possible ligands for new dye molecules to be used in DSSCs. Results support the copolymerization of ttp-H with EDOT and suggest ttp-Br does not polymerize. Using the ligands ttp-H and ttp-Br, new dye molecules have been synthesized and characterized with UV-Vis. The molar extinction coefficients for the new dyes rival the N3 dye which is commonly used in DSSCs.

While dyes have been synthesized, crystal structures are needed to confirm the successful synthesis of the molecules. Solar cells can then be fabricated using each dye and compared to determine the role polymerizing the dye into the PEDOT layer has on the solar cell efficiencies. Other thiophene ligands can be explored, specifically looking at effect of chain length between the thiophene and dye as well as bipyridine derivatives. It is proposed by polymerizing the dye into PEDOT, the regeneration of the dye will occur through bond like in the electron injection into the semiconductor material. This could be tested by changing the linkage between the thiophene and dye. Comparing different length conjugated and unconjugated chains would alter electron transfer rates if the process occurred through bond. Utilizing bipryidine ligands instead of terpyridine can allow for

the synthesis of neutral dyes instead of positively charged dyes. Starting in the neutral state could help with the injection of an excited electron into the $TiO_2$ layer.

The focus of Chapter 4 was comparing the photocatalytic activity of $TiO_2$ and dye-sensitized $TiO_2$ fibers in UV/Visible and Visible irradiation for the degradation of PAP. The results showed that incorporating a ruthenium sensitizer does not enhance the degradation rate under visible irradiation which gives insight into the mechanism. One possibility is the dye provides an alternative pathway for the relaxation of electrons, reducing the number of electrons reaching the surface of $TiO_2$. Another possibility is the degradation of PAP is predominately from the hydroxyl radical formation which would not be enhanced with an electron injecting dye. This contributed to previous work in the area of modified $TiO_2$ under visible irradiation, specifically using dye anchoring.

To further understand the reason for the reduced degradation rate, it is important to determine the degradation pathway of PAP. This could be done using GC-MS and NMR to determine the degradation products, giving insight if the major radical is hydroxyl or peroxide. It is also possible to explore other surface modifications. Other studies in the group showed PEDOT improved the degradation rates of PAP. Exploring the use of P3HT on the surface of $TiO_2$ could improve the rates under visible irradiation. P3HT is commonly used in organic solar cells as part of the photosensitizer layer while being conductive like PEDOT. This could provide absorbance in the visible region while extending the lifetime of the electron-hole pair through charge separation.

Chapter five discussed the fabrication and characterization of conducting electrospun nanofibers using different template polymers and PEDOT. The results show that the choice of the template polymer plays a major role in the conductivity of the

resulting fibers. We were also able to demonstrate using FTIR electrospun PVDF produces the β-phase of the polymer which is a known piezoelectric material. This is important because normally to prepare β-phase PVDF a poling step is required.

Although FTIR shows the PVDF is β-phase which is piezoelectric, it is important to determine the piezoelectric coefficient. This would quantify how piezoelectric the materials are and can be compared to thin films. Another application of the materials is in super capacitors. The group has made super capacitators using PEDOT with very high capacitance and showed increasing the surface area is important in capacitance performance. Electrospun fibers can have high surface area which would increase the loading of PEDOT in the material. Comparing the difference composite materials would show the effect of conductivity and surface area on the capacitance of the materials.